Structural studies of E1-E2 interactions in the ubiquitin cascade

Carlos Riechmann
St Hugh's College, University of Oxford
A thesis submitted for the degree of *Doctor of Philosophy*
Michaelmas 2025

Abstract

The conjugation of ubiquitin to substrate proteins underpins nearly all eukaryotic cellular pathways. In vertebrates, this process is initiated by two essential ubiquitin-activating enzymes (E1s), UBA1 and UBA6. Recent studies have shown that each E1 directs independent downstream pathways through distinct ubiquitin-conjugating enzymes (E2s), yet the mechanisms governing E2 selection remain unclear.

Here, in vitro E2 activity screens combined with cryoEM structures of the two UBA6-specific E2s in complex with UBA6 provide new insight into the molecular interactions driving E1-E2 specificity in the ubiquitin cascade. This framework was then applied to generate E2 mutants with altered E1 specificities, offering potential tools to dissect E1-specific pathways in cells.

Additionally, this work identifies a unique priority mechanism for the UBA6-specific E2 BIRC6, enabled by a uniquely high affinity E1-E2 interaction. Further analysis revealed that the Cys-cap loop of UBA6 dampens E2 affinities, which allows UBA6 to function with a high affinity E2 without being inhibited. These findings outline an affinity-driven hierarchy among E2s, balanced by an E1 regulatory element to ensure efficient E2 turnover.

Overall, this work provides key mechanistic insights into how E1-E2 specificity is achieved in the ubiquitin system, highlighting both structural determinants and regulatory mechanisms that shape pathway selectivity. By uncovering unique features of UBA6-mediated interactions and identifying principles that govern E2 hierarchy, these findings not only expand our fundamental understanding of the ubiquitin cascade but also lay the groundwork for new molecular tools to probe and manipulate E1-specific cellular pathways.

Acknowledgements

I would like to thank past and present members of the Elliott Lab for their invaluable contributions to this work, without which this thesis would not be possible:

Paul Elliott, for designing the project, assisting with the writing process, and completing the FP measurements in Figures 36, 38.

Cara Ellison, for assisting with the writing process of the associated manuscript, helping assemble the E2 panel, and other experimental work not included in this thesis.

Jake Anderson, for purifying UBA6 mutants in Figure 16.

Tim Western, for assisting with optimisation of the dUBA1-dBIRC6 cryoEM sample.

I also acknowledge the assistance from staff in both COSMIC and eBIC cryoEM facilities, in particular Teige Matthews-Palmer, Yuewen Sheng, and Karen Davies.

Table of contents

List of figures

List of tables

List of acronyms

3DVA	3-Dimensional variability analysis
AAD	Active adenylation domain
AMP	Adenosine monophosphate
APC/C	Anaphase-promoting complex/cyclosome
ATG-3	Autophagy-related protein 3
ATP	Adenosine triphosphate
BIR	Baculoviral IAP repeat
BIRC6	BIR-containing protein 6
BSA	Bovine serum albumin
cIAP	Cellular inhibitor of apoptosis
COOT	Crystallographic object-oriented toolkit
COSMIC	Central Oxford structural molecular imaging centre
cryoEM	Electron cryo-microscopy
crYOLO	(Cryo) you only look once
cryoSPARC	CryoEM single particle ab-initio reconstruction and classification
CTF	Contrast transfer function
Cy5	Cyanine5
CYLD	Cylindromatosis tumour suppressor protein
DBHDA	2,5-dibromohexanediamide
Dha	Dehydroalanine
DMSO	Dimethyl sulfoxide
DNA	Deoxyribonucleic acid
DTT	Dithiothreitol
DUB	Deubiquitinating enzyme
E1	Ubiquitin activating enzyme
E2	Ubiquitin conjugating enzyme
E3	Ubiquitin ligase (transferase)
eBIC	Electron bio-imaging centre
EDTA	Ethylenediaminetetraacetic acid
FAT10	Human leukocyte antigen-F adjacent transcript 10
FCCH	First catalytic cysteine half domain
FOM	Fluorinated octyl maltoside
FP	Fluorescence polarisation

FSC	Fourier shell correlation
HECT	Homologous to E6AP C-Terminus
HEPES	4-(2-hydroxyethyl)-1-piperazineethanesulfonic acid
IAD	Inactive adenylation domain
IAP	Inhibitor of apoptosis protein
IKK	Nuclear factor-κB kinase
IP6	Inositol-6-phosphate
ISG15	Interferon-stimulated gene 15
LC3	Microtubule-associated protein 1 light chain 3
mRNA	Messenger ribonucleic acid
NAE1	NEDD8 activating protein 1
NEDD8	Neural precursor cell expressed developmentally downregulated protein 8
NF-κB	Nuclear factor-κB
NHS	N-Hydroxysuccinimide
NMR	Nuclear magnetic resonance
PATo	Single particle analysis and tomography data visualisation interface
PCR	Polymerase chain reaction
PDB	Protein data bank
PEI	Polyethylenimine
PHENIX	Python-based hierarchical environment for integrated xtallography
PMSF	Phenylmethylsulfonyl fluoride
PPi	Pyrophosphate
PSAN	Bis-electrophilic 3-(phenylsulfonyl)-4-aminobut-2-enenitrile
RBR	RING-between-RING
RELION	Regularised likelihood optimisation
RHD	Rhodanese homology domain
RING	Really interesting new gene
RMSD	Root mean squared deviation
SAE1	Sumo activating protein 1
SAXS	Small-angle X-ray scattering
SCCH	Second catalytic cysteine half domain
SDS-PAGE	Sodium dodecyl sulphate polyacrylamide gel electrophoresis
SEC	Size exclusion chromatography
SIMPLE	Single-particle image processing linux engine

SUMO	Small ubiquitin-like modifier
TAB2/3	TAK1-binding proteins 2/3
TAK1	Transforming growth factor β-activated protein 1
TY	Tryptone-yeast extract
Ub	Ubiquitin
UBA	Ubiquitin activating protein
UBD	Ubiquitin binding domain
UbDha	Ubiquitin dehydroalanine
UBE	Ubiquitin conjugating enzyme
UBL	Ubiquitin-like protein
UFD	Ubiquitin fold domain
VEXAS	Vacuole, E1 enzyme, x-linked, autoinflammatory, somatic syndrome
VMX	5'-(((3-aminopropyl)sulfonyl)amino)-5'-deoxyadenosine
XIAP	X-linked inhibitor of apoptosis

1. Introduction

1.1. Introduction

1.1.1. The ubiquitin cascade

Ubiquitin is a highly conserved 76-amino acid protein (**Fig. 1a**) found across all eukaryotes, from yeast to humans[1]. Covalent attachment of ubiquitin to target proteins, typically via an isopeptide bond formed between the ubiquitin C-terminus and a surface-exposed primary amine on the substrate (**Fig. 1b**), facilitates a vast array of post-translational regulatory mechanisms[2]. Underpinning ubiquitin's versatility are its seven internal lysine residues: K6, K11, K27, K29, K33, K48, K63, and an amino terminus, M1, which enable ubiquitin molecules to form polyubiquitin chains of diverse topologies. These chain configurations are recognized by "reader" proteins, which interpret linkage-specific signals through ubiquitin binding domains (UBDs) to direct downstream cellular processes[3]. Ubiquitin signalling is also antagonised by "eraser" proteins, also known as deubiquitinating enzymes (DUBs) which either cleave thioester linkages within ubiquitin chains to shorten them, or prune chains directly off substrates[4].

Among these processes, the ubiquitin–proteasome system is the most extensively characterized. The attachment of K48-linked ubiquitin chains marks substrates for recognition and degradation by the 26S proteasome, a large, multi-subunit complex that hydrolyses unfolded polypeptide chains into short peptides[5] (**Fig. 1c**). This process not only maintains protein homeostasis but also serves as a rapid means of silencing protein activity. A notable example is progression through the cell cycle, in which each stage is coordinated by cell cycle checkpoints. This is achieved through

switching the substrate specificity of a single ubiquitin ligase (E3) enzyme, the anaphase-promoting complex/cyclosome (APC/C)[6]. When initially activated, APC/C ubiquitinates Cyclin A, however once the spindle assembly checkpoint is satisfied, further activation by Cdh1 allows APC/C to switch substrates and instead ubiquitinate Securin[7] and Cyclin B, thereby allowing sister chromatid separation and releasing cells from mitosis[8]. The specificity and rapid action of the ubiquitin-proteasome system give the cell exquisite temporal control over cell division, and the modular nature of the APC/C allows one master regulator to mediate the process.

Ubiquitin is also involved in non-degradative processes such as immune signalling, where non-degradative K63-linked ubiquitin chains play a key role in the activation of transforming growth factor β–activated protein 1 (TAK1) through the recruitment of TAK1-binding proteins 2/3 (TAB2/3)[9]. Activated TAK1 can then phosphorylate nuclear factor-κB (NF-κB) kinase (IKK), which in turn activates NF-κB transcription factors leading to the induction of proinflammatory cytokines[10]. This process is negatively regulated by DUBs such as Cylindromatosis tumour suppressor protein (CYLD) and A20[11], which suppress proinflammatory signals by cleaving the K63-linked ubiquitin chains and preventing TAK1 activation.

Given ubiquitin's central role in regulating essential processes, its attachment to substrates is tightly controlled[2]. Ubiquitin itself is chemically inert and must undergo sequential licensing steps before transfer to a substrate by ubiquitin "writer" enzymes (**Fig. 1d**). This process, known as the ubiquitin cascade, comprises three steps: first, an E1 activates ubiquitin's C-terminal carboxyl group; second, an E2 accepts ubiquitin from the E1 via a thioester transfer; and finally, an E3 binds the substrate and catalyses ubiquitin transfer either directly from the E2 or through an additional E3-mediated

intermediate[2]. This thesis focuses primarily on the interactions between E1s and E2s, which will be introduced in the following sections.

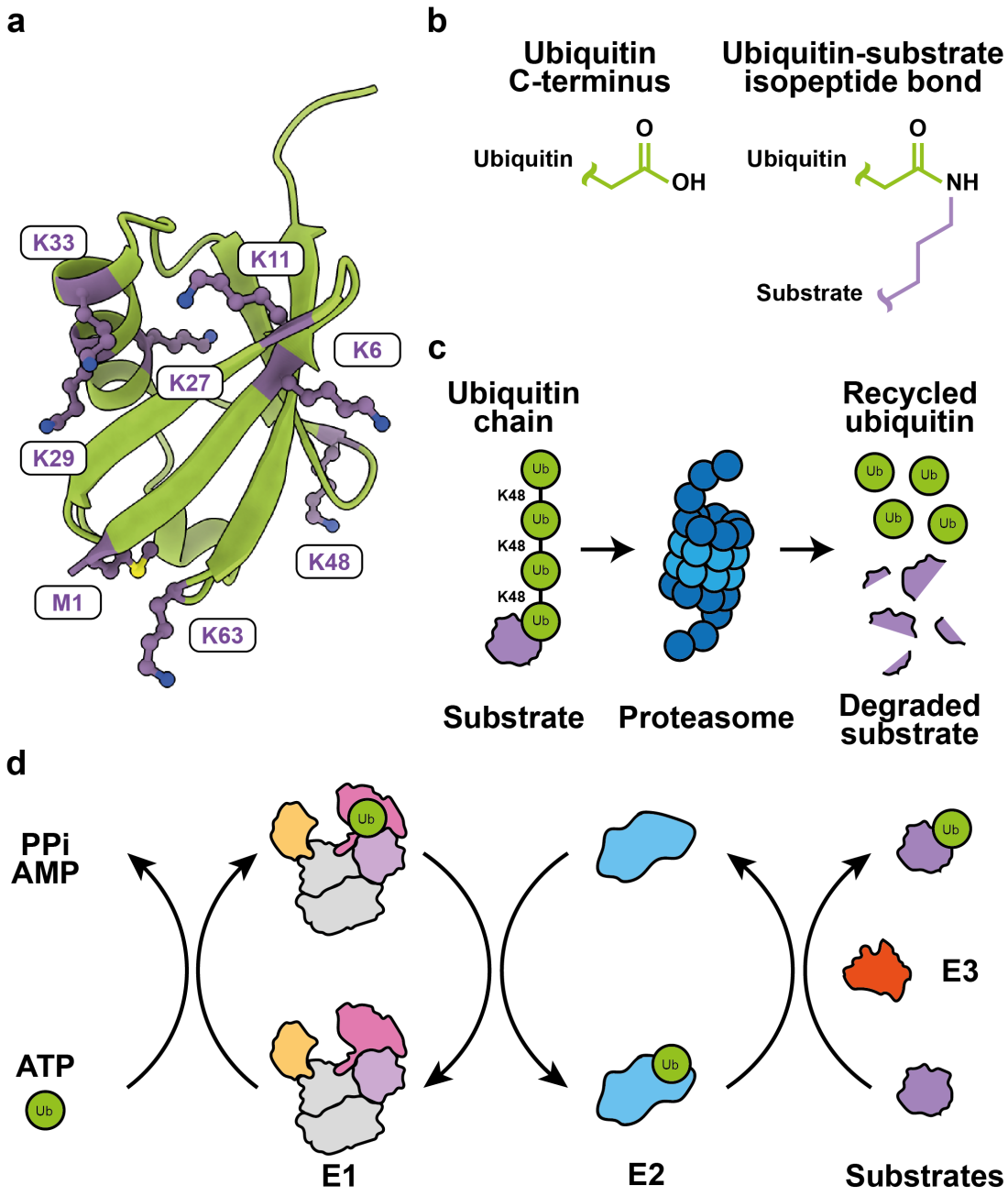
a
K33
K11
K6
K27
K29
K48
M1
K63
b
Ubiquitin
C-terminus
Ubiquitin
O
OH
Ubiquitin-substrate
isopeptide bond
Ubiquitin
O
NH
Substrate
c
Ubiquitin
chain
K48
K48
K48
Ub
Substrate
Proteasome
Recycled
ubiquitin
Degraded
substrate
d
PPi
AMP
ATP
Ub
E1
E2
E3
Substrates

Figure 1. Overview of the ubiquitin cascade

a. Model of ubiquitin (PDB: 1UBQ[12]) with lysine residues labelled.

b. Illustration of how the ubiquitin C-terminus (left) is conjugated to substrates through an isopeptide linkage (right).

c. Cartoon of the ubiquitin-proteasome system.

d. Schematic of ubiquitin licensing by the E1-E2-E3 cascade. Ubiquitin is activated by an E1, transferred to an E2, then conjugated to substrates through the action of an E3.

1.1.2. Ubiquitin activation by E1 enzymes

Humans encode eight E1 proteins in their genome, two of which activate ubiquitin[13]. The remaining E1s catalyse activation of structurally related but functionally distinct ubiquitin-like proteins (UBLs). Even when not directly involved in the ubiquitin cascade, these proteins are typically named UBAX (ubiquitin activating protein X). Despite their diverse functions, all human E1s share a common evolutionary origin and can be broadly divided into two categories based on domain organization[13] (**Fig. 2a**).

Non-canonical E1s, which are less relevant to this thesis, form homodimeric complexes built around a single active adenylation domain (AAD) with minimal additional structural features (**Fig. 2b**). In contrast, canonical E1s, including the ubiquitin-activating UBA1 and UBA6, exist either as heterodimers or monomers in which two non-identical E1-like sequences are combined (**Fig. 2c-d**). These enzymes retain one AAD, while the second adenylation domain is inactive (IAD) and serves as a non-catalytic scaffold. In canonical E1s, the catalytic cysteine is embedded within an auxiliary domain split into two subdomains: the first and second catalytic cysteine half-domains (FCCH and SCCH, respectively). The C-terminal region of all canonical E1s also harbours a ubiquitin-fold domain (UFD), which mediates downstream interactions.

Extensive biochemical and structural studies have elucidated the mechanism of ubiquitin activation by UBA1 in detail[13–15]. The process begins in the AAD with an adenosine triphosphate (ATP)-dependent adenylation reaction (**Fig. 3a-c**), in which the α-phosphate of ATP is attacked by the carboxyl group of ubiquitin's C-terminal glycine, generating a ubiquitin adenylate (ubiquitin-AMP) intermediate and releasing pyrophosphate (PPi). In the subsequent thioesterification step (**Fig. 3d**), the thiol group

of the catalytic cysteine attacks the acyl carbon of the ubiquitin-AMP, displacing AMP and forming a high-energy thioester linkage between ubiquitin and UBA1. This step is accompanied by a dramatic rearrangement of the SCCH domain, which shifts from its resting $SCCH^{UP}$ conformation (**Fig. 3e**) to a compact $SCCH^{DOWN}$ conformation (**Fig. 3f**) to position the catalytic cysteine for nucleophilic attack. After ubiquitin transfer to the cysteine, the SCCH domain resets to the $SCCH^{UP}$ conformation, enabling the AAD to perform a second adenylation reaction. This generates a doubly loaded E1: one ubiquitin remains thioester-linked at the SCCH, while a second ubiquitin is adenylated at the AAD[15]. At this stage, the E1 is poised to transfer ubiquitin to an incoming E2.

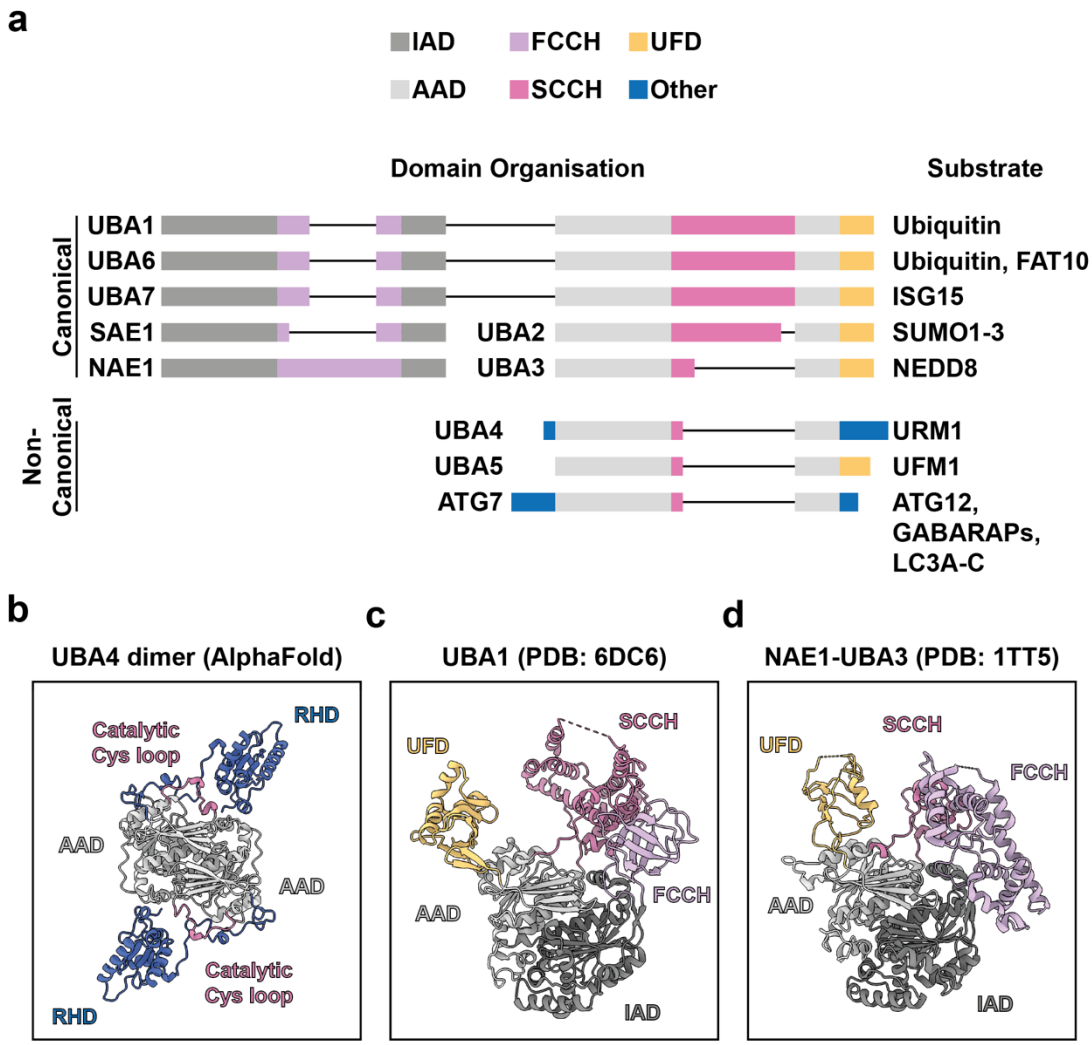
a
IAD
FCCH
UFD
AAD
SCCH
Other
Domain Organisation
Substrate
Canonical
UBA1
UBA6
UBA7
SAE1
NAE1
UBA2
UBA3
Ubiquitin
Ubiquitin, FAT10
ISG15
SUMO1-3
NEDD8
Non-Canonical
UBA4
UBA5
ATG7
URM1
UFM1
ATG12, GABARAPs, LC3A-C
b
UBA4 dimer (AlphaFold)
Catalytic Cys loop
RHD
AAD
AAD
Catalytic Cys loop
RHD
c
UBA1 (PDB: 6DC6)
SCCH
UFD
FCCH
AAD
IAD
d
NAE1-UBA3 (PDB: 1TT5)
SCCH
UFD
FCCH
AAD
IAD

Figure 2. Domain architecture of E1 enzymes

a. Schematic of the domain architectures found in canonical and non-canonical E1s (left), followed by their substrates (right). Non-canonical E1s exist as constitutive homodimers. Figure adapted from Schulman and Harper, 2009[13].

b-d. Atomic models for selected canonical (a, UBA1 (PDB: 6DC6[16]); b, NAE1-UBA3 (PDB: 1TT5[17])) and non-canonical (c, UBA4 Alphafold) E1s. UBA4 contains a unique rhodanese homology domain (RHD, blue).

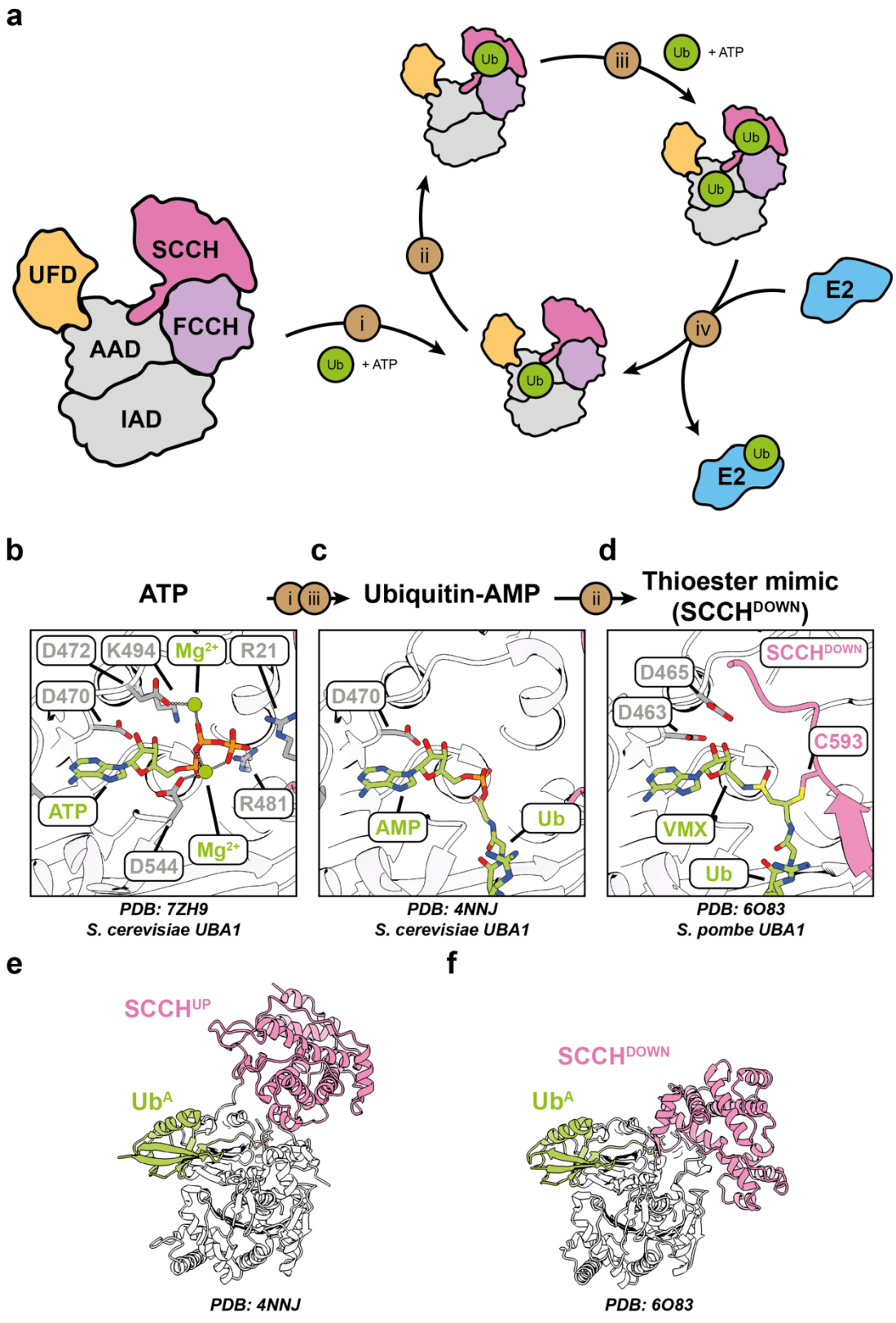
a
UFD
SCCH
FCCH
AAD
IAD
i
Ub
+ ATP
ii
iii
Ub
+ ATP
iv
E2
E2
Ub
b
c
d
ATP
i iii
Ubiquitin-AMP
ii
Thioester mimic
(SCCHDOWN)
D472
K494
Mg2+
R21
D470
ATP
R481
Mg2+
D544
PDB: 7ZH9
S. cerevisiae UBA1
D470
AMP
Ub
PDB: 4NNJ
S. cerevisiae UBA1
SCCHDOWN
D465
D463
C593
VMX
Ub
PDB: 6O83
S. pombe UBA1
e
SCCHUP
UbA
PDB: 4NNJ
f
SCCHDOWN
UbA
PDB: 6O83

Figure 3. Catalytic cycle of ubiquitin activation by E1 enzymes

a. Schematic of the cyclical activation of ubiquitin by E1 enzymes. i) A first ubiquitin molecule is adenylated in an ATP-dependent process. ii) The first ubiquitin is transferred onto the E1 catalytic cysteine. iii) A second ubiquitin molecule is adenylated. iv) An E2 is recruited, and the first ubiquitin is transferred to the E2 through a transthiolation reaction, regenerating a singly loaded E1 complex.

b. Structure of the E1 adenylation site occupied by ATP and Mg^{2+} prior to ubiquitin binding (PDB: 7ZH9[18]).

c. Structure of the E1 adenylation site occupied by the product of the adenylation reaction, ubiquitin AMP (PDB: 4NNJ[19]).

d. Structure of an E1 in a state mimicking thioesterification trapped using VMX-ubiquitin (PDB: 6O83[20]).

e-f. Structures of UBA1 with its SCCH domain in the UP (e, PDB: 4NNJ[19]) and DOWN (f, PDB: 6O83[20]) conformations.

1.1.3. Ubiquitin transthiolation to E2 enzymes

In contrast to the eight E1s, the human genome encodes approximately 39 E2s, 29 of which participate in the ubiquitin cascade. E2s are defined by the presence of a conserved ubiquitin-conjugating (UBC) domain of roughly 150 amino acids, which contains several structural features essential for interactions with both E1s and E3s[21,22] (**Fig. 4a**). The UBC domain adopts a compact α/β-fold, comprising a central four-stranded β-sheet flanked by α-helices, with key protein-protein interaction surfaces contributed by the L2 loop as well as the H1 and H2 helices.

Binding of an E2 to a loaded E1 results in transfer of ubiquitin from the active site cysteine of the E1 onto the active site cysteine of the E2 through a transthiolation reaction (**Fig. 4b**). Crystal structures of the NEDD8 E1 (NAE1-UBA3; NAE1 is also known as APPBP1) alone[23,24] and in complex with UBE2M[25,26] revealed how interactions between the E2 H1 and E1 UFD facilitate initial E2 binding, which is followed by a rotation of the UFD, drawing the E2 into the E1 catalytic site.

Once an E2 has fully entered the E1 catalytic site, nucleophilic attack from the E2 cysteine on the carbonyl of the E1~ubiquitin thioester bond (**Fig. 4c i**) results in the formation of a transient E1-Ub-E2 tetrahedral intermediate (**Fig. 4c ii**), stabilised by active site residues within the E1[27]. This intermediate rapidly collapses, leaving the ubiquitin C-terminus covalently linked to the E2 cysteine, and the loaded E2 is released from the complex (**Fig. 4c iii**).

Given that the transthiolation process is energetically identical in either direction, understanding how the ubiquitin cascade prevents the reverse reaction has long been a topic of interest[13]. It has been shown that E1-E2 transthiolation is coupled to the E1 adenylation site[28,29]. Recent structural data has shown that occupancy of the

adenylation site affects rotation of the E1 SCCH domain and bound E2, positioning the E1 optimally for transthiolation[30]. Consequently, transthiolation is more efficient when the E1 is doubly loaded with ubiquitin. This discourages any reverse transfer of ubiquitin through the cascade, as the ubiquitin-AMP already present at the E1 AAD can be rapidly loaded onto the E1 catalytic cysteine before a loaded E2 approaches. Directionality of transthiolation is also enforced through exclusion of the UBL-loaded product, which will be discussed further in **Chapter 4.1.2**.

In addition to the UBC catalytic core, many E2s contain extensions or insertions in peripheral loops. Such extensions have been shown to have a variety of functions in different E2s, from regulating processivity of ubiquitin chain formation[31–33], substrate selection[34], and recruitment to E3 complexes[35]. While most extensions consist of short, unstructured loops, certain E2s contain an auxiliary folded domain, such as UBE2K and the UBE2Q subfamily. Two E2s, UBE2O and BIRC6, exist as large multidomain proteins, and in these cases the additional domains function as substrate binding modules, allowing these enzymes to bypass an E3 and directly ubiquitinate substrates[36,37]. A comprehensive list of E2 enzymes, including the lengths of N- and C-terminal extensions can be found in **Table 1**.

Once ubiquitin is loaded onto the E2 catalytic cysteine and the E2 is released, the folded ubiquitin domain does not remain bound to the E2 and is instead conformationally dynamic[38]. Nuclear magnetic resonance (NMR) and small-angle X-ray scattering (SAXS) data suggest that the poses available to the thioester linked ubiquitin range from a ‘closed’ conformation resembling the ‘post-transfer’ state in which ubiquitin interacts with the E2 ‘H2’, to a ‘backbent’ conformation where ubiquitin instead interacts with the E2 ‘L5’ loop[38]. The preferred ubiquitin orientation within this distribution differs between E2s[38] and can also be affected by association of E3s[39].

In summary, E1-E2 transthiolation represents a highly coordinated molecular handoff that relies on precise structural alignment and is coupled to the E1 adenylation reaction. This coordination not only ensures efficient ubiquitin transfer but also enforces strict directionality through the cascade, preventing reverse reactions and maintaining processivity. This thesis will focus primarily on the protein-protein interactions formed immediately before and after transthiolation, which are crucial for determining E1-E2 compatibility.

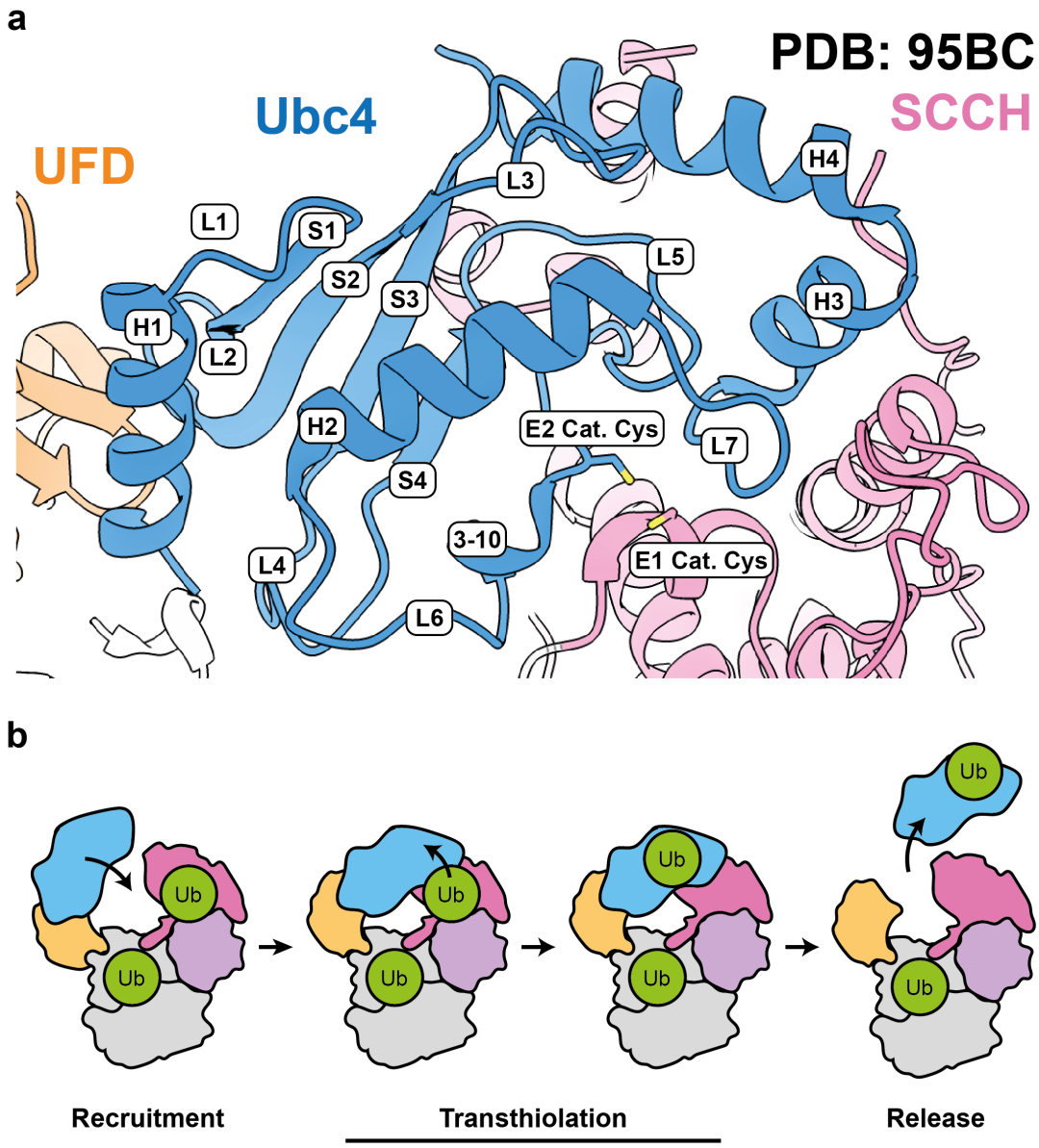
a
PDB: 95BC
Ubc4
SCCH
UFD
L1
S1
S2
S3
L3
H4
L5
H3
H1
L2
H2
E2 Cat. Cys
L7
S4
3-10
L4
E1 Cat. Cys
L6
b
Ub
Recruitment
Transthiolation
Release
c
i) Nucleophilic attack
ii) Tetrahedral intermediate
iii) Product
Ub
O
S
E1
E2

Figure 4. The UBC domain facilitates ubiquitin transthiolation

a. Annotated model of the Ubc4 UBC domain bound to UBA1 (PDB: 9B5C[30])

b. Cartoon overview of the E1-E2 transthiolation reaction.

c. Chemical mechanism for E1-E2 transthiolation, depicting initial nucleophilic attack by the E2 catalytic cysteine (i), formation of the E1-Ub-E2 tetrahedral intermediate (ii), and generation of the E2~Ub thioester product (iiii).

1.1.4. Mechanisms of ubiquitin transfer by E3 enzymes

E3 enzymes facilitate the transfer of ubiquitin from a loaded E2 to a substrate, conferring specificity to the final step of ubiquitination. They are classified into three major classes, Really Interesting New Gene (RING), Homologous to E6AP C-Terminus (HECT), and RING-between-RING (RBR) ligases, distinguished by their mechanisms of action[2].

RING E3s are the most abundant class of E3, and do not contain any inherent catalytic activity[40]. Instead, they act as scaffolds, bringing a ubiquitin-loaded E2 into proximity with a substrate. As a result, the nature of the ubiquitin signal applied to a substrate is decided by the E2, with certain E2s favouring addition of a single ubiquitin to a substrate, such as UBE2W, while others promote ubiquitin chain extension, like the heterodimeric E2 UBE2N/UBE2V which specifically assemble K63-linked ubiquitin chains[41]. RING domain containing proteins, such as those within the Cullin-RING ligase family (including the APC/C), are incorporated into large multi-subunit complexes, allowing for modular assembly of E2 and substrate recognition domains.[42]

The HECT class of E3s are functionally distinct, containing two conserved N- and C-lobes[43]. The N-lobe functions like a RING in that it binds a ubiquitin-loaded E2, however ubiquitin is transferred to a cysteine residue within the HECT C-lobe instead of directly to a substrate. The flexible C-lobe then swings between E2 and substrate to catalyse a second ubiquitin transfer. In contrast to RING E3s, HECT E3s dictate ubiquitin chain topology themselves[2,43].

Finally, RBR E3s unify the mechanisms of both classes described above: their catalytic machinery includes two RING domains, the first of which recruits the ubiquitin-loaded

E2, while the second harbours a catalytic cysteine which receives ubiquitin in a HECT-like intermediate through which substrates are ubiquitinated[44].

In summary, E2-E3 interactions are critical to ubiquitination, with each E3 class engaging E2 enzymes in distinct ways to dictate ubiquitin transfer dynamics and chain architecture. This specificity ensures precise control of substrate modification and signalling outcomes. That the topology of ubiquitin chains formed by RING E3s, the largest E3 class, are dictated by the recruited E2s, reinforces the importance of understanding E2-specific pathways and their initiation by E1s.

1.1.5. Ubiquitin-like protein cascades

Beyond UBA1 and UBA6, the remaining E1 enzymes activate closely related but functionally distinct ubiquitin-like proteins (UBLs)[13]. UBLs share the ubiquitin fold and are conjugated onto substrates through their C-terminus by parallel cascades of enzymes which mirror the ubiquitin system. While the cellular functions of each UBL cascade are not relevant to this thesis, many of the fundamental processes of E1-E2-E3 pathways were first uncovered in the NEDD8 and SUMO systems[13], and they are an invaluable reference point for understanding the ubiquitin pathway.

For example, the E1-E2 specificity is one of the major topics addressed in this thesis. UBL cascades are strictly independent of the ubiquitin machinery, with no cross-reactivity. This separation is maintained at two levels: E1 enzymes are highly specific for which UBLs they can activate; E2 enzymes are specifically recruited to their cognate E1 only. As such, understanding the mechanisms by which the closely related E2 enzymes within UBL cascades select for their cognate E1s is an important starting point for considering specificity within the ubiquitin cascade. These mechanisms are described in detail in **Chapter 3.1.2**.

However, it is also important to appreciate the difference in complexity between UBL cascades and the ubiquitin system. In general, UBL cascades consist of a single E1 enzyme and small number of E2s (**Fig. 5**)[13,45,46]. In contrast, the ubiquitin system, which contains two E1s and 29 E2s, has unique constraints on E1-E2 selection: while UBA1 and UBA6 must display features to exclude unwanted E2s, both enzymes must also remain similar enough to service a shared pool of non-specific E2s.

To summarise, UBL cascades provide a simplified yet instructive context for understanding the principles of E1-E2 specificity. Their strict segregation highlights mechanisms by which selectivity can be achieved while also offering a valuable contrast to the ubiquitin system, where evolutionary pressures have resulted in a more interconnected network.

	Ubiquitin	FAT10	ISG15	SUMO1-3	NEDD8
 E1	UBA1 UBA6	UBA6	UBA7	SAE1-UBA2	NAE1-UBA3
 E2	29	UBE2Z	UBE2L6	UBE2I	UBE2F UBE2M
 E3	> 600	?	2	9	2

Figure 5. Numbers of enzymes in UBL cascades containing canonical E1s

Numbers of proteins were collated from various reviews making similar comparisons[13,45,46].

1.2. Project aims

1.2.1. E1-E2 specificity in the ubiquitin cascade (E2 recruitment)

Aim 1: Catalogue E1 specificity across the ubiquitin-conjugating E2s

In vitro biochemical assays were used to establish a catalogue of E1 specificity across the ubiquitin-conjugating E2 family. Domain-swapped UBA1/UBA6 chimeras were then used to narrow down the exact interfaces driving E1 specificity for each individual E2 enzyme.

Aim 2: Understand the molecular basis for UBA1/UBA6 selectivity

A ubiquitin probe was utilised to stabilise E1-E2 complexes for structural studies. This technique was applied to both UBA6-specific E2s, providing structures of both complexes for the first time, revealing the interactions required for productive E2 recruitment to UBA6.

Aim 3: Generate mutations in E2s which alter E1 specificity

Based on the structural data of UBA6-E2 interactions, mutations were designed to modulate the UBA6 reactivity of selected E2s. In addition, novel functions of UBC domain extensions in regulating E1 specificity were found in the UBE2Q family.

1.2.2. UBA6 and BIRC6 (E2 release)

Aim 1: Characterise the UBA6-BIRC6 interaction

Structural and biophysical characterisation of the UBA6-BIRC6 complex revealed a uniquely strong E1-E2 interaction. The functional consequences of this interaction on E2 competition were then investigated *in vitro*.

Aim 2: Understand the structural features enabling release of BIRC6 from UBA6

Using a combination of biophysical and biochemical assays, thioester switching to promote product release is shown to be required to prevent inhibition of UBA6 by the high affinity interaction with BIRC6. A structural feature within UBA6 which limits the interaction of E2s was identified, removal of which causes potent inhibition of E1-E2 transthiolation by BIRC6.

2. Materials and methods

2.1. Cloning, expression and purification of proteins

2.1.1. Cloning

Expression vectors for recombinant protein expression were assembled from synthesised gene fragments (codon optimised for *E. coli* expression where appropriate), which were amplified by PCR (Q5 polymerase, NEB) and inserted into linearised expression vectors by Gibson assembly (NEB). Site directed mutagenesis was performed by PCR overlap extension using primers containing mutated codons. Chimeric constructs were generated by assembling gene sections from different proteins which were PCR amplified to introduce complementary overhangs. A complete list of expression vectors used for each protein and their associated affinity tags can be found in **Table 2**.

2.1.2. Protein expression in Escherichia coli (E. coli)

Vectors for *E. coli* expression were transformed by heat shock into Rosetta DE3 *E. coli*. Cultures were grown in 2xTY medium supplemented with 34 µg/mL chloramphenicol and 30 µg/mL kanamycin for approximately 5 hours at 30 °C, then induced with 400 µM isopropyl β-D-thiogalactopyranoside at 18 °C overnight. Cells were harvested by centrifugation at 4,000 rpm and stored at -80 °C.

2.1.3. Protein expression in Spodoptera frugiperda (Sf9)

Protein expression in Sf9 was performed following the Bac-to-Bac™ (Thermofisher) protocol: Vectors were transformed by heat shock into DH10Bac cells (Invitrogen) and selected for kanamycin, gentamicin and tetracycline resistance. Bacmids were then

isolated by isopropanol precipitation and transfected using PEI into Sf9 cells to produce initial baculovirus. For each transfection, 90 µg PEI was combined with 30 µg DNA and incubated for 20 minutes at room temperature before adding to a 25 mL Sf9 cells at a density of 0.7 x 10^6 cells/mL. A subsequent passage in a larger volume of Sf9 cells was performed to amplify the virus titre. 1 L cultures of Sf9 cells were then infected using amplified virus and harvested 72 hrs post-infection.

2.1.4. Protein purification from Sf9

E1 enzymes (wild-type, mutants and chimeras), full-length BIRC6 and UBE2O were purified recombinantly from Sf9 (**Table 2**). All buffer compositions are listed in **Table 3**.

Sf9 cell pellets were resuspended in either *Sf9 lysis buffer* or *Nickel A buffer* supplemented with cOmplete protease inhibitor tablets (Roche), 1 µM pepstatin, 2 µM leupeptin, 1 mM PMSF, and 0.5% (v/v) Tween-20. Lysis was then performed through manual homogenization followed by sonication. Cell lysate was clarified by centrifugation at 4,000 rpm for 20 minutes and applied to either Strep-Tactin (GE healthcare) or nickel affinity resin (Takara Bio). Strep-Tactin bound proteins were eluted by incubation with 3C protease, whereas nickel bound proteins were eluted in *Nickel B buffer*. Proteins were then either diluted or dialysed into *Anion exchange buffer A* for purification by anion exchange chromatography (Resource Q, Cytiva) and eluted with a linear gradient up to 1 M NaCl (*Anion exchange buffer B*). Finally, proteins were purified by size exclusion chromatography (SEC) in *SEC buffer*, concentrated (Centrifugal concentrators, Amicon), and flash-frozen in liquid nitrogen for storage.

2.1.5. Protein purification from E. coli

E2 enzymes (including any mutants or chimeras but not full-length BIRC6 and UBE2O) were purified after recombinant expression in *E. coli* (**Table 2**). All buffer compositions are listed in **Table 3**.

E. coli cell pellets were resuspended in *Nickel A buffer* supplemented with protease inhibitors (1 µM pepstatin, 2 µM leupeptin, 1 mM PMSF), DNAse and lysozyme. The cells were lysed by sonication, and the lysate was clarified by centrifugation at 18,000 rpm for 45 minutes. Recombinant proteins were purified using immobilized metal affinity chromatography (IMAC) and eluted in *Nickel B buffer*. Eluted proteins were incubated overnight with SENP1 or 3C protease to cleave affinity tags. Proteins were then either directly purified by SEC (Superdex 75, Cytiva) in *SEC buffer* or (in these cases affinity tag cleavage was performed during overnight dialysis into *Anion/Cation exchange buffer A*), applied to an ion exchange column (Resource Q or S, Cytiva), and eluted with a linear gradient up to 1 M NaCl (*Anion/Cation exchange buffer B*) prior to SEC. Proteins were then concentrated (Centrifugal concentrators, Amicon), and flash-frozen in liquid nitrogen for storage.

2.1.6. Protein purification from E. coli: Ubiquitin variants

Ubiquitin (WT, MC-, G76C) was purified using the acid precipitation method of Pickart and Rassi[47]. All buffer compositions are listed in **Table 3**. Briefly, after lysing *E. coli* cultures as described above, the clarified lysate was dropped to pH 4.0 by dropwise addition of perchloric acid and left stirring for 2-3 hours on ice. The resulting precipitate was pelleted by centrifugation, and the supernatant containing ubiquitin was further purified by cation exchange chromatography (SP, Cytiva) in *SP buffer A* and eluted in 1M NaCl (*SP buffer B*). A final SEC purification in *SEC buffer* was used to further clean the proteins. 1 mM DTT was added to buffers for purification of cysteine-containing

ubiquitin variants to prevent disulfide bond formation. After SEC, proteins were then concentrated (Centrifugal concentrators, Amicon), and flash-frozen in liquid nitrogen for storage.

2.1.7 Fluorescent labelling of ubiquitin

MC-ubiquitin, purified as described above, was reacted in 20 mM HEPES (pH 7.4), 200 mM NaCl with 20-fold molar excess of BDP FL maleimide (Lumiprobe) dissolved in DMSO. The labelling reaction was incubated overnight at 4 °C protected from light, followed by purification of fluorescently labelled ubiquitin from unreacted dye by SEC (Superdex 75, Cytiva) in 20 mM HEPES (pH 7.4), 200 mM NaCl. Fluorescent labelling of ubiquitin was performed by Paul Elliott.

2.2. Transthiolation assays

2.2.1. Multiple turnover reactions

In vitro transthiolation assays were used to observe and quantify ubiquitin transfer to E2 enzymes. In these reactions recombinantly purified E1, E2 and ubiquitin are combined and ubiquitin transfer is initiated by addition of ATP. Reactions were subsequently stopped and analysed by SDS-PAGE. Two methods were used to observe ubiquitin loading: fluorescence imaging when BDP-labelled ubiquitin was used, or Coomassie staining of unlabelled proteins. All quantification was performed using unlabelled ubiquitin so that relative intensities of loaded and unloaded E2 could be compared within each gel lane. Statistical analysis (calculating means, standard deviations, and unpaired *t*-tests) were performed in R.

E1-E2 transthiolation assays were performed at concentrations of 0.5 μM E1, 3 μM E2, 5 μM ubiquitin, 10 mM ATP in buffer containing 40 mM HEPES (pH 7.3), 10 mM

$MgCl_2$ and 0.6 mM DTT. All reactions were stopped at the time points indicated in figure legends after addition of ATP by mixing 1:1 with non-reducing SDS sample buffer. End point reactions were stopped at 5 minutes. Samples were then analysed by SDS-PAGE and Coomassie staining.

The proportion of E2~Ub thioester relative to total E2 within each lane was measured by quantification of Coomassie stained bands in ImageJ. Subsequent data analysis and plotting was performed in R (R version 4.4.0).

2.2.2. E2 competition assays

Single turnover

Single-turnover competition assays were performed with reagents at the concentrations described above (**Chapter 2.2.1.**). Prior to assembling the reaction, E1 was first loaded with ubiquitin for 15 minutes at room temperature, followed by addition of EDTA to a final concentration of 50 mM to prevent further ubiquitin adenylation. E2s were then added to a final concentration of 3 μM per E2 and samples taken at the indicated time points.

C4666A BIRC6 panel

The catalytically inactive BIRC6 (BIRC6 C4666A) competition panel was performed identically to the multiple turnover reactions described above (**Chapter 2.2.1.**), with the addition of 3 μM BIRC6 C4666A to each reaction prior to addition of ATP.

Multiple turnover

Multiple turnover competition assays were performed with reagents at the concentrations described above (**Chapter 2.2.1.**), except for Ubiquitin, which was present at twice the concentration (10 μM). UBE2D2 was kept at 3 μM while competitor

E2s were added at the following concentrations: 0.75, 1.5, 3.0, 4.5, 6.0 μM. After assembling the reactions, ATP was added and end points taken at 5 minutes.

2.3. Ubiquitin dehydroalanine cross-linking

2.3.1. Ubiquitin dehydroalanine probe generation

Purified ubiquitin G76C in 50 mM sodium phosphate (pH 8.0) was mixed with 2,5-dibromohexanediamide (DBHDA, Bio-Techne) solubilized in DMSO at final concentrations of 2 mg/mL ubiquitin and 5.5 mg/mL DBHDA (a 10-fold molar excess of DBHDA to ubiquitin). The reaction was incubated overnight at 37 °C, followed by separation of UbDha from unreacted starting materials by SEC (Superdex 75, Cytiva) in 50 mM $NaPO_4$ (pH 8.0).

2.3.2. E1-E2 cross-linking reaction

E1 (4 μM) was reacted with UbDha (40 μM) overnight in a reaction buffer containing 40 mM HEPES (pH 7.3), 10 mM $MgCl_2$, 0.6 mM DTT, and 10 mM ATP at room temperature. Following this reaction, E2 was added to a final concentration of 10 μM and incubated for 2 hours at room temperature.

To generate a stable mimic of ubiquitin-loaded E2, the UbDha cross-linking reaction was performed as described above, the reaction was diluted in *Anion exchange buffer A*, then DTT was added to a final concentration of 50 mM to reduce any thioester bonds to ubiquitin. E2-UbDha was then separated from the other reaction components by anion exchange chromatography (MonoQ, Cytiva).

2.4. Electron cryomicroscopy

2.4.1. Sample preparation

UBA6-UbDha-BIRC6^{UBC}, UBA6-UbDha-UBE2Z, and dUBA1-UbDha-dBIRC6^{UBC}

E1-UbDha-E2 cross-linking was performed as described above and purified by SEC (Superdex 200, Cytiva). Fractions containing E1-UbDha-E2 complexes were pooled and concentrated to approximately 50 µM (8 mg/mL).

To resolve preferred orientation observed in initial screening trials, all cryoEM samples were supplemented with 0.01% (w/v) fluorinated octyl maltoside immediately prior to vitrification. Vitrification in liquid ethane was performed using an automated plunge-freezing device (Vitrobot IV, Thermo Fisher Scientific) operated at 6 °C and 100% humidity with a blot time of 7 seconds.

UBA6-BIRC6^{UBC}

Non-covalent UBA6-BIRC6^{UBC} complex was generated during optimisation of the UbDha-trapped samples using a batch of UbDha probe with reduced activity. Proteins were mixed at the concentrations described above and the complex was purified by SEC (Superdex 200, Cytiva). Fractions containing both UBA6 coeluting with BIRC6^{UBC} were pooled and concentrated to approximately 50 µM (8 mg/mL). FOM was added to 0.01% (w/v) and then the sample was applied to grids and plunge frozen.

UBA6-BIRC6^{FL}

Non-covalent UBA6-BIRC6^{FL} complex was generated intentionally by combining UBA6 (16 µM) with BIRC6^{FL} (8 µM). FOM was added to 0.01% (w/v) and then the sample was applied to grids and plunge frozen.

2.4.2. Data collection

Preliminary grid screening was performed on a Talos Arctica microscope (Thermo Fisher Scientific, COSMIC facility) to assess sample quality. High resolution datasets

were collected on Titan Krios G3 instruments (Thermo Fisher Scientific, located at the eBIC and COSMIC cryoEM facilities) with Gatan BioQuantum image filters (20 eV slit width) and Gatan K3 direct electron detectors. Additional data collection parameters are described in Tables 4-6. The UBA6-BIRC6^{FL} dataset was collected on a Talos Arctica (Thermo Fischer Scientific) instrument located at the COSMIC cryoEM facility.

2.4.3. Data processing

UBA6-UbDha-BIRC6^{UBC}, UBA6-UbDha-UBE2Z, and dUBA1-UbDha-dBIRC6^{UBC}

Preprocessing (motion correction, CTF estimation and template picking) for the UBA6-UbDha-BIRC6^{UBC}, UBA6-UbDha-UBE2Z, and dUBA1-UbDha-dBIRC6^{UBC} datasets was performed in SIMPLE v3.3.070[48]. Volumes for template-based picking were derived from low resolution maps from initial grid screening. Particles for all datasets were then cleaned in cryoSPARC v4.4[49] using 2D classification and heterogeneous refinement. The UBA6-UbDha-BIRC6^{UBC} complex was found both singly and doubly loaded with ubiquitin. The singly loaded state was refined directly in cryoSPARC v4.4[49] to produce a consensus map without further processing. The doubly loaded state was exported to RELION v5.0[50,51], further cleaned by 3D classification and subjected to Bayesian polishing and CTF refinement before a final non-uniform refinement in cryoSPARC v4.4[49].

The UBA6-UbDha-UBE2Z complex was only found in the singly loaded state. Particles for this class were exported to RELION v5.0[50,51] for polishing and CTF refinement and finally refined in cryoSPARC v4.4[49].

The dUBA1-UbDha-dBIRC6^{UBC} complex was only found in the doubly loaded state. Particles for this class were exported to RELION v5.0[50,51] for polishing and CTF refinement and finally refined in cryoSPARC v4.4[49].

UBA6-BIRC6^{UBC}

Preprocessing (MotionCor2[52], CTFFind4[53] and crYOLO[54] particle picking) for the UBA6-BIRC6^{UBC} dataset was performed using the PATo on-the-fly processing interface available at eBIC[55]. Downstream processing was done in cryoSPARC v4.4[49]. The particles were initially cleaned by two rounds of 2D classification. Ab-initio model generation and heterogeneous refinement followed by 3D classification was then used to identify three states within the dataset (UBA6^{APO}, UBA6-BIRC6^{UBC-IN} and UBA6-BIRC6$^{UBC-OUT}$). These classes were then refined independently using non-uniform refinement to produce consensus maps.

UBA6-BIRC6^{FL}

Preprocessing (motion correction, CTF estimation and template picking) for the UBA6-BIRC6^{FL} dataset was performed in cryoSPARC v4.4[49]. UBA6 particles were cleaned by 2D classification, then APO and BIRC6-bound classes were separated by focused 3D classification. BIRC6 particles were cleaned by 2D classification, then refined to a consensus map using homogeneous refinement with C2 symmetry relaxation applied.

2.4.4. Model building and refinement

Initial models for all proteins were produced in AlphaFold[56], except for ubiquitin adenylate, which was derived from PDB 9B5C[30]. Models were initially refined using ISOLDE[57], followed by multiple rounds of real-space refinement in Phenix v1.21.2[58] and manual editing in COOT v0.9.8.92m[59].

2.4.4. Particle 3D variability analysis

3D variability analysis within particle stacks from the *UBA6-UbDha-BIRC6^{UBC}, dUBA1-UbDha-dBIRC6^{UBC},* and *UBA6-BIRC6^{UBC}* datasets were performed by the same

method in cryoSPARC v4.4[60]. First, consensus particle stacks were generated for each state using 3D classification tools. The particle stacks were then analysed by principal component analysis using the 3D variability analysis tool in cryoSPARC with the filter resolution set to 4 Å. Particles were then clustered into 5 groups along the primary component by the 3D variability display tool set to cluster mode. Particles within clusters at extreme ends of each component were then refined independently.

2.4.5. Particle distance analysis

Distances between particles in the UBA6-BIRC6FL dataset were analysed using a custom script written in R (R version 4.4.0). Briefly, particles from each class (UBA6^{APO}, UBA6-BIRC6^{FL} and BIRC6^{FL}) were exported into separate star files, from which particle coordinates within each micrograph were extracted. For every micrograph, the nearest BIRC6 particle was found for each UBA6 particle, and the distance was recorded. This process was repeated for UBA6 particles in UBA6^{APO} and UBA6-BIRC6^{FL} stacks. To generate synthetic particle locations for comparison, random coordinates were generated for UBA6 (equal to UBA6^{APO} + UBA6-BIRC6^{FL}) and BIRC6 particles and distributed over the same number of micrographs. The same distance analysis algorithm was then repeated for the synthetic data.

Histograms of the calculated distances for each particle group were then plotted in R (R version 4.4.0).

2.5. Analysis of protein-protein interactions

2.5.1. Analytical size exclusion chromatography

Analytical SEC of UBA6-BIRC6^{UBC}, UBA1-BIRC6^{UBC}, UBA6-UBE2D2, UBA6-UBE2Z, UBA1-dBIRC6^{UBC} and UBA6-dBIRC6^{UBC} interactions were performed by combining

E1 and E2 proteins at concentrations of 10 µM each in 20 mM HEPES pH 7.5, 200 mM NaCl and 4 mM DTT and injecting into a Superdex 200 Increase 3.2/300 column (Cytiva). For analysis of the dUBA1-dBIRC6^{UBC} interaction, proteins were combined at 5 µM in the same buffer and the sample was applied to a Superdex 200 10/300 column (Cytiva). Selected fractions from each run were mixed with SDS sample buffer and analysed by SDS-PAGE and Coomassie staining.

2.5.2. Fluorescence polarisation (FP)

Cy5-labelling of E2s was performed in a buffer containing 20 mM HEPES pH 7.8, 200 mM NaCl, 2 mM DTT. E2s were incubated with an eight-fold molar excess of sulfo-Cyanine5 (Cy5) N-Hydroxysuccinimide (NHS) ester (Lumiprobe) at room temperature for 2 hours. The reaction was quenched with 1M Tris pH 8.5, and Cy5-labelled proteins were separated from unreacted Cy5 via SEC (Superdex 75, Cytiva) and flash-frozen in liquid nitrogen.

FP assays were performed on a Clariostar plate reader (BMG Labtech) using 635 (20) nm and 680 (20) nm excitation and emission channels, respectively. Serial dilutions of UBA6 variants were prepared in FP buffer: 20 mM HEPES pH 7.5, 150 mM NaCl, 5 mM DTT, 0.05 % (w/v) CHAPS and 0.04 mg mL-1 BSA and pipetted into a 384-well black low binding plate (Corning) containing a final concentration of 15 nM Cy5 labelled-E2 variants. All graphs are representative of at least three independent repeats performed in technical triplicate. Data were plotted and fitted in GraphPad Prism 9 using the equation for specific binding: $Y = B_{max} * X / (X + K_d)$. Initial optimisation of E2 labelling and FP assay setup were performed by Carlos Riechmann. Final FP measurements and repeats were performed by Paul Elliott.

3. E1-E2 specificity in the ubiquitin cascade

3.1. Introduction

3.1.1. UBA1 and UBA6

Humans, among other higher eukaryotes, have two genes encoding E1 enzymes that activate ubiquitin, UBA1 and UBA6[61–63]. Of these, UBA1 is the predominant E1 and is responsible for most of the ubiquitination events in cells[64,65]. Consequently, UBA6 was discovered later[61–63] and less is known about the pathways it regulates.

UBA1 and UBA6 share the canonical multidomain E1 fold and activate ubiquitin through the same mechanism[20,66]. They are broadly well conserved (overall 42% identity, **Fig. 6a, b**). Nevertheless, subtle differences are present throughout their structures, the most striking functional consequence of which allows UBA6 to bind and activate a second UBL, FAT10, in addition to ubiquitin[18,66] (**Fig. 6c, d**).

While UBA1 mRNA transcripts and protein levels are approximately 10 times as abundant as for UBA6[63,67], both E1s are expressed across all tissues[63], highlighting their broad roles in essential cell functions. Indeed, while UBA1 has long been known to be an essential gene for eukaryotic cell survival[64,65], UBA6 has also been shown to be required for embryonic development[62].

Growing evidence points towards UBA1 and UBA6 serving independent ubiquitination cascades within the cell[63,68]. Knockout of UBA1 cannot be compensated by UBA6 and is therefore lethal[64,65,69]. This is further supported by the recent discovery of Vacuole, E1 enzyme, X-linked, Autoinflammatory, Somatic (VEXAS) syndrome[70]. VEXAS syndrome is caused by mutations effecting UBA1 in certain somatic cell types where partial loss of UBA1 activity can be tolerated (robust UBA1 activity is essential for most

cells). The disease is caused by either mutation of the alternative UBA1 start site used to produce cytosolic UBA1, which instead causes the production of a shortened, inactive cytosolic isoform of the protein through a third start site (normally not produced in healthy cells)[70], or various other activity-reducing amino acid substitutions throughout the E1[71]. The effects of these mutations result in loss of cytosolic ubiquitination, upregulation of the unfolded protein response, and proteotoxic stress[70]. The effects of this disease highlight how even partial loss of UBA1 activity, as found in in the less disruptive VEXAS mutations, cannot be compensated by UBA6[71].

For UBA6, knockout of the gene is embryonically lethal in mice[62] and can cause loss of viability in cell culture[72]. Neuron-specific loss of UBA6 in mice has been associated with pathologies in brain development, leading to impaired social interaction, learning defects and memory issues[73]. These effects can be attributed to loss of UBA6 ubiquitination specifically, as mice lacking the second UBL activated by UBA6, FAT10, are healthy[74,75]. As such, each ubiquitin E1 supplies ubiquitin to essential pathways which are not compensated by the remaining E1 when either UBA1/UBA6 is removed.

In 2017, Liu *et al.* began untangling the pathways downstream from UBA1 and UBA6 by expressing engineered orthogonal UBA1 and UBA6 ubiquitin systems in cells[68]. Their proteomic analysis revealed 269 UBA1-specific, 439 UBA6-specific and 258 shared substrates. While limitations of mass-spectrometry methods mean that their results likely do not encompass the full range of substrates targeted by the ubiquitin pathway, this paper established an important step towards the identification of E1-specific cascades. They followed up this analysis by validating CUGBP1 and ezrin as bona-fide UBA6-specific substrates with distinct cellular phenotypes by knockdown of UBA6 and, importantly, the UBA6-specific E2 UBE2Z[68].

All E1-specific ubiquitination pathways must necessarily pass through an E1-specific E2 enzyme (and an E3 enzyme independent of the other E1, **Fig. 6e**). As a result, a thorough understanding of the rules governing E1-E2 specificity is required for any further work targeting ubiquitination pathways affecting a given substrate. Since the discovery of UBA6, profiling the E1-specificity of ubiquitin E2s has been a priority, from initial *in vitro* screens[62,63] to later proteomic studies[68]. A pattern has emerged from these studies, in that the majority of E2s either work specifically downstream of UBA1, or non-specifically with both E1s[63,68]. In fact, only two UBA6-specific E2s have been identified, UBE2Z[62,63,68] and BIRC6[68,76–78]. However, the molecular basis governing how E2s in the ubiquitin system achieve specificity for either UBA1 or UBA6 is not yet understood.

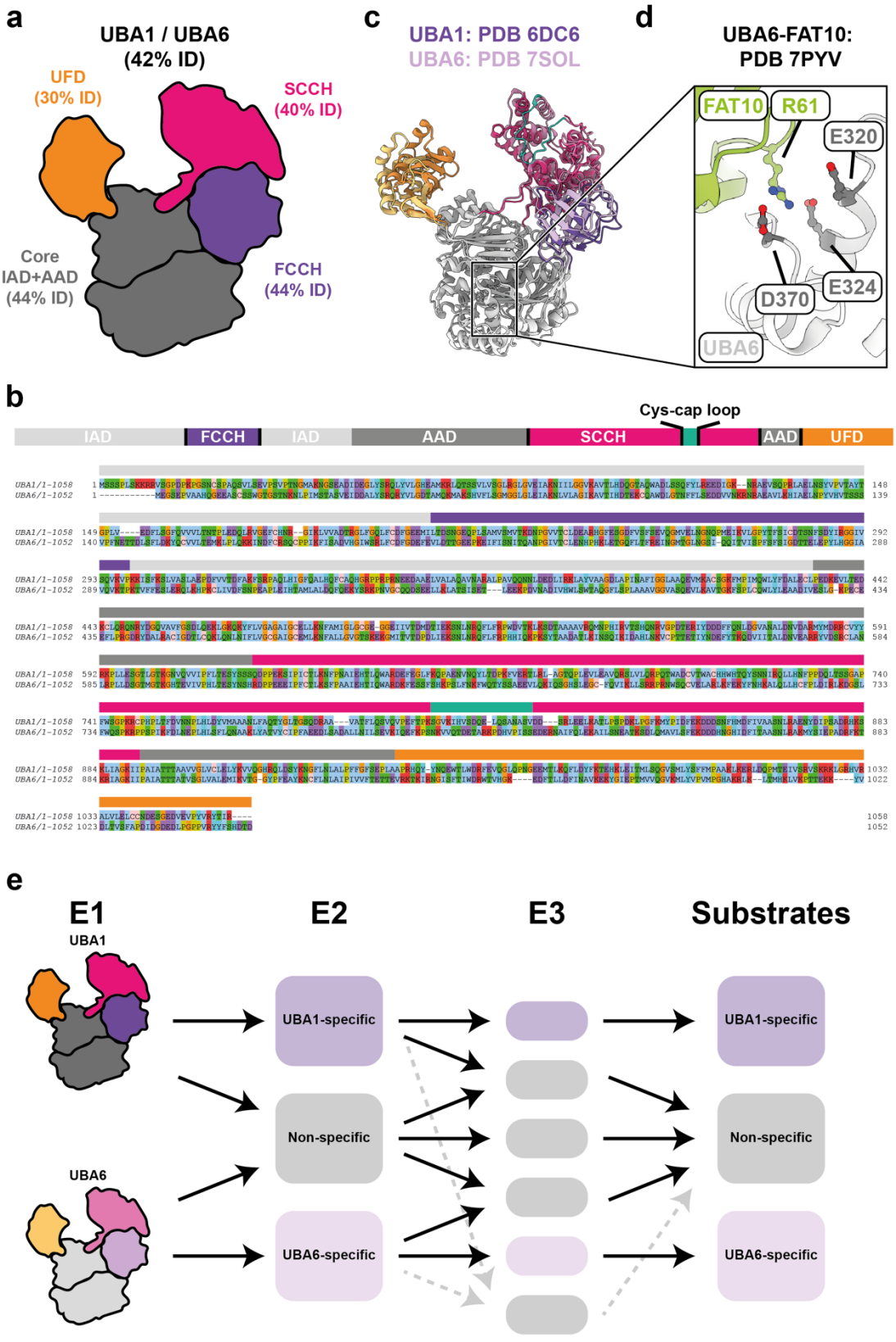
a
UBA1 / UBA6
(42% ID)
UFD
(30% ID)
SCCH
(40% ID)
Core
IAD+AAD
(44% ID)
FCCH
(44% ID)
c
UBA1: PDB 6DC6
UBA6: PDB 7SOL
d
UBA6-FAT10:
PDB 7PYV
FAT10
R61
E320
D370
E324
UBA6
b
Cys-cap loop
IAD
FCCH
IAD
AAD
SCCH
AAD
UFD
e
E1
E2
E3
Substrates
UBA1
UBA6
UBA1-specific
Non-specific
UBA6-specific
UBA1-specific
Non-specific
UBA6-specific

Figure 6. Structural comparison of UBA1 and UBA6

a. Cartoon of E1 domain architecture with each domain annotated with the respective sequence identity between UBA1 and UBA6.

b. Alignment of UBA1 and UBA6 sequences with domains annotated.

c. Alignment of UBA1[16] and UBA6[66] crystal structures.

d. Close-up view of the UBA6-specific FAT10 binding site within the IAD from a FAT10-bound crystal structure of UBA6[18].

e. Schematic showing how specificity of components in the ubiquitin cascade may lead to independent regulation of substrates by UBA1 and UBA6.

3.1.2. E1-E2 specificity in UBL cascades

While E1-E2 specificity within the ubiquitin cascade is not yet understood, much more is known regarding parallel UBL cascades. E2s have exquisite specificity for their cognate E1s, which is necessary to avoid mischarging E2s with the incorrect UBL. Structural and biochemical studies have shown that this specificity is achieved at the earliest stage of E1-E2 interaction, during E2 recruitment by the E1 UFD. Each UFD contains unique features which are recognised by complementary interactions within the H1 and L2 motifs of cognate E2s (**Fig. 7a-d**).

Specificity in the NEDD8 system is enforced by several interactions throughout the UFD interface. L32 of UBE2M is directed towards a hydrophobic patch containing residue A424 of UBA3[26] (**Fig. 7b**). Ubiquitin E2s tend to contain arginine or lysine in this position (K4 in UBE2D/Ubc4), and the UBA1 UFD correspondingly contains a glutamic acid (E992 in *S. pombe*) in place of UBA3's A424, which would be incompatible with UBE2M binding (**Fig. 7a**). Furthermore, the 'H1' helix of UBE2M is one turn shorter than those found in most other E2s, which allows UBE2M to avoid clashes to an extension of the NAE1-UBA3 UFD which would otherwise prevent E2 recruitment[26] (**Fig. 7e**).

Similar comparisons can be made for the ISG15-specific E2 UBE2L6 and its E1, UBA7. K9 of UBE2L6 forms a salt bridge with D999 and S995 in UBA7 (**Fig. 7c**), the latter of which is replaced by M994 in UBA1[79,80] (**Fig. 7a**). This interaction is in part mediated by an acidic loop in the UBA7 UFD which wraps around the UBE2L6 'H1'[80], a conformation not seen in UBA1 and UBA6. Like UBE2M, UBE2L6 also contains an uncharged residue (M5) in place of the UBE2D K4, which inserts directly the UFD interface, forming hydrophobic interactions with I945 and L947 of UBA7 (**Fig. 7c**).

How do the ubiquitin E1s compare to these parallel UBL systems? The UBA1 and UBA6 UFDs do not contain such striking features as the UBA3 extension and UBA7 acidic loop. As noted by previous analysis of the UFD sequences[63], there are slight differences across the E2 binding surfaces: human UBA1 has negatively charged residues E992 and E1004 in place of T1025 and P1039 in UBA6; UBA6 contains bulkier hydrophobic residues in positions V987 and M992 (corresponding to S946 and L951 in *S. pombe* UBA1, respectively) (**Fig. 7a, d**). However, assessing the consequences of these residues on E2 interactions is challenging, as no structures of E2s bound to UBA6 have yet been solved.

Beyond the UFD interface, UBE2M has been shown to use additional interactions to prevent reactivity with UBA1. Alanine scanning revealed two charged sidechains facing the SCCH interface, which when removed, enhanced ubiquitin loading on UBE2M[81] (**Fig. 7e**). In addition, UBE2M also contains a 26-residue N-terminal extension which binds to a dedicated groove below the UFD of NAE1-UBA3. This interaction is required to achieve robust recruitment of UBE2M[17] and discourages binding to UBA1, which does not have an equivalent groove[81].

Together, these findings illustrate how E1-E2 specificity in parallel UBL cascades is driven by a network of finely tuned structural features, with UFD-H1 complementarity forming the foundation of selectivity. While the NEDD8 and ISG15 systems rely on distinctive elements such as the UBA3 extension, UBA7 acidic loop, and accessory N-terminal motifs of their cognate E2s, ubiquitin E1s appear to employ subtler variations that remain less well understood. The following chapter aims to address this important issue by providing a structural basis for UBA1/UBA6 selectivity across the ubiquitin E2s.

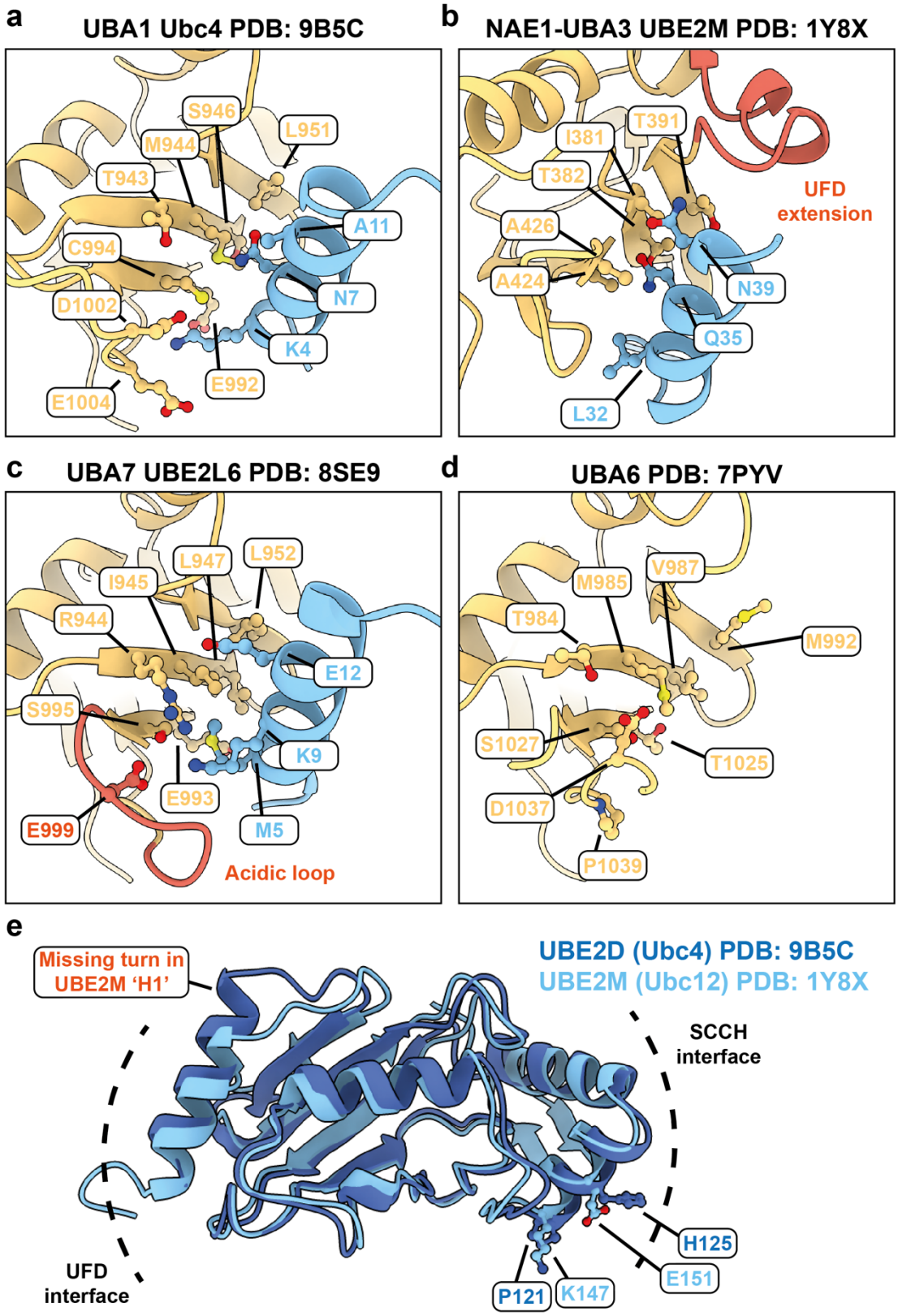
a
UBA1 Ubc4 PDB: 9B5C
S946
L951
M944
T943
A11
C994
N7
D1002
K4
E992
E1004
b
NAE1-UBA3 UBE2M PDB: 1Y8X
T391
I381
T382
UFD
extension
A426
A424
N39
Q35
L32
c
UBA7 UBE2L6 PDB: 8SE9
L947
L952
I945
R944
E12
S995
K9
E993
E999
M5
Acidic loop
d
UBA6 PDB: 7PYV
V987
M985
T984
M992
S1027
T1025
D1037
P1039
e
Missing turn in
UBE2M 'H1'
UBE2D (Ubc4) PDB: 9B5C
UBE2M (Ubc12) PDB: 1Y8X
SCCH
interface
UFD
interface
H125
E151
P121
K147

Figure 7. Mechanisms of E1-E2 specificity in UBL cascades

a-d. Atomic models of E1 UFDs bound to their cognate E2s (where available). Residues lining the E1-E2 interface are annotated, and E1-specific features are highlighted in red.

e. Alignment of Ubc4 and UBE2M atomic models. Regions contacting the E1 UFD and SCCH domains are indicated with dashed lines. Key differences between the E2s are annotated: UBE2M has a shorter ‘H1’ and additional charged residues at the SCCH interface.

3.2. Results

3.2.1. Generating a panel of human ubiquitin E2 enzymes

To begin our investigation into E1-E2 specificity, generated a panel of recombinantly purified E2s was generated. E2s which activate other UBL proteins (UBE2F, UBE2I, UBE2L6, UBE2M, ATG10, ATG3), the catalytically inactive UBE2NL, and the UBE2N-associated UBE2V subfamily were excluded to focus the panel on active ubiquitin-conjugating enzymes.

While most E2s could be readily purified as full-length constructs, alterations were made to certain enzymes to improve protein expression: the C-terminal transmembrane helices from UBE2J1 and UBE2J2 were removed, as was the unstructured C-terminal extension to UBE2U. While UBE2Q1 and UBE2Q2 could be readily expressed, soluble protein for the final member of the UBE2Q sub-family UBE2QL could not be obtained. The largest E2s (UBE2O and BIRC6) required expression in Sf9 cells. A general strategy of affinity capture followed by ion exchange chromatography and size exclusion chromatography was used for purification of all selected E2 constructs (see Methods, **Table 2**).

3.2.2. E1 reactivity profile across the E2 panel

After assembling the panel of E2 constructs, E2s were then tested for their ability to receive ubiquitin from UBA1 and UBA6 during *in vitro* E1-E2 transthiolation assays. First, E2s were qualitatively assessed for UBA1/UBA6 charging by observing transfer of fluorescently labelled ubiquitin (**Fig. 8a**). Next, the proportion of E2 loading was quantified using Coomassie staining of equivalent transthiolation reactions performed using unlabelled ubiquitin (**Fig. 8b**).

All the purified E2s showed activity with at least one E1, confirming that our purified enzymes were active. Some E2s clearly showed a difference in activity between UBA1 and UBA6, so to further aid comparison, the percentage of E2~Ub thioester formed was quantified by analysis of coomassie-stained gels (**Fig. 8b**).

To aid further analysis, the E2s were then classified depending on E1 specificity. While preference for UBA1 over UBA6 exists along a continuum, a fourfold activity difference between E1s was applied as a threshold to define classes of E1 specificity. This corresponds to an empirical limit for manual observation of Coomassie stained E2~Ub bands in the assay, as for E2s such as UBE2A loading with UBA6 was only just visible by eye (**Appendix Figures 1, 2**).

14 E2s exhibited specificity for UBA1, two for UBA6 and the remaining 13 non-specific E2s showed activity with both E1s (**Fig. 8c**). In some cases, specificity was preserved across members of the same E2 subfamily, such as the UBA1-specific UBE2E1-3 (84% lowest pairwise identity), and the non-specific UBE2D1-4 (88% lowest pairwise identity). Interestingly, this was not always the case: the UBE2G and UBE2J subfamilies each consist of two members, only one of which is UBA1-specific while the other is non-specific. While E2s within the UBE2G/J subfamilies are less well conserved (50% and 33% pairwise identity respectively), these results still suggest that subtle differences can be sufficient to alter E1 specificity of an E2 and simple phylogenetic clustering of whole E2 sequences is not sufficient to group E2s by specificity (**Fig. 8b**, top).

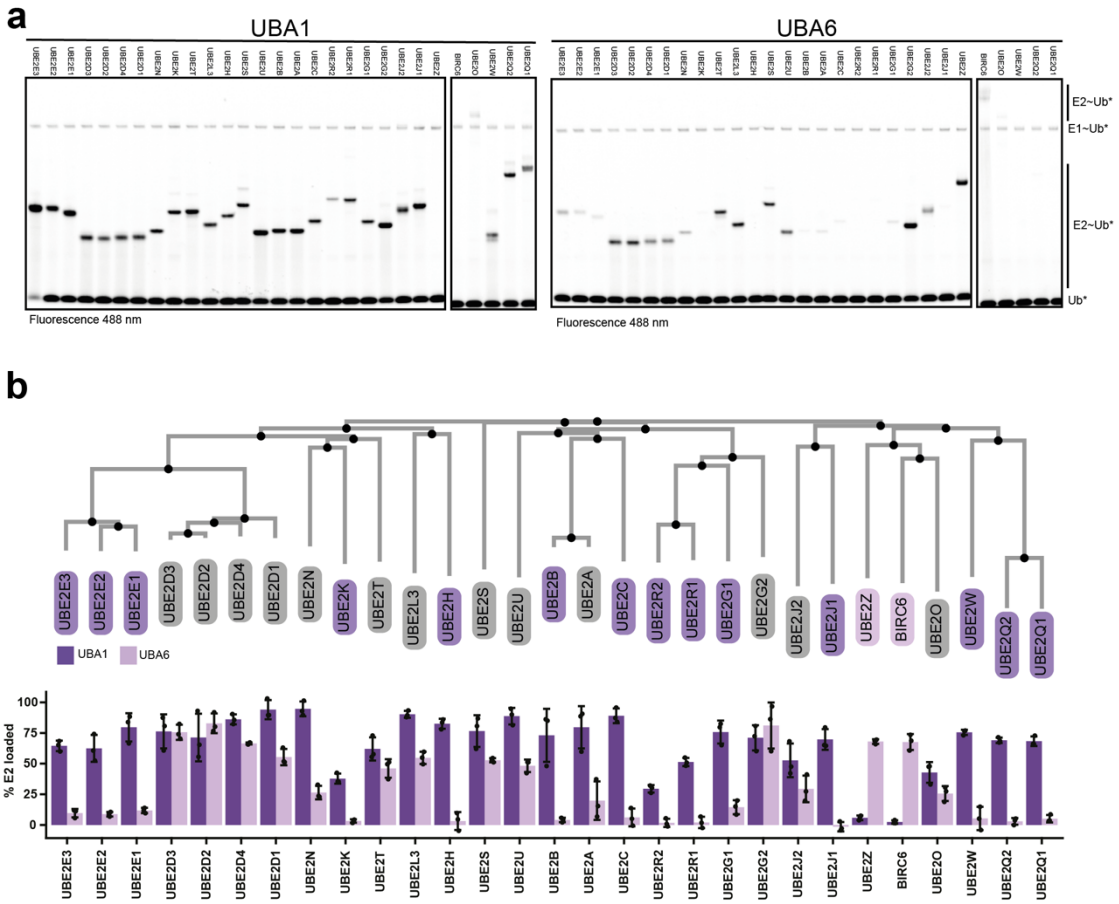

UBA1-specific (14)		Non-specific (13)		UBA6-specific (2)
UBE2B	UBE2J1	UBE2A	UBE2L3	UBE2Z
UBE2C	UBE2K	UBE2D1	UBE2N	BIRC6
UBE2E1	UBE2Q1	UBE2D2	UBE2O	
UBE2E2	UBE2Q2	UBE2D3	UBE2S	
UBE2E3	UBE2R1	UBE2D4	UBE2T	
UBE2G1	UBE2R2	UBE2G2	UBE2U	
UBE2H	UBE2W	UBE2J2		

Figure 8. E1 reactivity profile across the E2 panel

a. SDS-PAGE analysis of i*n vitro* transthiolation reactions for all human E2s in the presence of either UBA1 (left) or UBA6 (right). The assay was performed with fluorescently labelled ubiquitin, and a fluorescence image showing labelled ubiquitin (Ub*) loading onto each human E2 is shown. Fluorescent bands not attributed to free ubiquitin or E1~Ub* thioester indicate the formation of E2~Ub* thioester. Some lanes contain additional bands due to E2 autoubiquitination.

b. Phylogenetic tree of aligned E2 sequences (top). Proportion of loaded E2 (E2~Ub) formed by each human E2 in the presence of UBA1 or UBA6, measured by Coomassie stained SDS-PAGE analysis of 5-minute transthiolation assays (representative gel panels shown in **Fig. 9b,** all unprocessed gels in **Appendix Figures 1, 2**) (bottom). Due to low activity, the assay duration was extended to 30 minutes for UBE2K. Quantification was performed across three technical repeats, and the plot displays the mean ± standard deviation.

c. Classification of E1 specificity across the E2 panel. Relative E1 activity was calculated by dividing the absolute values of the proportion of E2 loaded with UBA1 by the proportion loaded with UBA6, then plotted on a log scale (top). E2s with UBA1/UBA6 activities within a 4-fold range were classified as non-specific. E1 specificities are summarised in a table (bottom).

3.2.3. E1 domain specificity across the E2 panel

While our initial panel demonstrated the E1 preference for each E2, it did not tell us which E1 features were required to drive specificity. To investigate this, a series of E1 chimeras were generated in which the SCCH and UFD domains were exchanged between UBA1/UBA6 (**Fig. 9a**). Each E2 from the panel was then tested for activity using each of the chimeric E1s, and classified according to which chimeras they were able to receive ubiquitin from (**Fig. 9b**).

Non-specific E2 enzymes

The majority of non-specific E2s showed activity with all the domain-swapped chimeras, demonstrating the compatibility of these enzymes with both variants of the SCCH and UFD domains and validating the activity of the chimeric E1s. Interestingly, five non-specific E2s lost activity with the chimeras. This suggests that for some (but not all) E2s, recruitment by the UFDs of UBA1/UBA6 is not equivalent and would therefore not necessarily grant activity with the SCCH of another E1.

UBA1-specific E2 enzymes

Transthiolation activity tracked directly with the identity of the UFD for eight of the UBA1-specific E2s. This remained consistent within the E1-specific E2 subfamilies, suggesting conserved specificity mechanisms within E2 groups (e.g. UFD recognition drives specificity for all UBE2E subfamily members). Of the remaining UBA1-specific E2s, four depended on both domains for activity, suggesting that features within the SCCH can also determine specificity among ubiquitin E2s. The final two E2s displayed a more complicated pattern, possibly due to these E2s depending on additional interfaces outside of the domains swapped in our chimeras.

UBA6-specific E2 enzymes

Surprisingly, the two UBA6-specific E2s use different strategies to achieve E1 specificity. BIRC6 (both as the full-length protein and when truncated to the catalytic domain) mirrored the more sensitive UBA1-specific enzymes, requiring both SCCH and UFD domains for robust activity. On the other hand, and uniquely across all E2s, UBE2Z activity tracked with the SCCH domain alone.

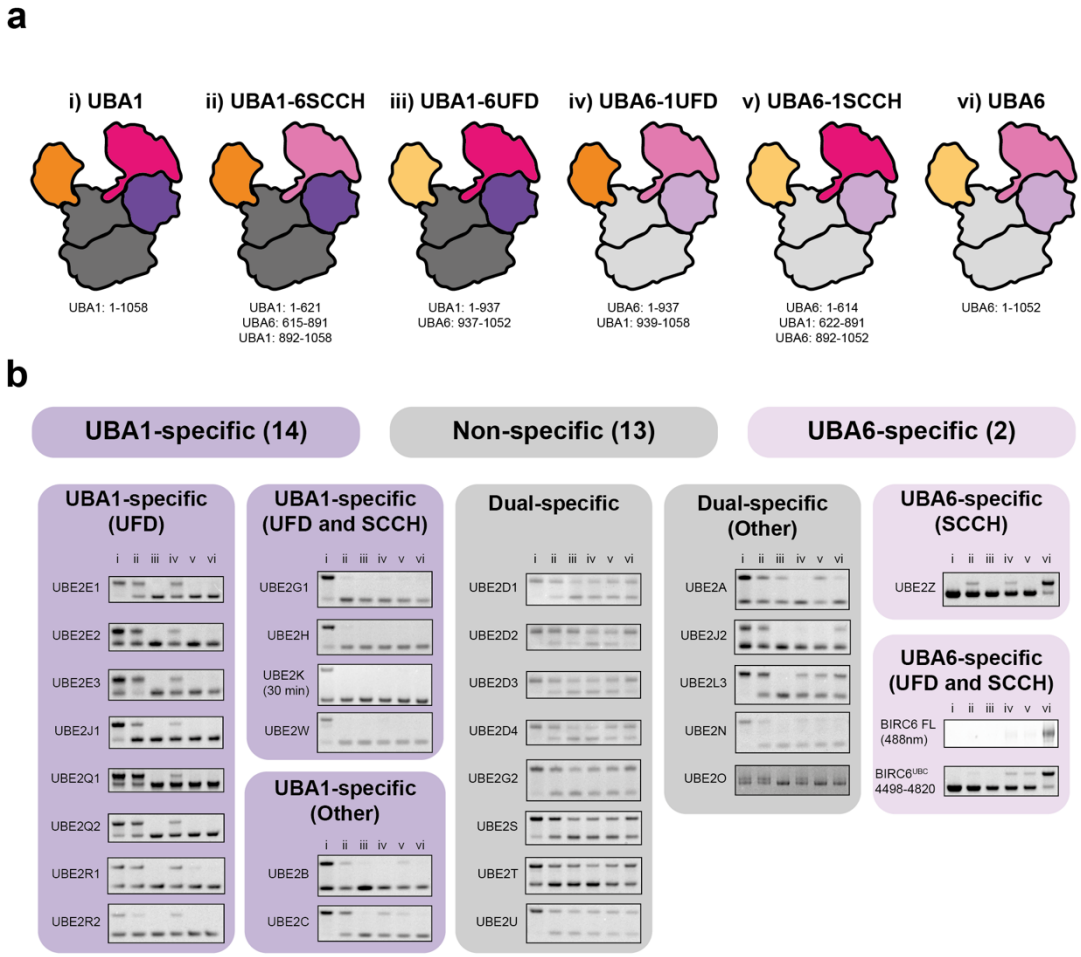
a
i) UBA1
ii) UBA1-6SCCH
iii) UBA1-6UFD
iv) UBA6-1UFD
v) UBA6-1SCCH
vi) UBA6
UBA1: 1-1058
UBA1: 1-621
UBA6: 615-891
UBA1: 892-1058
UBA1: 1-937
UBA6: 937-1052
UBA6: 1-937
UBA1: 939-1058
UBA6: 1-614
UBA1: 622-891
UBA6: 892-1052
UBA6: 1-1052
b
UBA1-specific (14)
Non-specific (13)
UBA6-specific (2)
UBA1-specific (UFD)
UBA1-specific (UFD and SCCH)
Dual-specific
Dual-specific (Other)
UBA6-specific (SCCH)
UBA6-specific (UFD and SCCH)
UBA1-specific (Other)
i ii iii iv v vi
UBE2E1
UBE2E2
UBE2E3
UBE2J1
UBE2Q1
UBE2Q2
UBE2R1
UBE2R2
UBE2G1
UBE2H
UBE2K (30 min)
UBE2W
UBE2D1
UBE2D2
UBE2D3
UBE2D4
UBE2G2
UBE2S
UBE2T
UBE2U
UBE2A
UBE2J2
UBE2L3
UBE2N
UBE2O
UBE2Z
BIRC6 FL (488nm)
BIRC6UBC 4498-4820
UBE2B
UBE2C

Figure 9. Classifying E1 domain specificity across E2 enzymes

a. Cartoons and amino acid boundaries for the UBA1/UBA6 chimeras.

b. Classification of all human ubiquitin E2 enzymes based on their activity pattern with the E1 chimeras. E2 loading was assessed by imaging Coomassie stained transthiolation reactions (in technical triplicate) using unlabelled ubiquitin, except for full-length BIRC6, which is too large to observe a mobility shift upon ubiquitin loading and so fluorescent ubiquitin was used instead. The E1 chimera specificity for full-length BIRC6, observed with fluorescent ubiquitin, agreed well with that for the isolated UBC domain, observed with Coomassie stained unlabelled ubiquitin. All unprocessed gels are included in **Appendix Figures 1, 2**.

3.2.4. Strategy to stabilise E1-E2 complexes

Ubiquitin E1-E2 complexes rapidly dissociate and therefore require chemical methods such as cross-linking by probes to stabilise interactions for structural studies[27,30,82,83]. A previously reported ubiquitin-dehydroalanine (UbDha) probe was chosen for use in this study[84].

UbDha consists of a ubiquitin molecule in which the final glycine is replaced by a reactive dehydroalanine residue, resulting in a probe containing an additional reactive group near the carboxyl-terminus (**Fig. 10a**). When mixed with a ubiquitin ligase, the incoming nucleophile from the E1/E2 can either attack the Dha sidechain or the C-terminus (**Fig. 10b**). If the UbDha probe reacts first through its carboxyl terminus with the E1 (**Fig. 10b**, 2), and then through its dehydroalanine sidechain to the E2 (**Fig. 10b**, 3), UbDha forms a covalent cross-link between E1 and E2 enzymes, stabilising their interaction in a conformation closely resembling the native tetrahedral intermediate. This pathway was outlined as an undesired side product in the first paper to use the UbDha probe[84]. In addition, mutation of the E1 catalytic cysteine to serine was reported to further stabilise the UbDha crosslink, so this mutation was introduced into UBA6 for the reactions.

UbDha synthesised in-house from recombinantly purified ubiquitin G76C cross-linked UBA6 C625S readily to both BIRC6 and UBE2Z, and the complex could be partially separated from unreacted species by gel filtration (**Fig. 10c-d**). Due to difficulties handling full-length BIRC6, cross-linking was performed with a shortened BIRC6 construct containing only the catalytic UBC domain (amino acids 4498-4820, $BIRC6^{UBC}$), which demonstrated the same E1 specificity as the full-length construct in our E1 chimera panel (**Fig. 9b**).

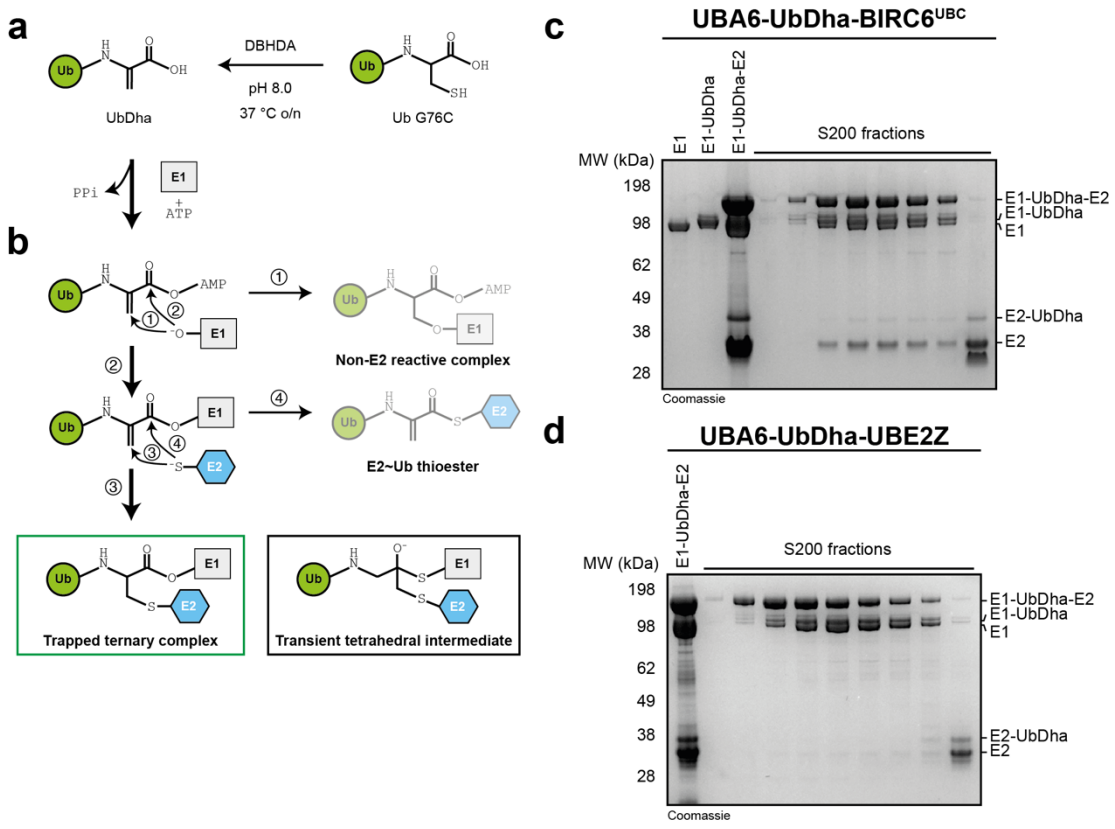

Figure 10. UbDha cross-links UBA6 to BIRC6^{UBC} and UBE2Z

a. Reaction to generate the UbDha probe.

b. Scheme for the UbDha cross-linking reaction between E1 and E2 enzymes. The E1 nucleophile attacks either (1) the Dha sidechain, generating a UbDha-E1 adduct, or (2) the C-terminus of UbDha. After reaction (2), the E2 nucleophile can again attack either (3) the Dha sidechain, generating the cross-linked E1-UbDha-E2 ternary complex, or (4) the C-terminus of UbDha, generating an E2~UbDha thioester. A comparison between the E1-UbDha-E2 trapped ternary complex and the native transient tetrahedral intermediate is shown below.

c. SDS-PAGE of samples taken from performing Dha cross-linking of UBA6 to BIRC6^{UBC} and subsequent purification by SEC.

d. SDS-PAGE of samples taken after Dha cross-linking of UBA6 to UBE2Z and subsequent purification by SEC.

3.2.5. Structures of UBA6-specific E2 enzymes bound to UBA6

Initial screening of E1-UbDha-E2 complexes by electron cryo-microscopy (cryoEM) proved challenging, as particles suffered from severe preferred orientation. After several rounds of sample optimisation, including tilted acquisitions, addition of a surfactant (0.01% fluorinated octyl maltoside) resolved the issue and allowed for the collection of high-quality datasets (**Fig. 11a-c**).

UBA6-UbDha-BIRC6^{UBC}

Multiple states of the UBA6-UbDha-BIRC6^{UBC} complex were identified during the initial stages of data processing (**Fig. 12a**). Two classes corresponding to either the presence or absence of ubiquitin in the E1 adenylation site (referred to as doubly or singly loaded) were observed. Further particle cleaning and refinement brought the singly and doubly loaded states to final resolutions of 3.6 Å and 3.1 Å respectively (**Fig. 12b**). Our data also included a third class with no observable ubiquitin density in either the adenylation or transfer sites. While the following analysis in this chapter focuses on the UbDha cross-linked maps, this third state (BIRC6^{OUT}) is revisited in **Chapter 4**.

Models were built for most residues in UBA6 and BIRC6^{UBC} in both cross-linked maps. While Ub^{A} could be confidently built in the doubly loaded map, due to the significant flexibility of Ub^{T} in both consensus maps, only the final residues contributing to the UbDha crosslink could be built. Further analysis of Ub^{T} mobility was performed in cryoSPARC, described in **Chapter 3.2.9**. The conformations of both UBA6 and BIRC6^{UBC} were identical in the singly and doubly loaded states, with the only difference being occupancy of the ubiquitin adenylation site. Detailed descriptions of data processing and structure validation can be found in **Figures 13a-d, 14**.

UBA6-UbDha-UBE2Z

Surprisingly, the UBA6-UbDha-UBE2Z dataset was more homogeneous, as only the singly loaded state was observed (**Fig. 12c**). Refinement of the particle stack yielded a map at a resolution of 2.9 Å (**Fig. 12d**). In contrast to the UBA6-UbDha-BIRC6^{UBC} maps, Ub^{T} was less dynamic, and a Ub^{T} could be built into the consensus map. Detailed descriptions of data processing and structure validation can be found in **Figure 15**.

General observations

Overall, our structures resemble those previously published for yeast UBA1 in complex with E2s[27,30,82,83]. As expected, both BIRC6 and UBE2Z bind between the UFD and SCCH domains of UBA6. Clear density for the UbDha cross-link between E1 and E2 catalytic residues was observed (**Fig. 12e**). The adenylation site was occupied in all structures; either with UbDha-AMP for doubly loaded states, or ATP for singly loaded states. Within the SCCH domain of both structures, consistent with other E1-E2 structures, the Cys-cap loop was displaced to allow access to the E1 catalytic site. Interestingly, clear density for IP6 was observed in both of our E2-bound structures (**Fig. 12f**), suggesting that IP6 is bound within the SCCH of UBA6 during transthiolation.

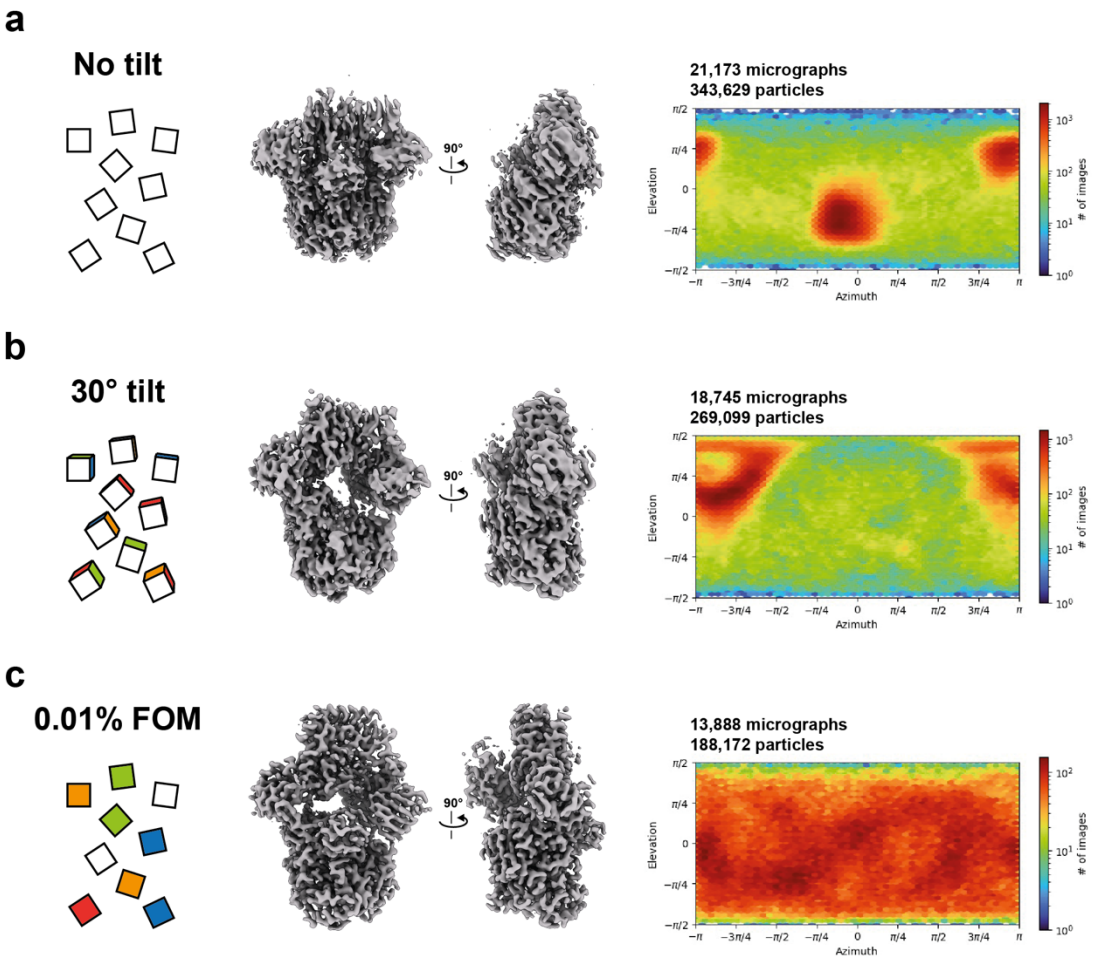
a
No tilt
90°
21,173 micrographs
343,629 particles
b
30° tilt
90°
18,745 micrographs
269,099 particles
c
0.01% FOM
90°
13,888 micrographs
188,172 particles
Elevation
Azimuth
# of images

Figure 11. Resolving preferred orientation in the E1-UbDha-E2 sample

a-c. Cartoon showing particle orientations (left), front and side views of consensus maps (centre) and particle orientation distribution diagrams (right) for separate cryoEM datasets collected on UBA6-UbDha-BIRC6^{UBC} samples.

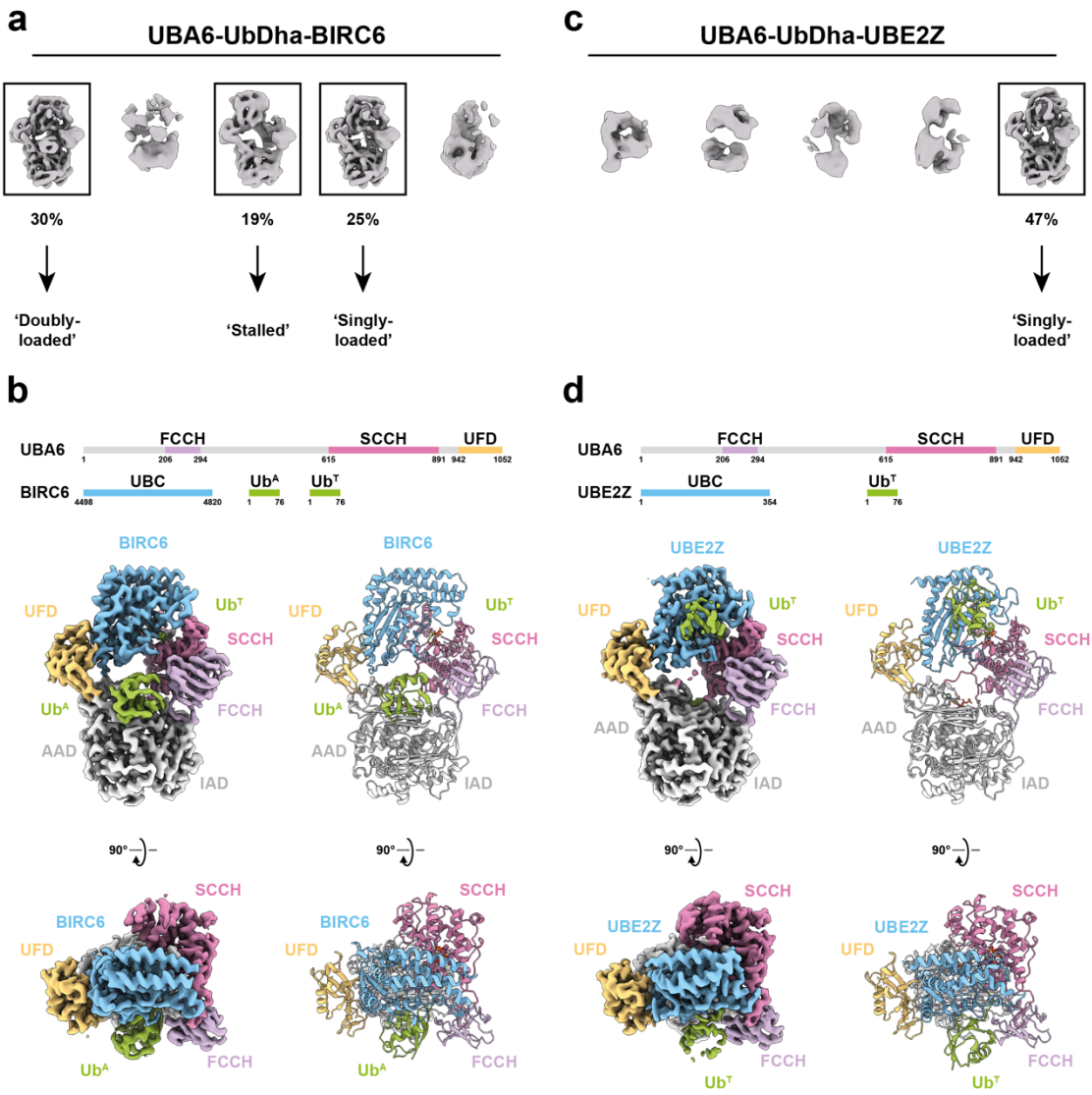
a
UBA6-UbDha-BIRC6
30%
19%
25%
'Doubly-loaded'
'Stalled'
'Singly-loaded'
c
UBA6-UbDha-UBE2Z
47%
'Singly-loaded'
b
UBA6
FCCH
SCCH
UFD
BIRC6
UBC
UbA
UbT
UFD
SCCH
FCCH
AAD
IAD
90°
d
UBE2Z
e
UBA6-UbDha-BIRC6UBC
C4666
Dha76
S625
f
UBA6-UbDha-BIRC6UBC
H4671
K687
Dha76
IP6
K652
K628
K714
K644
K706
UBA6-UbDha-UBE2Z
R183

Figure 12. Trapped CryoEM structures of UBA6 transferring ubiquitin to BIRC6^{UBC} and UBE2Z

a. Classes produced by heterogeneous refinement of the UBA6-UbDha-BIRC6^{UBC} dataset.

b. Front and top views of the doubly loaded UBA6-UbDha-BIRC6^{UBC} map and model.

c. Classes produced by heterogeneous refinement of the UBA6-UbDha-UBE2Z dataset.

d. Front and side views of the singly loaded UBA6-UbDha-UBE2Z map and model.

e. Density for the UbDha cross-link between UBA6 and BIRC6.

f. Density for IP6 in the UBA6-UbDha-BIRC6^{UBC} and UBA6-UbDha-UBE2Z maps.

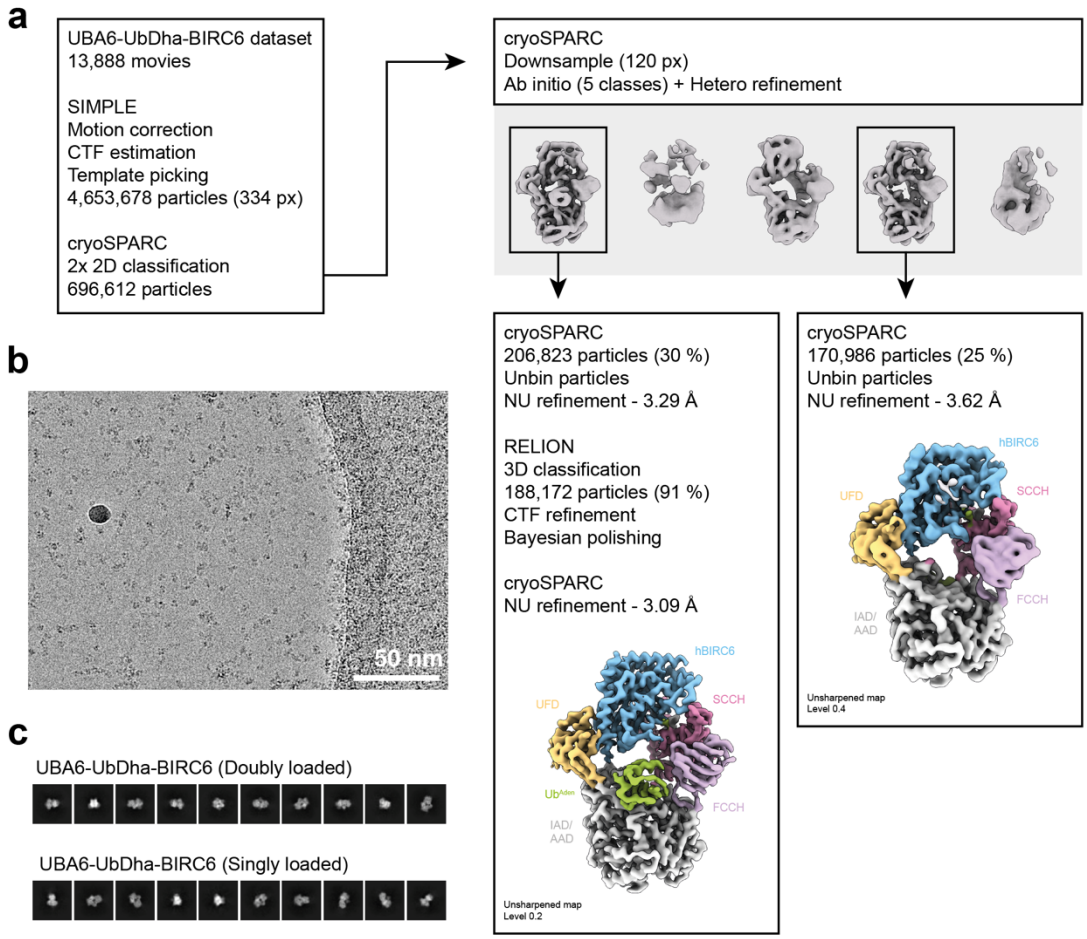
a
UBA6-UbDha-BIRC6 dataset
13,888 movies
SIMPLE
Motion correction
CTF estimation
Template picking
4,653,678 particles (334 px)
cryoSPARC
2x 2D classification
696,612 particles
cryoSPARC
Downsample (120 px)
Ab initio (5 classes) + Hetero refinement
cryoSPARC
206,823 particles (30 %)
Unbin particles
NU refinement - 3.29 Å
RELION
3D classification
188,172 particles (91 %)
CTF refinement
Bayesian polishing
cryoSPARC
NU refinement - 3.09 Å
hBIRC6
UFD
SCCH
UbAdea
FCCH
IAD/
AAD
Unsharpened map
Level 0.2
cryoSPARC
170,986 particles (25 %)
Unbin particles
NU refinement - 3.62 Å
hBIRC6
UFD
SCCH
FCCH
IAD/
AAD
Unsharpened map
Level 0.4
b
50 nm
c
UBA6-UbDha-BIRC6 (Doubly loaded)
UBA6-UbDha-BIRC6 (Singly loaded)

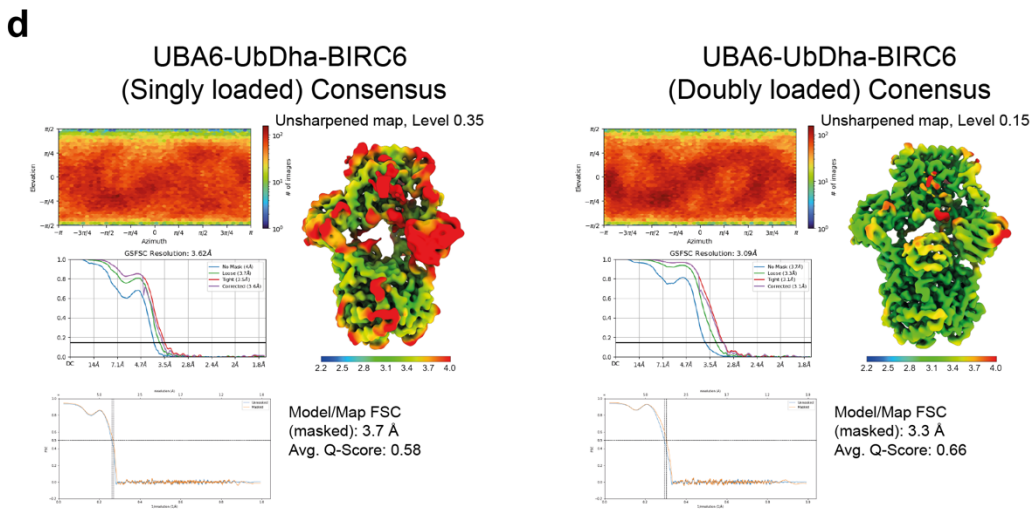
d
UBA6-UbDha-BIRC6
(Singly loaded) Consensus
Unsharpened map, Level 0.35
GSFSC Resolution: 3.62Å
Model/Map FSC
(masked): 3.7 Å
Avg. Q-Score: 0.58
UBA6-UbDha-BIRC6
(Doubly loaded) Conensus
Unsharpened map, Level 0.15
GSFSC Resolution: 3.09Å
Model/Map FSC
(masked): 3.3 Å
Avg. Q-Score: 0.66

Figure 13. CryoEM processing and validation for the UBA6-UbDha-BIRC6 sample

a. Preprocessing, classification and refinement steps used to generate consensus maps for singly and doubly loaded states of UBA6-UbDha-BIRC6.

b. A representative micrograph image.

c. Representative 2D classes for particles used in each class.

d. Particle orientation distribution diagram, local resolution map, GSFSC and model-map FSC curves for each consensus map.

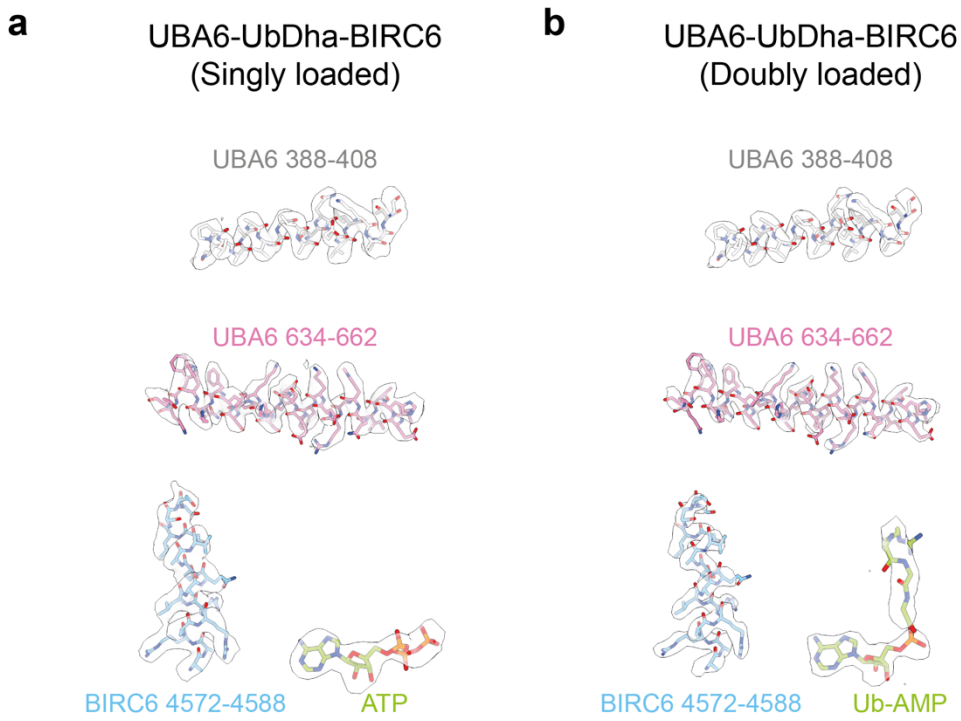

Figure 14. Representative densities for selected regions within the singly and doubly loaded UBA6-UbDha-BIRC6 structures

Cryo-EM density and associated atomic model for selected regions in the singly (a) and doubly (b) loaded UBA6-UbDha-BIRC6 structures: UBA6 core (residues 388-406), UBA6 SCCH domain (residues 634-662), BIRC6 helix 1 (residues 4572-4588), and ATP/Ubiquitin-AMP.

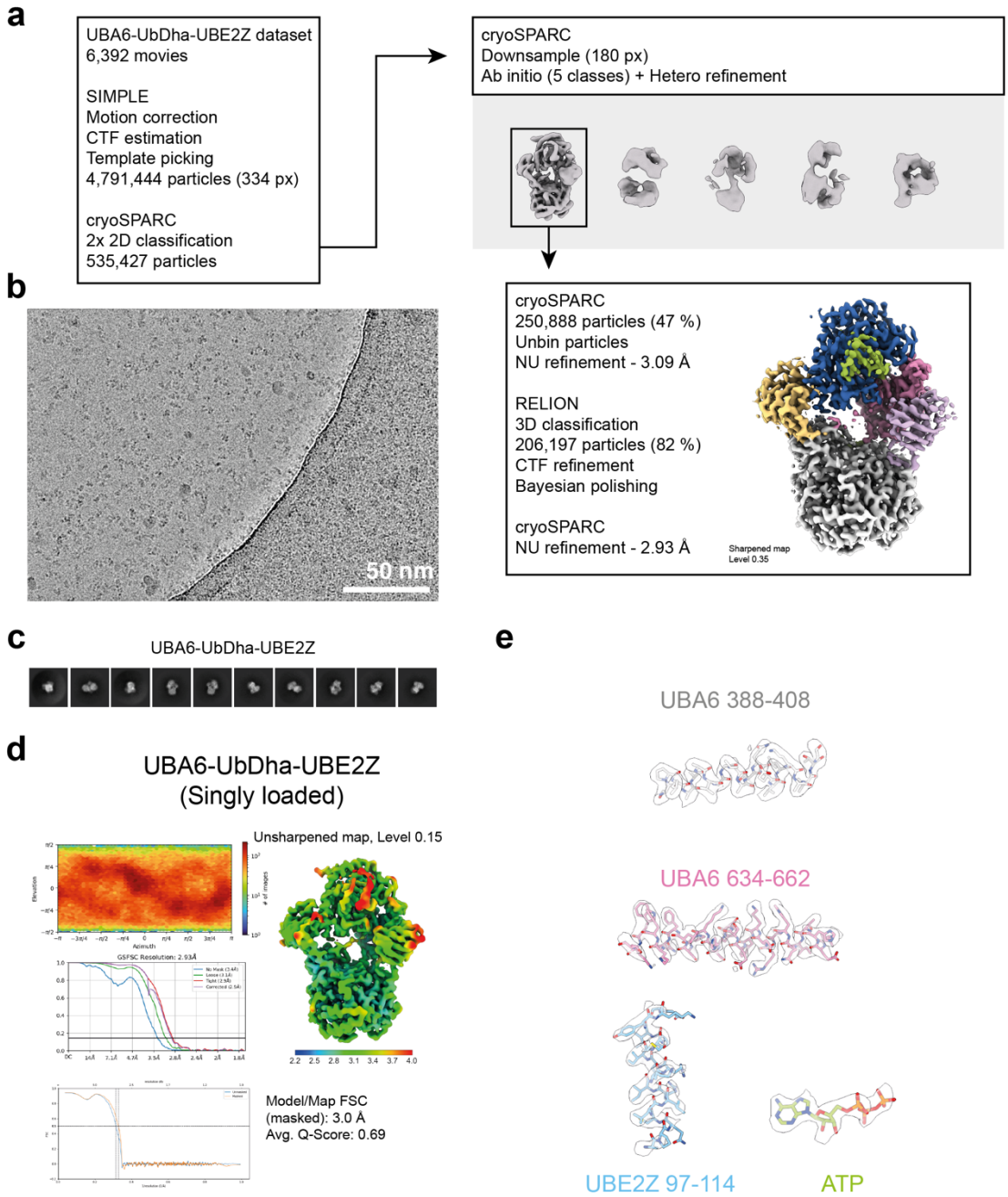
a
UBA6-UbDha-UBE2Z dataset
6,392 movies
SIMPLE
Motion correction
CTF estimation
Template picking
4,791,444 particles (334 px)
cryoSPARC
2x 2D classification
535,427 particles
cryoSPARC
Downsample (180 px)
Ab initio (5 classes) + Hetero refinement
b
50 nm
cryoSPARC
250,888 particles (47 %)
Unbin particles
NU refinement - 3.09 Å
RELION
3D classification
206,197 particles (82 %)
CTF refinement
Bayesian polishing
cryoSPARC
NU refinement - 2.93 Å
Sharpened map
Level 0.35
c
UBA6-UbDha-UBE2Z
d
UBA6-UbDha-UBE2Z
(Singly loaded)
Unsharpened map, Level 0.15
GSFSC Resolution: 2.93Å
Model/Map FSC
(masked): 3.0 Å
Avg. Q-Score: 0.69
e
UBA6 388-408
UBA6 634-662
UBE2Z 97-114
ATP

Figure 15. CryoEM processing and validation for the UBA6-UbDha-UBE2Z sample

a. Preprocessing, classification and refinement steps used to generate the consensus map for singly loaded UBA6-UbDha-UBE2Z.

b. A representative micrograph image.

c. Representative 2D classes for particles used in each class.

d. Particle orientation distribution diagram, local resolution map, GSFSC and model-map FSC curves for the consensus map.

e. Cryo-EM density and associated atomic model for selected regions in the UBA6-UbDha-UBE2Z structure: UBA6 core (residues 388-406), UBA6 SCCH domain (residues 634-662), UBE2Z helix 1 (residues 97-114), and ATP.

3.2.6. Validating interfaces within E1-UbDha-E2 structures

A series of point mutations in BIRC6 and UBE2Z were then designed to validate the key interfaces revealed by the atomic models.

Disruptive mutations at the BIRC6-UFD interface had a range of effects (**Fig. 16a**). Introducing charged residues into positions originally occupied by uncharged residues (A4575, A4579, L4606) generally reduced BIRC6 loading, particularly L4606R. L4606 is part of the canonical 'L2' of BIRC6 which, alongside 'H1', binds a cleft formed by beta-strands in the UFD. While the charge swap mutation of R4576E had a large impact on activity, mutations of other charged residues (Q4580R, E4604R) were less significant. No mutations within the 'H1' of UBE2Z affected E2 loading (**Fig. 16b**), consistent with the relative unimportance of the UBE2Z for E1 specificity. However, mutating 'L2' residue M128 to a charged side chain was able the effect of the L4606R mutation in BIRC6, knocking out activity.

Mutations at the SCCH interface were generally less effective at disrupting E2 loading. In BIRC6 only the Y4711R mutation reduced activity (**Fig. 16c**), possibly by loss of favourable interactions with a series of hydrophobic residues in UBA6 (F722, I726 and L728). For UBE2Z, mutation of the hydrophobic residue Y182 to alanine had no effect, but swapping the charge of the neighbouring R183 resulted in a slight reduction in activity (**Fig. 16d**). Interestingly, this arginine in UBE2Z coordinates the cofactor IP6, which is found in the SCCH of UBA6 only.

In addition to probing sites of E1-E2 interactions, residues within the post-transfer ubiquitin-binding surface of both E2s were also mutated. Previous studies have found that mutations in the equivalent site of Cdc34 (yeast UBE2R1) reduce ubiquitin transfer[27], which is consistent with the thioester switch model proposed for UBA1

(discussed in **Chapter 4.1.2.**). Unexpectedly, most of the mutations we designed for both E2s at this interface had little effect (**Fig. 16e, f**). While this may be due to the selection of residues, it also raises the possibility that UBA6-specific E2s may not depend on the same thioester switch mechanism as UBE2R1.

To complement mutations within the E2s, corresponding disruptive mutations within the UBA6 UFD were also designed (**Fig. 16g**). Interestingly, different effects were observed when testing each of the mutations with multiple E2s. Activity of both UBE2Z and UBE2D2 was drastically lowered by the M992E mutation, however BIRC6 was only slightly affected. Likewise, only UBE2Z was affected by the M998R mutation. Together, this suggests that there is variation across E2s for susceptibility to E1 mutations, with BIRC6 being more tolerant to mutations in the E1 UFD than UBE2D2 and UBE2Z.

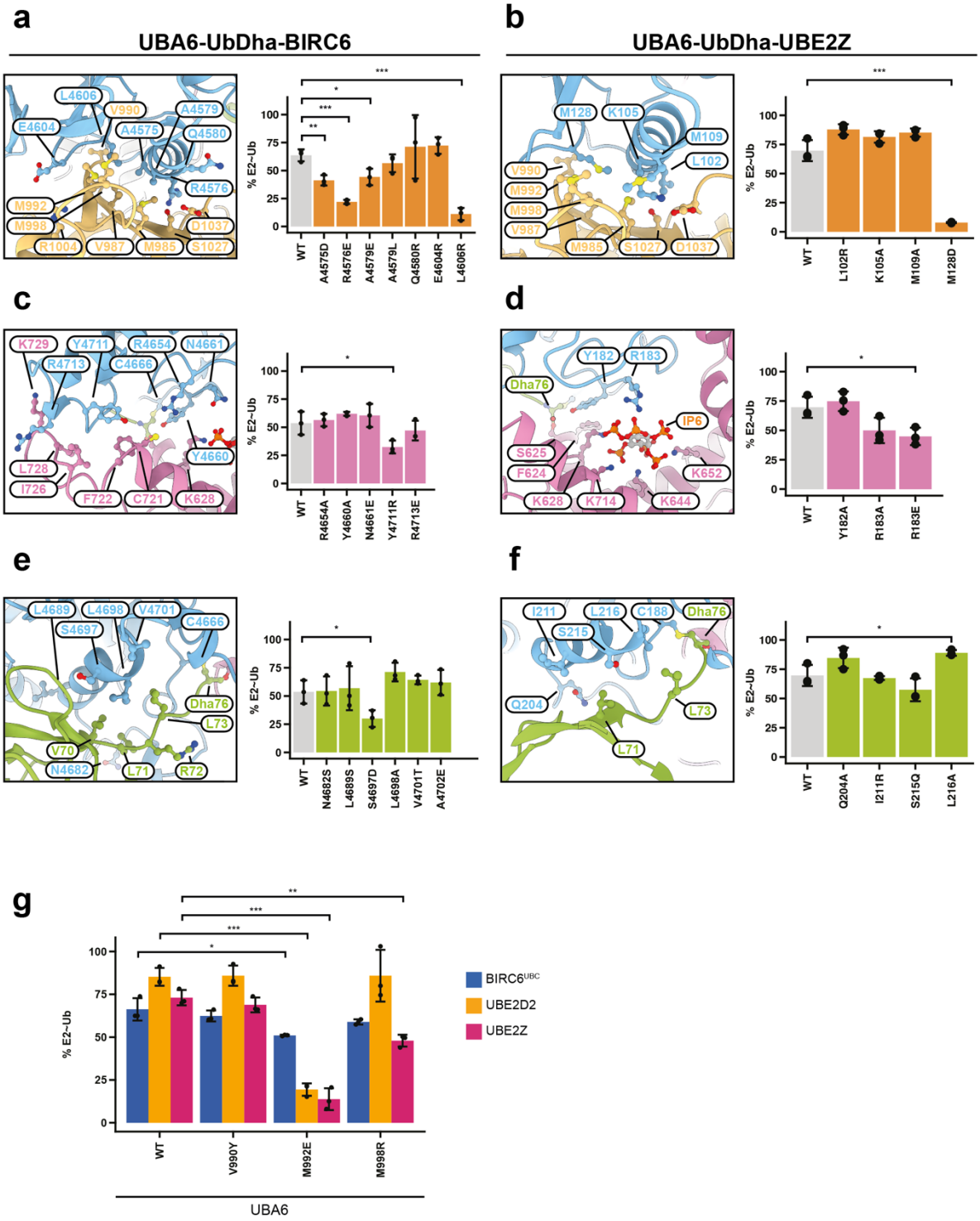
a
UBA6-UbDha-BIRC6
L4606
V990
A4579
E4604
A4575
Q4580
R4576
M992
M998
Q1037
R1004
V987
M985
S1027
% E2~Ub
WT
A4575D
R4576E
A4579E
A4579L
Q4580R
E4604R
L4606R
b
UBA6-UbDha-UBE2Z
M128
K105
M109
L102
V990
M992
M998
V987
M985
S1027
Q1037
WT
L102R
K105A
M109A
M128D
c
K729
Y4711
R4654
N4661
R4713
C4660
L728
I726
Y4660
F722
C721
K628
WT
R4654A
Y4660A
N4661E
Y4711R
R4713E
d
Y182
R183
Dha76
IP6
S625
F624
K652
K628
K714
K644
WT
Y182A
R183A
R183E
e
L4689
L4698
V4701
S4697
C4666
Dha76
L73
V70
N4682
L71
R72
WT
N4682S
L4689S
S4697D
L4698A
V4701T
A4702E
f
I211
L216
C188
Dha76
S215
Q204
L73
L71
WT
Q204A
I211R
S215Q
L216A
g
BIRC6UBC
UBE2D2
UBE2Z
WT
V990Y
M992E
M998R
UBA6

Figure 16. Validating UBA6-E2 interfaces through site-directed mutagenesis

Close-up view (left) and quantification of E2~Ub thioester formation for E2 mutants (right) at the following interfaces:

a. $UBA6^{UFD}$-BIRC6

b. $UBA6^{UFD}$-UBE2Z

c. $UBA6^{SCCH}$-BIRC6

d. $UBA6^{SCCH}$-UBE2Z

e. Ub^{T}-BIRC6

f. Ub^{T}-UEB2Z

g. Quantification of E2~Ub thioester formation for E1 mutants with WT $BIRC6^{UBC}$, UBE2Z and UBE2D2.

Proportion of loaded E2 (E2~Ub) was measured by Coomassie stained SDS-PAGE analysis of 5-minute transthiolation assays. Quantification was performed across three technical repeats, and the plot displays the mean ± standard deviation. Statistical analysis between reactions was performed using an unpaired *t*-test, and significant differences are indicated with the following levels:

(*** $p < 0.001$, ** $p < 0.01$, * $p < 0.05$)

3.2.7. Structure of an E1-bispecific BIRC6 orthologue bound to UBA1

Phylogenetic analysis of UBA6 and BIRC6 conservation (Paul Elliott and Kay Hofmann) revealed an orthologue of BIRC6 which was potentially compatible with UBA1: While BIRC6 is widely conserved, UBA6 is missing in Nematoda and Insecta (**Fig. 17a**). Given that BIRC6 is known to have biological functions dependent on its ubiquitination activity in drosophila[85,86], we checked to see if the drosophila BIRC6 protein (dBIRC6) had adapted to function with UBA1 in the absence of UBA6. Indeed, not only did recombinantly expressed dBIRC6 show activity with drosophila UBA1 (dUBA1), but it was also compatible with both human E1s (**Fig. 17b**). UbDha-crosslinking was then repeated with dUBA1 and dBIRC6^{UBC} to determine a structure of the E1-nonspecific BIRC6 variant (**Fig. 17c**), which could then be used to understand differences between the two BIRC6 orthologues which enable UBA6-specificity in human BIRC6.

The dUBA1-UbDha-dBIRC6^{UBC} cryoEM dataset only contained the doubly loaded complex (**Fig. 18a**), which was refined to a 2.6 Å consensus map (**Fig. 18b**). As seen in the UBA6-UbDha-BIRC6^{UBC} consensus map, most of the density corresponding to Ub^{T} was blurred due to flexibility, however the UbDha cross-link could be built confidently (**Fig. 18c**). Overall, the arrangement of E1 and E2 proteins in the drosophila complex closely resembled the human complex, suggesting that E1 specificity would be driven by subtle differences between the two BIRC6 orthologues (**Fig. 18d**). Detailed descriptions of data processing and structure validation can be found in **Figure 19**.

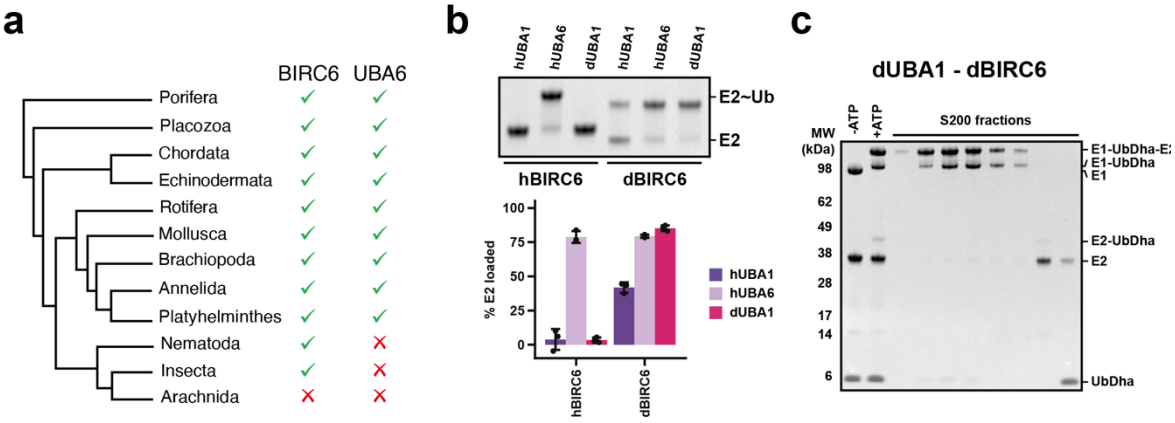

Figure 17. Drosophila melanogaster contains a UBA1-active BIRC6 orthologue

a. Phylogenetic analysis of UBA6 and BIRC6 conservation across animal clades.

b. Quantification of E2~Ub thioester formation of h/dBIRC6^{UBC} with human and drosophila E1s. Proportion of loaded E2 (E2~Ub) was measured by Coomassie stained SDS-PAGE analysis of 5-minute transthiolation assays (representative gel panel shown above). Quantification was performed across three technical repeats, and the plot displays the mean ± standard deviation.

c. UbDha cross-linking of dUBA1 and dBIRC6 for cryoEM analysis.

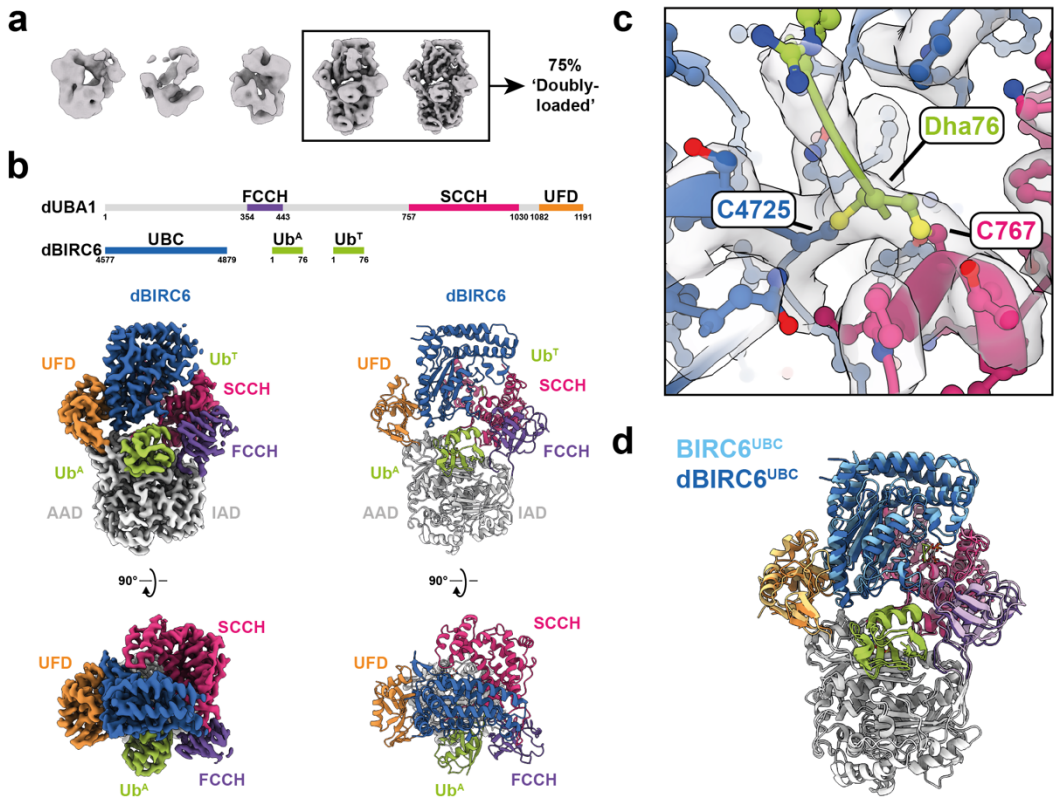

Figure 18. Trapped CryoEM structure of drosophila UBA1 transferring ubiquitin to a non-specific BIRC6 orthologue

a. Classes produced by heterogeneous refinement of the dUBA1-UbDha-dBIRC6^{UBC} dataset.

b. Front and top views of the doubly loaded dUBA1-UbDha-dBIRC6^{UBC} map and model.

c. Density for the UbDha cross-link between dUBA1 and dBIRC6.

d. Aligned models of the UBA6-UbDha-BIRC6^{UBC} and dUBA1-UbDha-dBIRC6^{UBC} complexes.

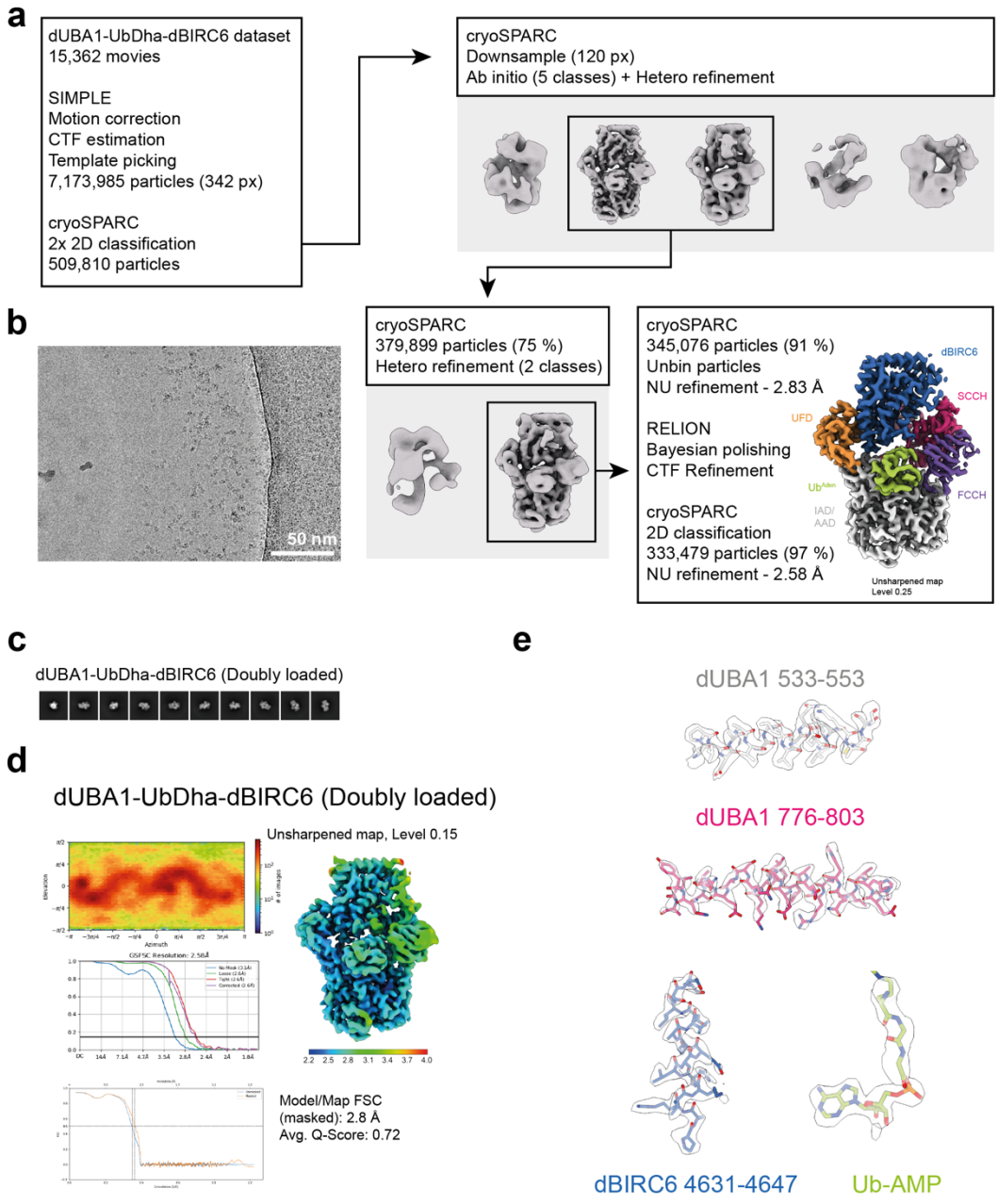
a
dUBA1-UbDha-dBIRC6 dataset
15,362 movies
SIMPLE
Motion correction
CTF estimation
Template picking
7,173,985 particles (342 px)
cryoSPARC
2x 2D classification
509,810 particles
cryoSPARC
Downsample (120 px)
Ab initio (5 classes) + Hetero refinement
b
50 nm
cryoSPARC
379,899 particles (75 %)
Hetero refinement (2 classes)
cryoSPARC
345,076 particles (91 %)
Unbin particles
NU refinement - 2.83 Å
RELION
Bayesian polishing
CTF Refinement
cryoSPARC
2D classification
333,479 particles (97 %)
NU refinement - 2.58 Å
dBIRC6
SCCH
UFD
FCCH
IAD/
AAD
Unsharpened map
Level 0.25
c
dUBA1-UbDha-dBIRC6 (Doubly loaded)
d
dUBA1-UbDha-dBIRC6 (Doubly loaded)
Unsharpened map, Level 0.15
Model/Map FSC
(masked): 2.8 Å
Avg. Q-Score: 0.72
e
dUBA1 533-553
dUBA1 776-803
dBIRC6 4631-4647
Ub-AMP

Figure 19. CryoEM processing and validation for the dUBA1-UbDha-dBIRC6 sample

a. Preprocessing, classification and refinement steps used to generate the consensus map for singly loaded dUBA1-UbDha-dBIRC6.

b. A representative micrograph image.

c. Representative 2D classes for particles used in each class.

d. Particle orientation distribution diagram, local resolution map, GSFSC and model-map FSC curves for the consensus map.

e. Cryo-EM density and associated atomic model for selected regions in the dUBA1-UbDha-dBIRC6 structure: dUBA1 core (residues 533-553), UBA1 SCCH domain (residues 776-803), dBIRC6 helix 1 (residues 4631-4647), and Ubiquitin-AMP.

3.2.8. BIRC6 constructs with altered E1-specificity

To systematically search for BIRC6 features within out structures which could affect E1 specificity, an alignment of human and drosophila BIRC6 sequences was generated and residues positioned near (<5 Å) to the E1 in either structure were inspected (**Fig. 20a**).

This analysis revealed a pair of glutamic acid residues (4603-4604, ‘EE’) within the ‘loop 2’ region of human BIRC6 (**Fig. 20b**). The equivalent residues in drosophila (4662-4663, ‘TD’) are threonine and aspartic acid, the sidechains of which are shorter than glutamic acid by one carbon atom. Crucially, both residues point directly towards a helix within the E1 UFD; in UBA1 this helix is extended by an additional turn, restricting the space available for the E2 and potentially causing a clash with the longer 'EE' sidechains in human BIRC6. The most significant residue substitution close to the SCCH interface was glycine 4650, which in drosophila BIRC6 is replaced by an arginine (**Fig. 20c**).

Based on these findings, a series of chimeric BIRC6 constructs were generated to test whether these residues do in fact drive E1 specificity in BIRC6 (**Fig. 20d**, top). These chimeras included substitutions of three larger BIRC6 sections: 'N-terminal', 'Core' and 'C-terminal'. More subtle amino acid substitutions within the 'Core' section were also included, which targeted both UFD and SCCH interfaces. The activity of each chimeric BIRC6 construct was then tested with both UBA1 and UBA6 (**Fig. 20d**, bottom).

All the chimeric BIRC6 constructs were active with UBA6. Substitution of any individual human BIRC6 section (Chimeras 1, 3, 10) with that of drosophila was not sufficient to gain activity with UBA1. Replacing either the 'N-terminal' or 'Core' sections of drosophila BIRC6 abolished UBA1 activity (Chimeras 4, 8), however the C-terminal

substitution (Chimera 9) was still active. Together, these results showed that simultaneous contributions from residues within the N-terminus and core of drosophila BIRC6 are required for activity with UBA1. Crucially, while not sufficient to restore activity alone (Chimera 7), for constructs already containing N-terminal substitutions from human to drosophila, mutation of the glutamic acid motif ‘EE’ to ‘TD’ restored activity with UBA1 (Chimeras 1 and 2, 4 and 5/6). No additional effect was observed when introducing the further amino acid substitutions to the BIRC6 core, including G4650R (Chimeras 5 and 6).

Overall, the activities of our chimeras support the importance of residues involved in the BIRC6-UFD interaction as the critical site for determining E1 specificity, particularly the 'EE'/'TD' motif. On the other hand, the glycine to arginine substitution towards the SCCH interface appears to not be as important for enabling UBA1 activity.

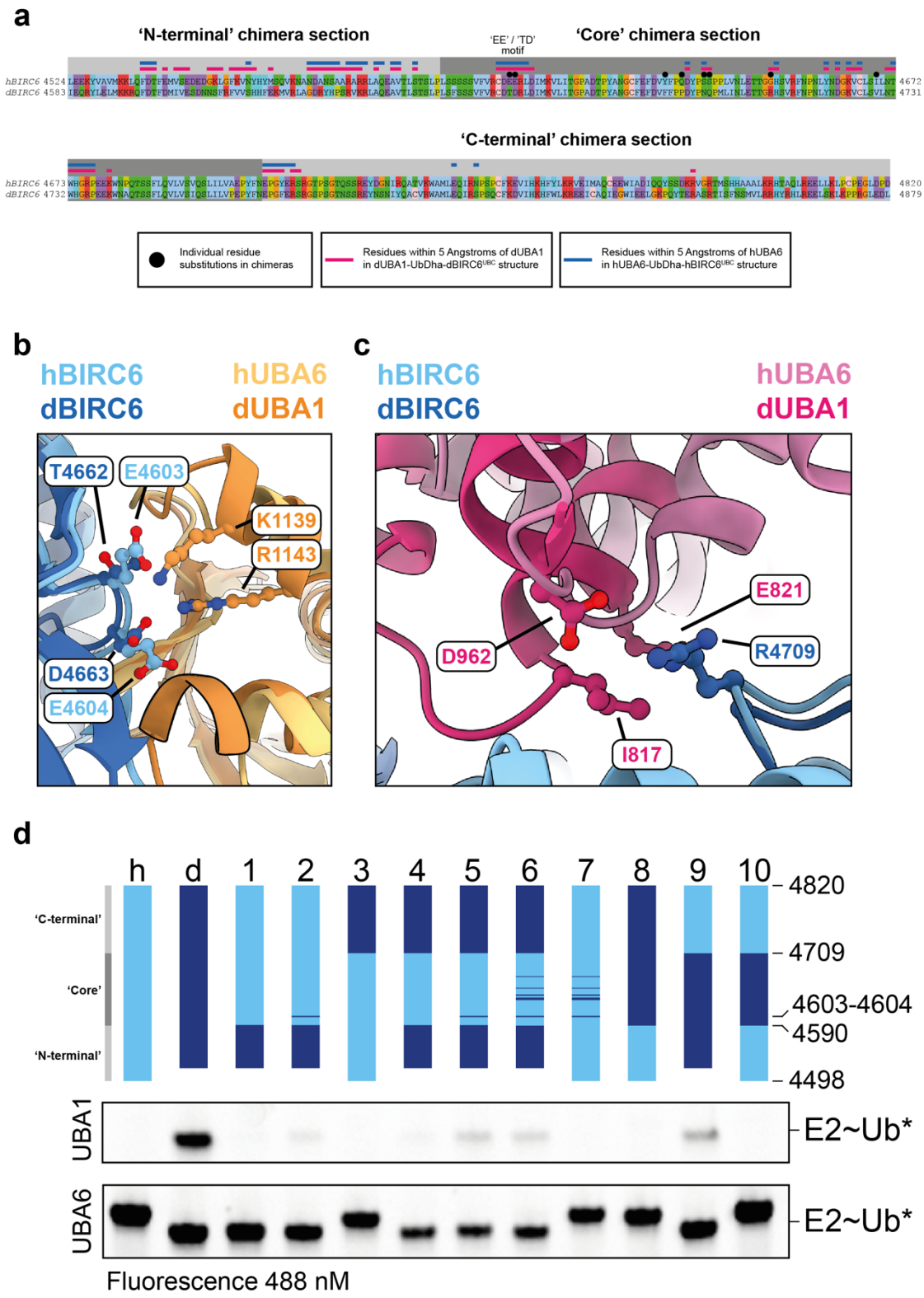
a
'N-terminal' chimera section
'EE' / 'TD' motif
'Core' chimera section
'C-terminal' chimera section
Individual residue substitutions in chimeras
Residues within 5 Angstroms of dUBA1 in dUBA1-UbDha-dBIRC6UBC structure
Residues within 5 Angstroms of hUBA6 in hUBA6-UbDha-hBIRC6UBC structure
b
hBIRC6
dBIRC6
hUBA6
dUBA1
T4662
E4603
K1139
R1143
D4663
E4604
c
hBIRC6
dBIRC6
hUBA6
dUBA1
E821
D962
R4709
I817
d
h
d
1
2
3
4
5
6
7
8
9
10
'C-terminal'
'Core'
'N-terminal'
4820
4709
4603-4604
4590
4498
UBA1
E2~Ub*
UBA6
E2~Ub*
Fluorescence 488 nM

Figure 20. Locating specificity-driving features in BIRC6

a. Annotated sequence alignment of human and drosophila BIRC6 orthologues.

b. Close-up view of the UFD-binding interface of human and drosophila BIRC6. The additional UFD helical turn in UBA1 is outlined for emphasis.

c. Close-up view of the SCCH-binding interface of drosophila BIRC6. Arginine 4709 is replaced by glycine in human BIRC6.

d. Cartoon of BIRC6 chimeras (top). Fluorescence image of SDS-PAGE analysis for *in vitro* transthiolation reactions containing each BIRC6 chimera with either UBA1 or UBA6 (bottom). Exact domain boundaries of chimeras 1-10, followed by additional residue substitutions are as follows:

1 dBIRC6 4577-4646, hBIRC6 4590-4820

2 dBIRC6 4577-4648, hBIRC6 4590-4820: E4603T, E4604D

3 hBIRC6 4498-4708, dBIRC6 4768-4879

4 dBIRC6 4577-4648, hBIRC6 4590-4708, dBIRC6 4768-4879

5 dBIRC6 4577-4648, hBIRC6 4590-4708, dBIRC6 4768-4879: E4603T, E4604D

6 dBIRC6 4577-4648, hBIRC6 4590-4708, dBIRC6 4768-4879: E4603T, E4604D, Y4631F, Q4634P, S4638N, S4639Q, G4650R, I4669V

7 hBIRC6 4498-4820: E4603T, E4604D, Y4631F, Q4634P, S4638N, S4639Q, G4650R, I4669V

8 hBIRC6 4498-4589, dBIRC6 4649-4879

9 dBIRC6 4577-4767, hBIRC6 4709-4820

10 hBIRC6 4498-4589, dBIRC6 4649-4767, hBIRC6 4709-4820

3.2.9. Designing E2 mutants with altered E1-specificity

To combine the results of the E2 specificity panel and new insights into E1 interactions from UBA6-specific E2s, E1-specificity altering mutations were designed for other E2s. Since all specific E2 enzymes (except for UBE2Z) depended at least in part on the UFD interaction to drive specificity, therefore these mutations were focused within the canonical UFD interacting motif of E2 enzymes, 'H1'.

As mentioned above, previous analysis of specificity determinants in UBA1 and UBA6[63] had been hindered by the selection of UBE2Z as a model UBA6-specific E2 (which is understandable, because UBE2Z was the only known UBA6-specific E2 at that time). The data in this thesis suggests that UBE2Z is in fact compatible with the UFD of UBA1 and therefore would not be useful for understanding UFD-driven specificity.

Instead, UBA1-specific E2s were compared to BIRC6 (**Fig. 21a**). From this a series of residues along the BIRC6 'H1' (positions '3', '7' and '11', as defined by the H1 sequence alignment in **Fig. 21a**) were identified, that, when viewed in the UbDha cross-linked structure (**Fig. 21b**), face a cleft formed by beta-sheets in the UBA6 UFD. In BIRC6 residues at these positions have hydrophobic or short side chains, whereas UBA1-specific E2s often contained a bulkier or charged residue in at least one of the three positions.

Based on these observations, mutations at the '3', '7' and '11' 'H1' sites in the UBA1-specific E2s UBE2H, UBE2E1 and UBE2W were generated (**Fig. 22a, b**). The mutations in UBE2E1 and UBE2W specifically increased activity with UBA6, confirming the importance of these residues in preventing recruitment to UBA6 for

these E2s. The UBE2H mutant was more active with both E1s, therefore the impact on specificity was unclear.

The same approach was then used to modify an E1-nonspecific enzyme, UBE2D2, and introduce specificity for UBA1 (**Fig. 22c, d**). Introducing lysine and aspartic acid residues into positions 3 and 7 of the UBE2D2 ‘H1’ drastically reduced activity with UBA6. Introducing a lysine into ‘L2’ (UBE2D2 M2, D28K) also specifically reduced UBA6 activity, suggesting that like in BIRC6, the ‘L2’ motif of UBE2D2 can be exploited to prevent favourable interactions with UBA6. A similar lysine substitution in the more distant ‘L4’ of UBE2D2 did not affect E1 specificity.

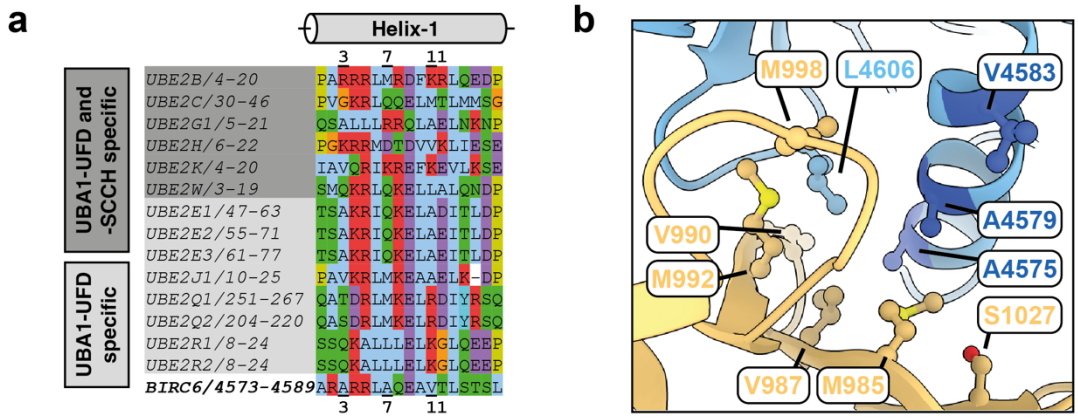

Figure 21. UBA1-specific E2s contain charged residues facing the E1 UFD

a. Sequence alignment of 'H1' sequences of UBA1-specific E2s. The BIRC6 'H1' is added below for comparison. Residues in positions '3', '7' and '11' are marked for emphasis.

b. Close-in view of the UBA6-BIRC6^{UBC} UFD interaction. The residues in positions '3', '7' and '11' are coloured dark blue for emphasis.

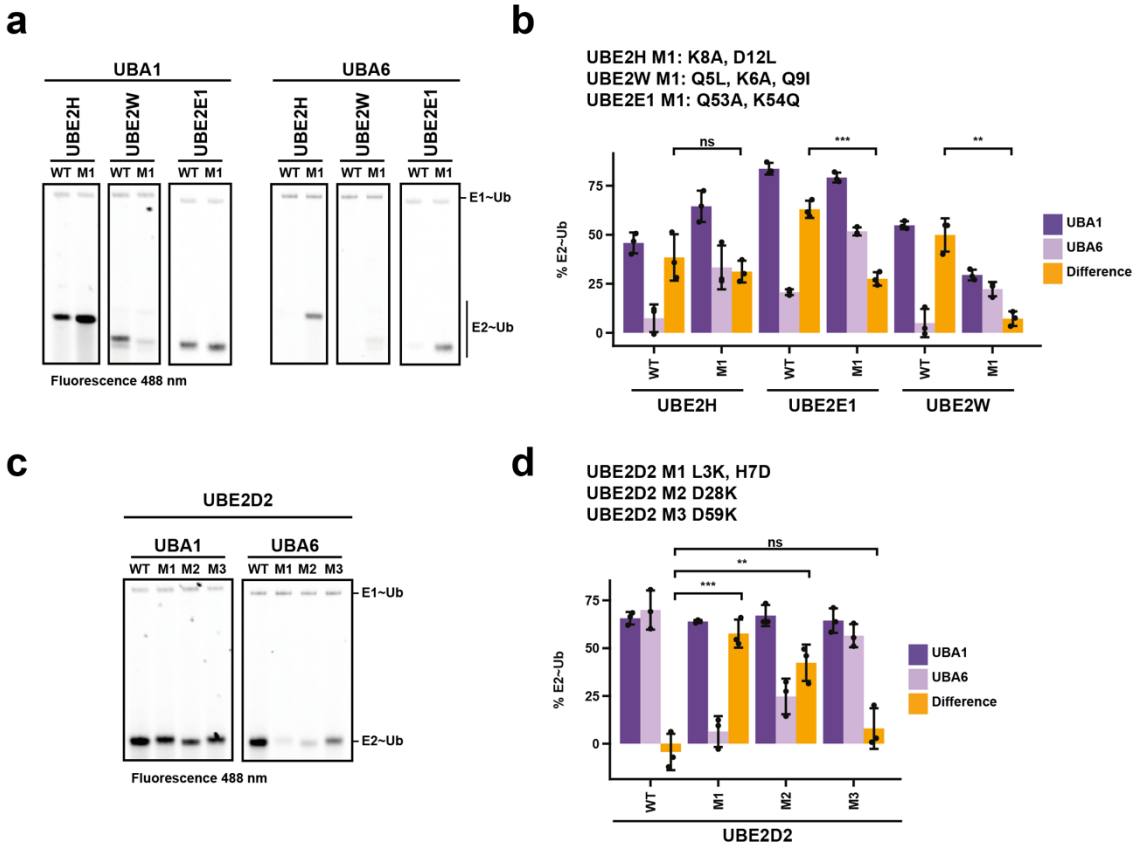

Figure 22. BIRC6-derived mutations at the UFD interface modulate E1-specificity

a-b. 'H1' mutations reduce specificity in UBA1-specific E2s in *in vitro* transthiolation assays. Assays were performed with fluorescently labelled ubiquitin, and imaged first using fluorescence (a), and later quantified by Coomassie staining (b).

c-d. 'H1' and 'L2' mutations decrease activity with UBA6 for the non-specific E2 UBE2D2 in *in vitro* transthiolation assays. Assays were performed with fluorescently labelled ubiquitin, and imaged first using fluorescence (c), and later quantified by Coomassie staining (d). While the gel shown in panel (c) appears to show a difference in UBA1/UBA6 activity for UBE2D2 M3, this difference was not significant across all three repeats (unprocessed gels included in **Appendix Figure 3**).

Proportion of loaded E2 (E2~Ub) was measured by Coomassie stained SDS-PAGE analysis of 5-minute transthiolation assays. Quantification was performed across three technical repeats, and the plot displays the mean ± standard deviation. Statistical analysis between reactions was performed using an unpaired *t*-test, and significant differences are indicated with the following levels:

(*** $p < 0.001$, ** $p < 0.01$, * $p < 0.05$)

3.2.10. Other mechanisms of E1-specificity

It is not known if extensions to the UBC domain could affect E1 specificity in ubiquitin E2s. The UBA1-specific UBE2Q subfamily turned out to be a convenient model system to test the impact of E2 extensions on E1-specificity. Full-length UBE2Q1 and UBE2Q2 both contain an N-terminal RWD domain, and a unique C-terminal fold with an extended unstructured tail (**Fig. 23a**). Fortunately, in the process of testing E2 constructs for the assembly of the E2 specificity panel, UBE2Q constructs with truncations at both N- and C-termini of both subfamily members had been generated (**Fig. 23b**). As a result, a complete panel of truncated variants of UBE2Q subfamily members was available to test for E1 specificity.

While individual truncations at either the N- or C-terminus had little effect, simultaneous truncation of both termini unmasked the core of both UBE2Q1 and UBE2Q2 to have significant cross-reactivity with UBA6 (**Fig. 23c, d**). As such, this represents the first evidence of extensions to a ubiquitin E2 enzyme affecting E1 specificity and invites further experiments into the extensions of other E2s (**Table 1**) and their effect on E1-specificity.

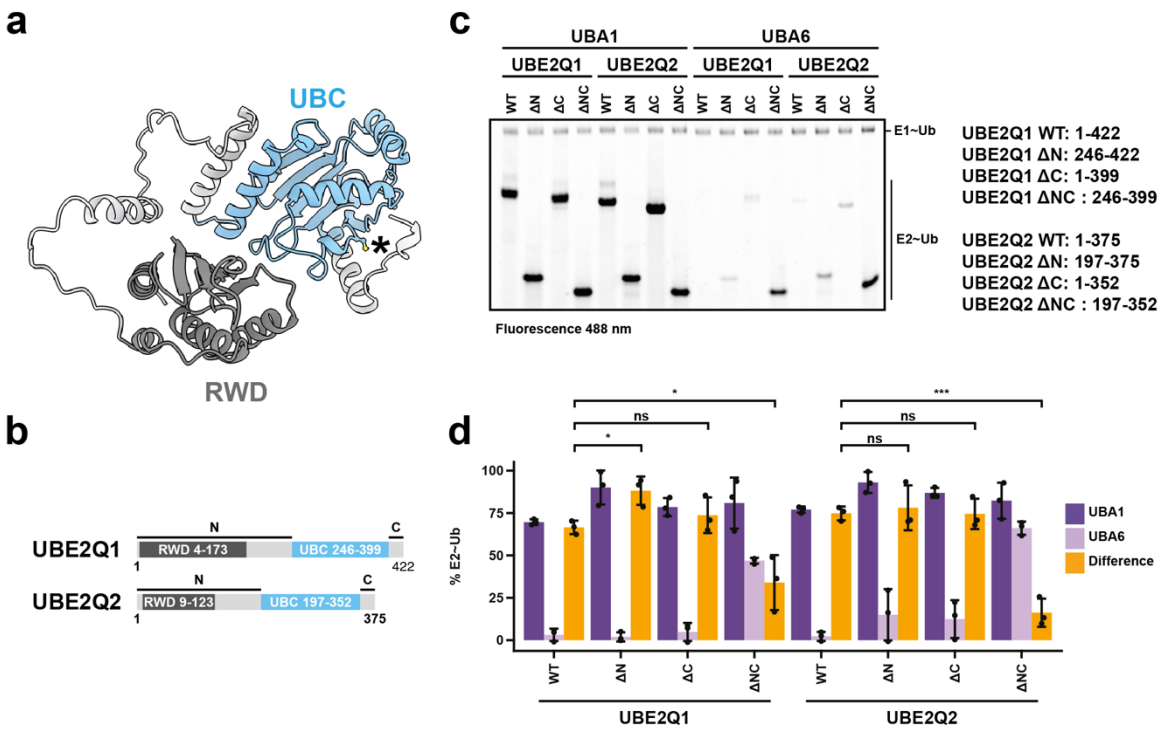

Figure 23. Removing extensions to the UBE2Q core UBC domain unmasks innate activity with UBA6

a. AlphaFold3 predicted model of full-length UBE2Q2. The catalytic cysteine residue is annotated with an asterisk.

b. Schematic of truncated UBE2Q constructs.

c-d. Truncated UBE2Q constructs reveal masked UBA6 activity in *in vitro* transthiolation assays. Assays were performed with fluorescently labelled ubiquitin, and imaged first using fluorescence (c), and later quantified by Coomassie staining (d).

Proportion of loaded E2 (E2~Ub) was measured by Coomassie stained SDS-PAGE analysis of 5-minute transthiolation assays. Quantification was performed across

three technical repeats, and the plot displays the mean ± standard deviation. Statistical analysis between reactions was performed using an unpaired *t*-test, and significant differences are indicated with the following levels:

(*** $p < 0.001$, ** $p < 0.01$, * $p < 0.05$)

3.2.11. 3D variability analysis of E1-UbDha-E2 structures

Finally, further effort was made to address the flexibility of Ub^T in the UbDha cross-linked structures. The 3D variability tool in CryoSPARC was used to describe Ub^T heterogeneity across the cryoEM datasets. Subsequent reconstructions of particles clustered along the identified principal components showed improved, albeit low resolution, density for Ub^T at snapshots across its range of motion (**Fig. 24a, b**), enabling docking of Ub^T models.

A variety in ranges of Ub^T motion were observed across the three E1-UbDha-E2 datasets (**Fig. 24c**). As previously mentioned, Ub^T was stably bound in the 'post-transfer' site of UBE2Z. The UBA6-UbDha-BIRC6 dataset contained a small (7 Å) range of Ub^T positions centred around the face of the E2, which we assumed to be the 'post-transfer' site. In contrast, Ub^T was found in a wider (17 Å) range of positions the drosophila dataset, reaching further towards the E1 FCCH domain and the presumed 'pre-transfer' site.

The Ub^T dynamics described here differ from those reported in previous studies[27,30]. Overall, Ub^T had a shorter range of movement; even the largest range of Ub^T motion in the drosophila dataset was below the 23 Å distance observed by Kochańczyk et al.[30] (**Fig. 24d**). Furthermore, the exact location of the endpoints of Ub^T motion were different. While the 'post-transfer' sites in our UBE2Z and BIRC6 datasets were similar (**Fig. 24c**), they were both positioned further towards the E2 than the 'post-transfer' site in UBA1-Ubc4 (**Fig. 24d**). In addition, the opposite end of Ub^T motion in the dUAB1-UbDha-dBIRC6 dataset was also positioned closer to the face of the E2 compared to the 'pre-transfer' state of UBA1-Ubc4, where rests on the E1 FCCH. This

could point towards fundamental differences in ubiquitin transfer mechanisms between E1s, or differences induced by E1-E2 cross-linking methods.

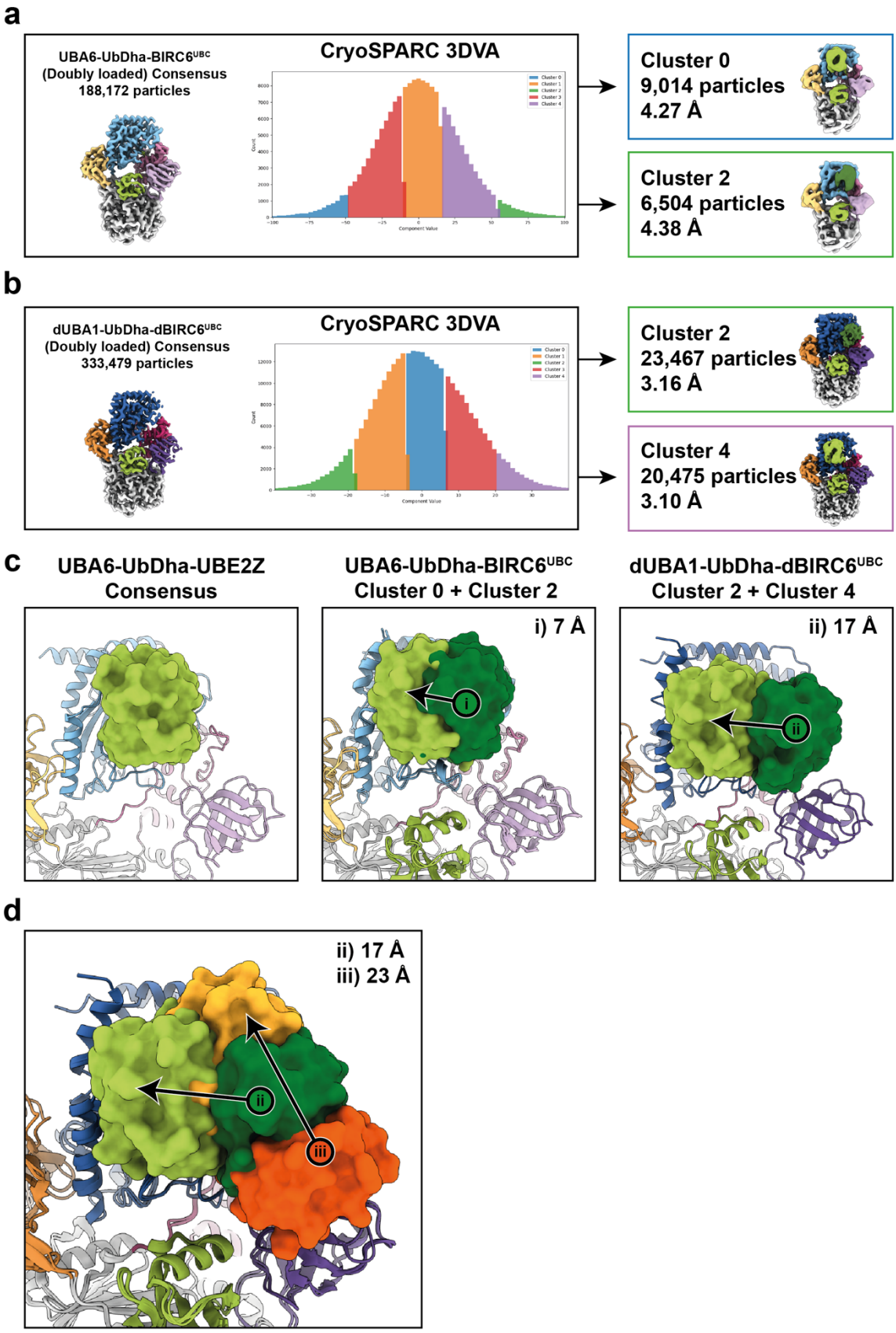
a
UBA6-UbDha-BIRC6UBC
(Doubly loaded) Consensus
188,172 particles
CryoSPARC 3DVA
Cluster 0
9,014 particles
4.27 Å
Cluster 2
6,504 particles
4.38 Å
b
dUBA1-UbDha-dBIRC6UBC
(Doubly loaded) Consensus
333,479 particles
CryoSPARC 3DVA
Cluster 2
23,467 particles
3.16 Å
Cluster 4
20,475 particles
3.10 Å
c
UBA6-UbDha-UBE2Z
Consensus
UBA6-UbDha-BIRC6UBC
Cluster 0 + Cluster 2
i) 7 Å
dUBA1-UbDha-dBIRC6UBC
Cluster 2 + Cluster 4
ii) 17 Å
d
ii) 17 Å
iii) 23 Å

Figure 24. Ub^T dynamics differ between structures of cross-linked E1-E2 complexes.

a. 3D variability analysis and clustering of particles from the UBA6-UbDha-$BIRC6^{UBC}$ dataset.

b. 3D variability analysis and clustering of particles from the dUBA1-UbDha-$dBIRC6^{UBC}$ dataset.

c. Aligned views of models showing the position of Ub^T in the UBA6-UbDha-UBE2Z map (left) and the extents of Ub^T motion captured by 3D variability analysis for human (middle) and drosophila (right) complexes. Ub^T displacement between pairs of models is annotated.

d. Models showing the extent of Ub^T motion in dUBA1-UbDha-$dBIRC6^{UBC}$ and yeast UBA1-UbPSAN-Ubc4 (PDBs: 9B5D, 9B5E). Ub^T displacement between pairs of models is annotated.

3.3. Discussion

3.3.1. E1 specificity across the ubiquitin E2 family

The E1-specificity panel presented here builds on previous UBA6 activity screens[61–63] through the inclusion of previously skipped E2s and the use of recombinantly purified proteins. The widest E2 panel prior to this work used *in vitro* translation with bacterial cell extracts to rapidly produce E2s without the need for laborious purification steps[63]. As a result, their analysis was limited to E2s which could be expressed with their *E. coli* system, and they did not have control of the exact amount of E2 present in each reaction. Consequently, their assay was of limited use for comparing relative activity between E2s and could not control for unknown effects the bacterial cell extract may have on E2 activity.

This study provides a more quantitative profile of E1-E2 reactivity, allowing for better comparisons between E2s. Most E2s showed robust loading under the assay conditions, with the least active E2 being UBE2K (for which we had to extend the assay duration to 30 minutes). This may be due to the C-terminal UBA domain in UBE2K, however further experiments would be required to demonstrate this.

The vast majority of E2s received ubiquitin from UBA1, consistent with its essential role as the predominant ubiquitin-activating enzyme[65]. Furthermore, even the non-specific E2s were generally more active with UBA1, however it is unclear whether this represents a wider trend in E2 specificity or if this reflects a subtly higher rate of ubiquitin activation by UBA1, as has been reported by Jin *et al.*[63].

The overall trend of E2 specificity is clear: the prevalence of UBA1-specific E2s combined with the lower levels of UBA6 found in cells[63] explain why UBA6 is unable to compensate for the loss of UBA1. Conversely, the *in vitro* results presented here

suggest that non-specific E2s may be well compensated by UBA1 when UBA6 is lost. Therefore, in lieu of data supporting differential subcellular localisation of UBA1 and UBA6 which could affect non-specific E2s in a local environment, the downstream effects of UBA6 knockouts could be solely attributed to loss of BIRC6 and UBE2Z activity.

3.3.2. Mechanisms of E1-E2 specificity in ubiquitin E2s

The main contribution of this thesis towards the understanding of E1 specificity across ubiquitin E2s was the inclusion of domain swapped E1 chimeras. A similar approach was used on a smaller scale to identify the role of the UFD in driving specific E2 recruitment to both NAE1-UBA3[87] and UBA7[79,80]. A chimeric UBA6 containing the UBA1 SCCH domain was previously generated to facilitate crystallisation with FAT10[18], however its role in driving E2 specificity was not examined. From the chimera panel, it can now be seen that ubiquitin E2s show different preferences for E1 domains, which is instructive for the design of E2s with altered E2 specificities.

Given its role in E2 recruitment and driving specificity for E2s of parallel UBL cascades, it is unsurprising that for most of the E2s with a preference between UBA1 and UBA6, activity tracked with the E1 UFD. As demonstrated by the specificity-changing E2 mutants, these interactions are largely driven through matching the surface charge of the E2 ‘H1’ to the corresponding binding cleft within the UFD; the UBA6 UFD is incompatible with bulky charged residues. Interactions from the E2 ‘L2’ are also important, as evidenced by the ‘EE’ motif responsible for UBA6 selectivity in BIRC6. Here, the sidechain length is especially critical given the effect of shortening both residues by one carbon, as seen in dBIRC6.

The results from the chimeric BIRC6 constructs point towards the UFD interaction as more important than that at the SCCH for driving specificity. However, the E1 chimera panel showed that inclusion of the UBA6 UFD (which should be able to recruit BIRC6) does not restore activity with BIRC6. This could be explained by slight differences in how each UFD recruits and positions bound E2s for transthiolation, such that (for some E2s) even successful recruitment by the UFD of one E1 is not sufficient to stimulate activity at the SCCH domain of a different E1. This would be consistent with the observation of E2s within the E1 specificity panel which worked with both UBA1 and UBA6, but lost activity with some of the chimeras.

UBE2Z was found to use a different specificity mechanism to BIRC6, driven instead by the SCCH domain. Indeed, at the equivalent position in 'L2' where BIRC6 bears the specificity-defining 'EE' motif, UBE2Z contains the residues threonine and valine, which are not long enough to clash with the UBA1 UFD. The IP6 binding site within the UBA6 SCCH is a significant difference between the two E1s. Earlier crystal structures of UBA6 identified the unique IP6 binding pocket within the SCCH domain and showed that while this site is occupied prior to ubiquitin thiolation, IP6 must be released when the SCCH transitions into the 'down' conformation[66]. Our cryoEM data suggests that IP6 returns to UBA6 prior to or during transthiolation and could thereby contribute to specific E2 recruitment. Indeed, UBE2Z coordinates IP6 in our UbDha-crosslinked structure, and mutation of the coordinating residue lowers transthiolation activity. Therefore, IP6 itself may be the feature within the SCCH domain driving specific recruitment of UBE2Z to UBA6 instead of UBA1.

Finally, the effect of UBC extensions on E1 specificity of ubiquitin E2s is a novel finding of this study. Given the importance of the UBC N-terminus in E2 recruitment[17,87,88], one may well expect that N-terminal extensions would likely affect interactions with

E1s. Indeed, addition of an N-terminal GST tag to UBE2B reduces transthiolation efficiency[87], however the effect of these extensions on activity with UBA6 was not examined. In the case of UBE2Q, combined N- and C-terminal extensions determine E1 specificity through specific loss-of-function with UBA6. As such, addition of the UBE2Q N-terminal RWD domain could be used as an alternative to 'H1' mutations as a method for engineering E1-specificity into non-specific E2s. Given the prevalence of UBC extensions in many other ubiquitin E2s (**Table 1**), it is possible that other examples of specificity-altering extensions remain to be discovered.

3.3.3. Comparison of E1-E2 complex trapping strategies

This study presents the first use of the UbDha probe to stabilise E1-E2 interactions for structural studies. Recently, Ub-PSAN was used to stabilise the UBA1-Ubc4 complex for cryoEM studies[30]. The Ub-PSAN probe contains two targets for nucleophilic attack, allowing for sequential reaction with E2, then E1, to generate a faithful analogue of the E1-Ub-E2 transthiolation intermediate. However, multiple steps of chemical synthesis are required to generate the Ub-PSAN probe, and additional mutations to remove surface exposed cysteines were required to prevent off-target cross-linking[30].

As a result, UbDha has several practical advantages over Ub-PSAN, given that a simple single-step reaction is required to generate the probe from recombinantly expressed Ub G76C, and removal of surface cysteine residues was not required for the cross-linking reactions demonstrated in this thesis. Consequently, UbDha may be much better suited for use with larger E2s such as full-length BIRC6 and UBE2O which contain many additional cysteines.

On the other hand, Ub-PSAN produces a more faithful mimic of the transthiolation intermediate than UbDha[30]. Clearly E1 enzymes can accommodate non-native cross-

linking strategies to bind E2 enzymes, as has been previously established with disulfide cross-linking[27,79,80,82,83]. As UBA1 and UBA6 natively recognise a range of E2 enzymes, it is perhaps unsurprising that they can adapt to small deviations to cross-linker geometry. However, just because an E1-E2 complex can still form does not mean certain aspects of the interaction have been affected by the nature of the cross-linker. Two aspects of the E1-Ub-E2 complexes presented in this thesis showed unexpected variations between each other and previously reported structures.

First, each of the UbDha cross-linked cryoEM samples exhibited different occupancy of Ub^A in the E1 adenylation site (singly loaded for UBA6-UBE2Z, singly and doubly loaded for UBA6-BIRC6, doubly loaded for dUBA1-dBIRC6). Since all samples from this thesis were all UbDha cross-linked, these results suggest that the differential Ub^A occupancy may be driven by innate properties of E1 and E2 enzymes. However, without controls using other cross-linking methods, it cannot be ruled out that these effects were due to the use of the UbDha probe, especially given the coupling of adenylation and transthiolation reactions. Interestingly, ubiquitin G76A was shown to favour formation of a singly loaded E1 complex rather than the normal doubly loaded state[29], yet despite the similarity between UbDha and G76A, we observed doubly loaded states for the human and drosophila BIRC6 cross-linked samples. For comparison, the Ub-PSAN cross-linked UBA1-Ubc4 structure was found in both singly and doubly loaded states, with a roughly equal distribution of particles between the two states[30].

Second, the 3D variability analysis revealed significant differences in both magnitude and direction of Ub^T motion between UbDha and Ub-PSAN cross-linked complexes. The range of Ub^T motion that observed in the data presented here was reduced and along a different axis to that from UBA1-Ubc4[30]. It is tempting to speculate that Ub^T

may indeed adopt different ‘pre-transfer’ and ‘post-transfer’ positions for different E1-E2 combinations, as was suggested in the discussion of a previous E1-E2 complex involving *S. pombe* Ubc15[89]. However, the present comparisons are limited to a small number of structures which have been cross-linked by different probes. Only two other structures with Ub^T mimics are available (UBA1-Ubc4[30] and UBA1-Cdc34[27]), both of which are in good agreement regarding Ub^T positioning. It should be noted that when not bound to an E1 or an E3, E2-specific differences have been seen for positioning of thioester-linked ubiquitin[38].

A direct comparison of structures of identical E1-E2 pairs with both UbDha and Ub-PSAN probes is needed to fairly investigate the effect of cross-linker geometry on both Ub^A occupancy and Ub^T dynamics. Additionally, applying either cross-linking method to a single E2 with both UBA1 and UBA6 would reveal any E1-specific effects on these aspects of the E1-Ub-E2 complex.

4. UBA6 and BIRC6

4.1. Introduction

4.1.1. Structure and function of BIRC6

The second half of this thesis focuses on a specific E1-E2 pair, UBA6 and BIRC6. Analysis of gene essentiality across human cancer cell lines has revealed a UBA6-dependent ubiquitination pathway exploited for survival in cell lines exhibiting aneuploidy[90]. Interestingly, this pathway involves only one of the two UBA6-specific E2s, BIRC6. Indeed, further analysis of the DepMap database[91] (Paul Elliott and Cara Ellison) revealed a significantly stronger correlation between UBA6 and BIRC6 than any other UBA6-active E2 (**Fig. 25a**).

UBA6's co-dependency with BIRC6 for cancer cell survival can be understood when considering the context of the known cellular functions of BIRC6. Recent studies have established BIRC6 as a bona-fide inhibitor of apoptosis (IAP), directly regulating caspases coordinating apoptosis[76–78,92]. Structural studies were key in revealing the intricate architecture of BIRC6 and the roles each domain plays in the recognition and ubiquitination of caspases[76–78,92] (**Fig. 25b**). BIRC6 contains a baculoviral inhibitor of apoptosis repeat (BIR) domain which binds activated caspases with nanomolar affinity. Like XIAP, binding of the BIRC6 BIR domain directly inhibits caspase activity[78,93–95]. In addition, while other IAPs such as XIAP and cIAP1/2 are E3s[96], BIRC6 contains an internal E2 UBC domain and therefore directly ubiquitinates caspases. As such, BIRC6 antagonises cell death signalling through direct inhibition by its BIR domain and ubiquitination by its UBC domain. BIRC6's role in inhibiting cell death is exploited by BIRC6-dependent cancer cell lines, as evidenced by an increase in the proportion of

cells undergoing early apoptosis when BIRC6 is knocked out, which also corresponds with a significant drop in cell viability[90].

BIRC6 has also been implicated in pathways beyond regulating cell death. Recent studies showed that BIRC6 works in concert with UBA6 to monoubiquitinate the autophagy marker LC3B-I[97], the precursor for LC3B-II[98], a protein involved in the assembly of autophagosomes[98,99]. LC3B-1 ubiquitination by BIRC6 primes it for degradation, removing the precursor for autophagosome formation and thereby reducing autophagic flux[97]. Consequently, knockout of BIRC6 promotes removal of autophagy substrates such as ubiquitinated protein aggregates[97].

In addition, genetic studies in mice reveal that BIRC6 is indispensable for embryonic viability. Mouse embryos containing BIRC6 mutants lacking its UBC domain exhibit defects in placental and yolk sac tissues, activation of mitochondrial apoptotic pathways, and p53 stabilization, culminating in loss of viability during early development[100].

In summary, the cellular functions of BIRC6, integrating both apoptotic suppression and autophagic control (**Fig. 25c**), along with its essential role in embryogenesis, underscore the biological and therapeutic importance of dissecting the UBA6-BIRC6 pathway. Previous data from the lab suggested that the UBA6 and BIRC6 may have a strong interaction, as UBA6 was identified as one of the top interaction partners of BIRC6 by affinity-purified mass spectrometry[78]. This, together with observations from our UbDha cross-linking reactions, led us to investigate the UBA6-BIRC6 interaction in more detail.

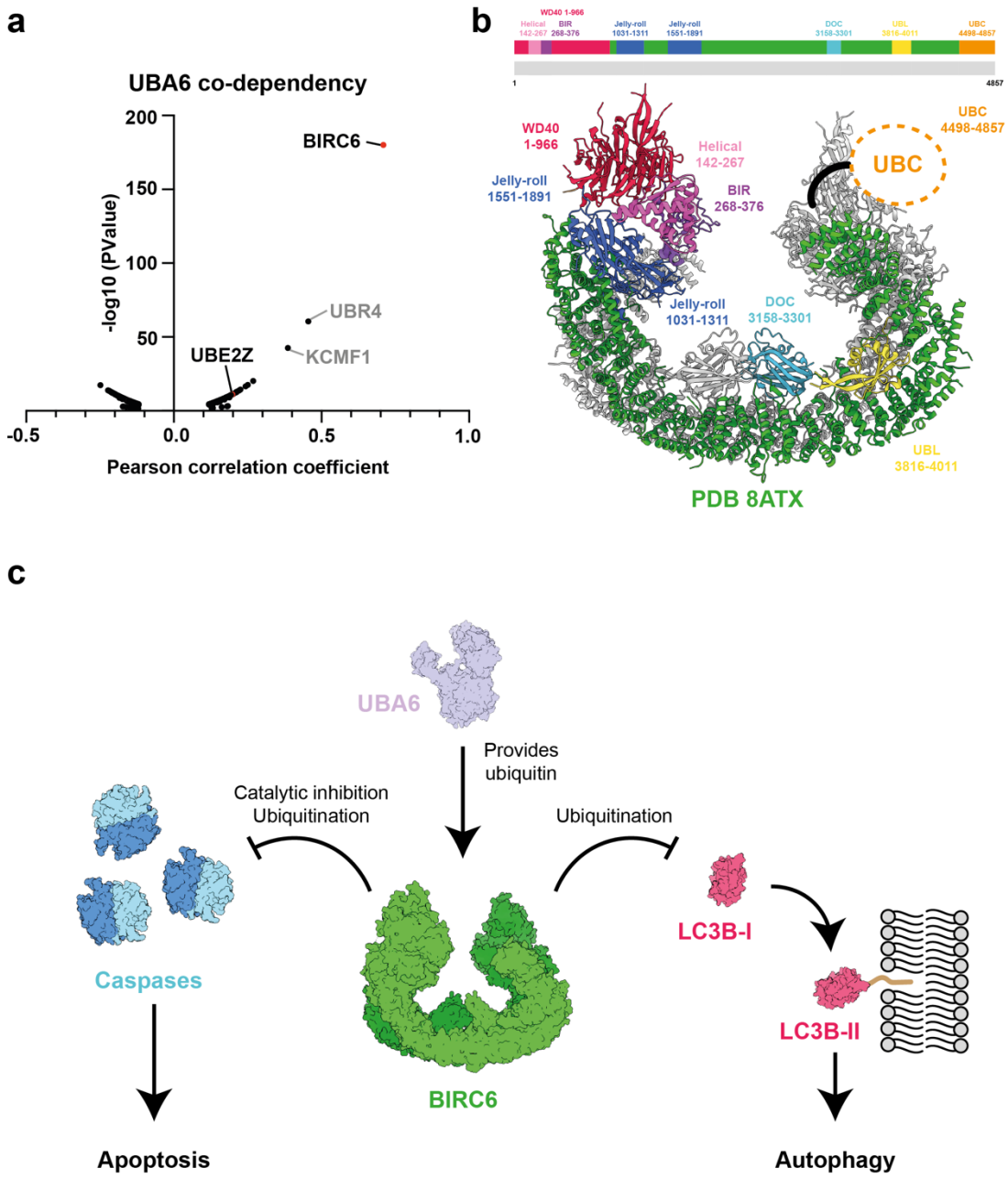
a
UBA6 co-dependency
200
150
100
50
-log10 (PValue)
BIRC6
UBR4
KCMF1
UBE2Z
-0.5
0.0
0.5
1.0
Pearson correlation coefficient
b
WD40 1-966
Helical 142-267
BIR 268-376
Jelly-roll 1031-1311
Jelly-roll 1551-1891
DOC 3158-3301
UBL 3816-4011
UBC 4498-4857
1
4857
WD40 1-966
Helical 142-267
BIR 268-376
Jelly-roll 1551-1891
Jelly-roll 1031-1311
DOC 3158-3301
UBL 3816-4011
UBC 4498-4857
UBC
PDB 8ATX
c
UBA6
Provides ubiquitin
Catalytic inhibition Ubiquitination
Ubiquitination
Caspases
BIRC6
LC3B-I
LC3B-II
Apoptosis
Autophagy

Figure 25. Importance of UBA6-BIRC6 pathways

a. Analysis of gene co-depencency with UBA6 across cancer cell lines across the DepMap database[91].

b. Domain schematic and atomic model of full-length BIRC6 (PDB: 8ATX[77]).

c. Schematic of two known cellular functions of BIRC6, inhibiting both apoptotic and autophagy pathways. Direct inhibition and ubiquitination of caspases by BIRC6 prevents them from initiating and executing apoptosis. Ubiquitination of the LC3B-II precursor, LC3B-I, limits autophagic flux.

4.1.2. The thioester switch: regulation of E1-E2 affinity during transthiolation

A key aspect of the interaction between UBA6 and BIRC6 explored in the following chapter is how E1-E2 binding is regulated throughout transthiolation. For some E1-E2 pairs, the UFD interaction alone forms a stable E1-E2 complex[24,101,102]. However, in the case of UBA1/UBA6, E2s do not interact strongly with unloaded E1[13,103,104]. While many of the E1-E2 interactions in the ubiquitin cascade have not been characterised, a recent study has shown that UBE2L3 indeed binds unloaded UBA1 weakly with a Kd of ~17 μM[105]. The affinity of E2s to the doubly loaded E1 complex is thought to be much higher[87,106], however the mechanism by which this is achieved is not fully understood.

After ubiquitin transfer has occurred, the affinity of the E1 to the loaded E2 must drop again to allow the product to be released. For UBA1, this is mediated by the loss of two E1-Ub^T interactions after transthiolation has occurred: First, the thioester bond from the ubiquitin C-terminus to the E1 catalytic cysteine is broken. Second, movement of Ub^T to the 'post-transfer' site loses contacts from Ub^T to the E1 FCCH domain (**Fig. 26a, b**)[27,89]. Without additional interfaces increasing E1-E2 affinity the loaded E2 dissociates from the E1. This mechanism has been described as a 'thioester switch', tuning the E1-E2 affinity to ensure recruitment of substrates and release of products from the E1 enzyme[13,25].

What about the E1s which have stronger interactions with their E2s? E2 release from both NAE1-UBA3 and SAE1-UBA2 is thought to coincide with reversal of the lateral UFD rotation which takes place during E2 recruitment, restoring the E1 to its resting conformation[25] (**Fig. 26c**). Superimposing NEDD8-loaded UBE2M (PDB: 4P5O[107])

onto the resting UFD orientation of NAE1-UBA3 (PDB: 1TT5[17]) shows that binding of the UBL-loaded E2 is incompatible, with severe clashes present between NEDD8 and the AAD (**Fig. 26d**). This is thought to drive loaded E2 release while also preventing return of the thioester product to the E1 active site.

Proper functioning of the E1 thioester switch is critical to avoid product inhibition of E1 enzymes[26,108]. The NAE1-UBA3 and SAE1-UBA2 systems demonstrate that when particularly strong E1-E2 interactions are present, more drastic thioester switching mechanisms are required to ensure proper functioning of the E1 enzyme (**Fig. 26e, f**). The following chapter will outline the discovery of a unique high-affinity E1-E2 interaction within the ubiquitin cascade, and corresponding features on the E1 which prevent inhibition of the pathway.

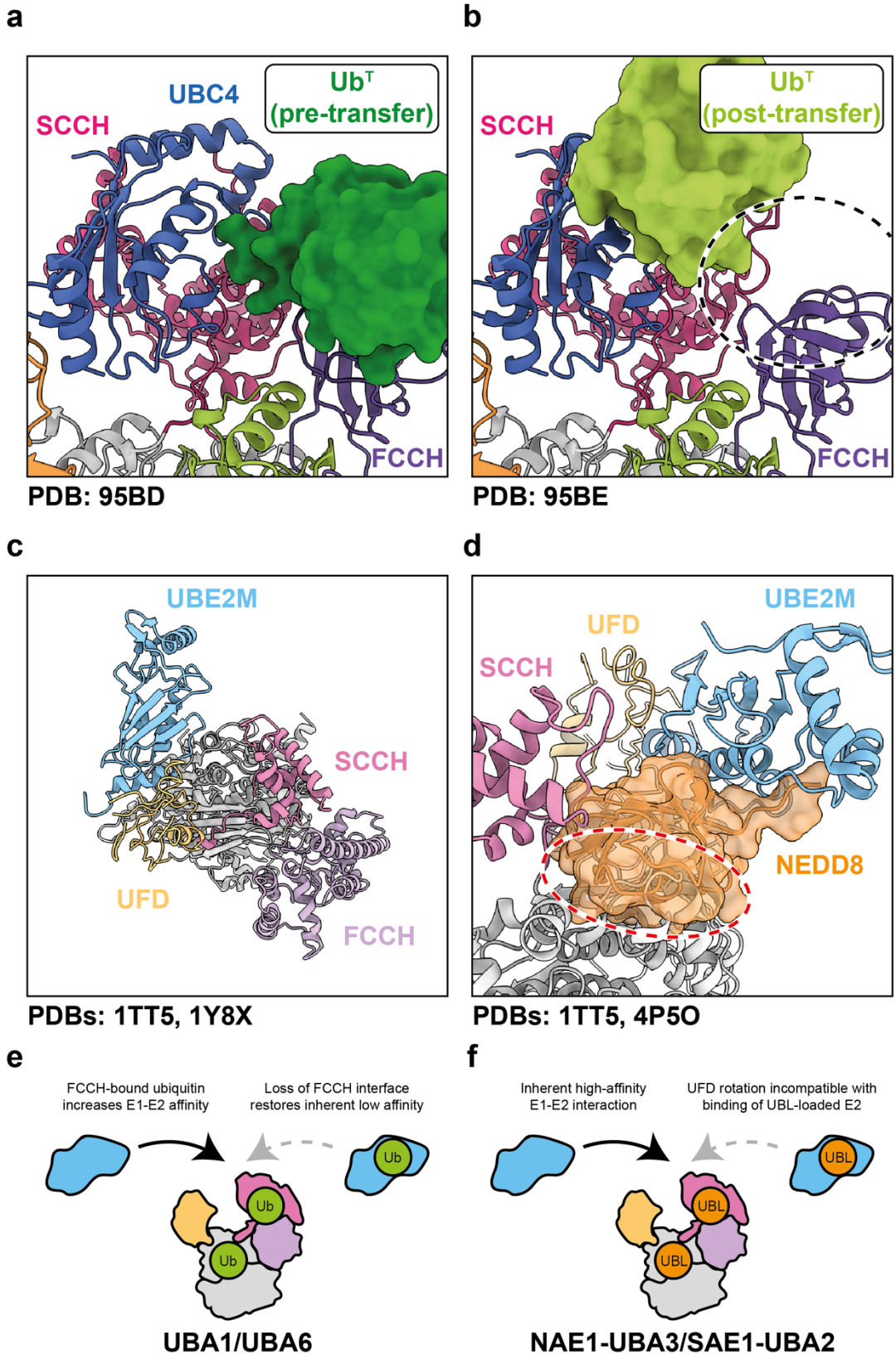
a
b
UBC4
SCCH
UbT
(pre-transfer)
FCCH
PDB: 95BD
SCCH
UbT
(post-transfer)
FCCH
PDB: 95BE
c
d
UBE2M
SCCH
UFD
FCCH
PDBs: 1TT5, 1Y8X
UBE2M
UFD
SCCH
NEDD8
PDBs: 1TT5, 4P5O
e
FCCH-bound ubiquitin
increases E1-E2 affinity
Loss of FCCH interface
restores inherent low affinity
Ub
Ub
Ub
UBA1/UBA6
f
Inherent high-affinity
E1-E2 interaction
UFD rotation incompatible with
binding of UBL-loaded E2
UBL
UBL
UBL
NAE1-UBA3/SAE1-UBA2

Figure 26. Thioester switching mechanisms in UBA1 and NAE1-UBA3

a-b. Structures of ubiquitin-PSAN cross-linked UBA1-Ubc4, with the transferred ubiquitin in the pre- (a, PDB: 9B5D[30]) and post-transfer (b, PDB: 9B5D[30]) states.

c-d. Composite models of NAE1-UBA3 bound to unloaded (c, PDBs: 1TT5[17], 1Y8X[26]) and loaded (d, PDBs: 1TT5[17], 4P5O[107]) UBE2M.

e-f. Cartoons summarising the two thioester switching mechanisms. For UBA1, innate low E1-E2 affinities are enhanced by E1-loading, then after post ubiquitin transfer. For NAE1-UBA3, a large rotation of the UFD after thioester transfer excludes loaded E2s from binding.

4.2. Results

4.2.1. BIRC6 binds UBA6 in the absence of ubiquitin

During the preparation of the UbDha cross-linked UBA6-BIRC6 complex, coelution of free BIRC6 with UBA6 was observed (**Fig. 10c**). Intrigued by this, other E1-E2 pairs were tested for similar coelution behaviour. First, BIRC6 was confirmed to only coelute with its cognate E1, UBA6, and not UBA1 (**Fig. 27a, b**). Further tests with the UBA6-compatible E2s UBE2Z and UBE2D2 showed no sign of coelution with UBA6 (**Fig. 27c, d**). Finally, no coelution of drosophila BIRC6 with either UBA1 orthologue was observed (consistent with the preparation of the UbDha cross-linked sample, **Fig. 27e, f**), however the interaction with UBA6 was still present, albeit weaker than for human BIRC6 (**Fig. 27g**).

Together, these results show that the majority of E2s tested behaved as expected, in that they do not form a stable interaction with E1 enzymes in the absence of ubiquitin. The behaviour of BIRC6 and UBA6 appears to be unique and is not conserved to the drosophila orthologue of BIRC6.

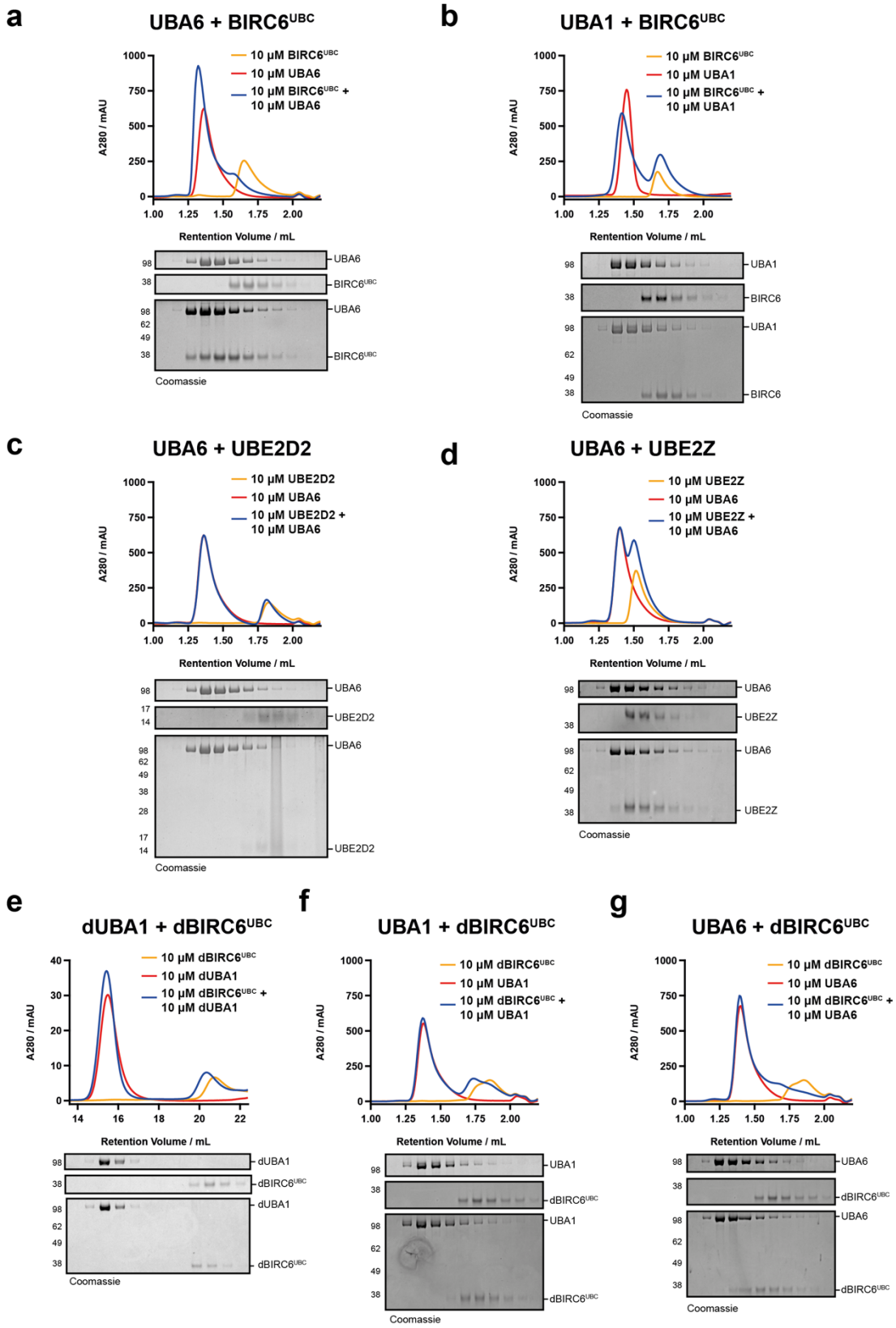
a
UBA6 + BIRC6UBC
10 µM BIRC6UBC
10 µM UBA6
10 µM BIRC6UBC + 10 µM UBA6
A280 / mAU
Rentention Volume / mL
UBA6
BIRC6UBC
Coomassie
b
UBA1 + BIRC6UBC
10 µM BIRC6UBC
10 µM UBA1
10 µM BIRC6UBC + 10 µM UBA1
A280 / mAU
Rentention Volume / mL
UBA1
BIRC6
Coomassie
c
UBA6 + UBE2D2
10 µM UBE2D2
10 µM UBA6
10 µM UBE2D2 + 10 µM UBA6
A280 / mAU
Rentention Volume / mL
UBA6
UBE2D2
Coomassie
d
UBA6 + UBE2Z
10 µM UBE2Z
10 µM UBA6
10 µM UBE2Z + 10 µM UBA6
A280 / mAU
Rentention Volume / mL
UBA6
UBE2Z
Coomassie
e
dUBA1 + dBIRC6UBC
10 µM dBIRC6UBC
10 µM dUBA1
10 µM dBIRC6UBC + 10 µM dUBA1
A280 / mAU
Retention Volume / mL
dUBA1
dBIRC6UBC
Coomassie
f
UBA1 + dBIRC6UBC
10 µM dBIRC6UBC
10 µM UBA1
10 µM dBIRC6UBC + 10 µM UBA1
A280 / mAU
Retention Volume / mL
UBA1
dBIRC6UBC
Coomassie
g
UBA6 + dBIRC6UBC
10 µM dBIRC6UBC
10 µM UBA6
10 µM dBIRC6UBC + 10 µM UBA6
A280 / mAU
Retention Volume / mL
UBA6
dBIRC6UBC
Coomassie

Figure 27. Unlike other E1-E2 combinations, BIRC6 forms a stable interaction with UBA6 during SEC

UV absorbance profiles and SDS-PAGE of corresponding fractions for size exclusion chromatography of the following E1-E2 pairs:

a. UBA6 + BIRC6

b. UBA1 + BIRC6

c. UBA6 + UBE2D2

d. UBA6 + UBE2Z

e. dUBA1 + dBIRC6

f. UBA1 + dBIRC6

g. UBA6 + dBIRC6

Experiments in panels (a, b, c, d, f, g) were performed using a micro S200 column, while experiment (e) was performed on a tricorn S200 column. While the A280 absorbance trace in panel (b) shows a shift for UBA1 in the presence of BIRC6, no coelution of the proteins was observed in SDS-PAGE analysis of the resulting fractions, and therefore the apparent shift may be an artifact caused by improper loading of the 100 uL sample loop.

4.2.2. BIRC6 has priority for UBA6 over other E2s

Next, the functional consequences of the unusually strong UBA6-BIRC6 interaction were considered. Stronger binding of BIRC6 to UBA6 may allow it to gain priority for transthiolation over other E2s as initial recruitment is driven by affinity. To test this, a single-turnover E2 competition assay was designed. Treatment of UBA6 with EDTA inhibits the Mg^{2+}-dependent adenylation of ubiquitin, thereby only allowing a single turnover of E1-E2 transthiolation to occur. As a result, the amount of loaded E2 observed in the competition assay reflects the initial competition for recruitment to the E1~Ub complex and would not be affected by E2-specific differences in rates of transthiolation.

When combined with BIRC6, loading of UBE2D2 by UBA6 was drastically reduced, whereas BIRC6 loading was unaffected (**Fig. 28a**, lanes i, ii, v). In comparison, addition of UBE2Z did not show a pattern of preferential ubiquitin transfer (**Fig. 28a**, lanes i, iii, vi). The priority of BIRC6 can be attributed to its high-affinity interaction with UBA6, as the A4575D mutant (which shall be confirmed later to interact with UBA6 significantly weaker than BIRC6 WT) was not able to outcompete UBE2D2 (**Fig. 28a**, lanes i, iv, vii).

To supplement this, a higher-throughput multiple turnover competition experiment was designed, in which each UBA6-active E2 identified in the specificity panel (**Fig. 8**) was mixed first with catalytically inactive BIRC6 (BIRC6 C4666A), then allowed to react with UBA6 (**Fig. 28b**). Despite robust loading of UBA6, all the E2s tested showed lower levels of thioester formation when BIRC6 C4666A was present, indicating that BIRC6 may indeed be able outcompete all other UBA6-active E2s for access to UBA6. BIRC6

did not affect UBE2D2 loading when UBA1 was used instead of UBA6, confirming that the priority affect was UBA6-specific.

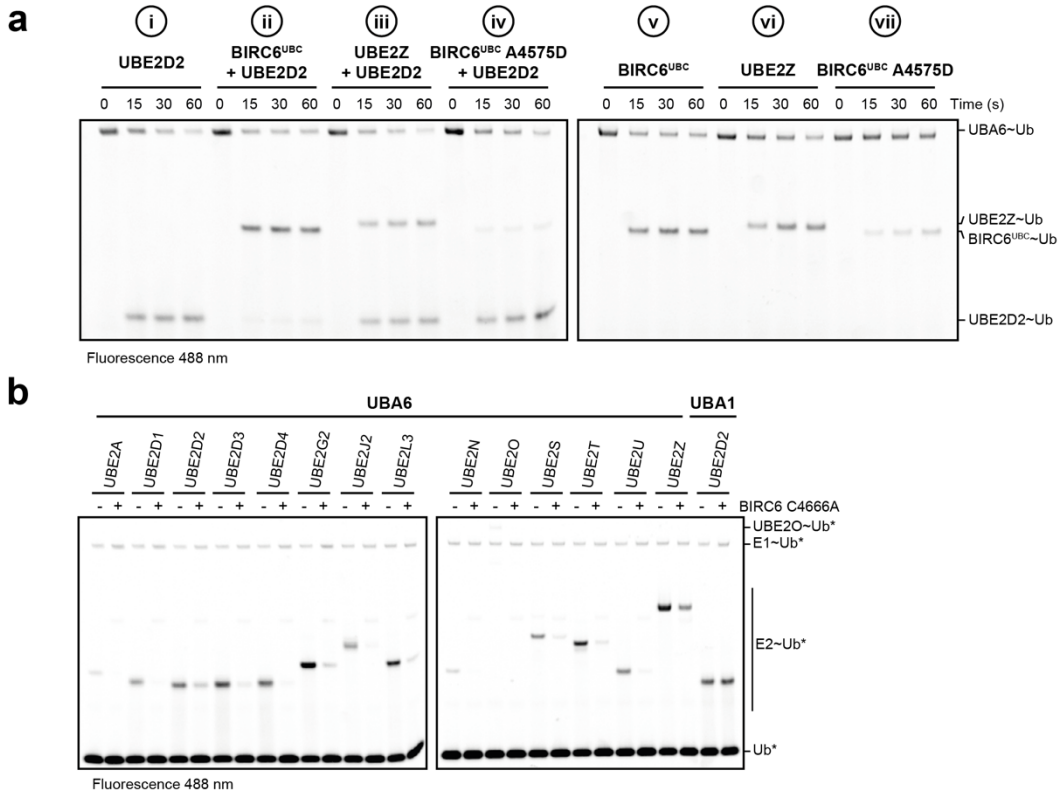

Figure 28. BIRC6 has priority over other E2s for UBA6

a. Fluorescence image of SDS-PAGE analysis of single-turnover transthiolation to UBE2D2 alone and in combination with BIRC6, UBE2Z and BIRC6 A4575D (left, i-iv). Control reactions for BIRC6, UBE2Z and BIRC6 A4575D receiving ubiquitin from UBA6 (right, v-vii). Due to the low levels of ubiquitin transfer under single-turnover conditions, reactions were performed with fluorescently labelled ubiquitin and were not quantified with Coomassie staining. Reactions were performed in technical triplicate, one representative gel is shown.

b. Fluorescence image of SDS-PAGE analysis of multiple turnover transthiolation from UBA6 to UBA6-active E2s with and without BIRC6 C4666A. A control reaction with UBA1 is included. Reactions were performed in technical triplicate, one representative gel is shown.

4.2.3. Structure of the non-covalent UBA6-BIRC6 complex

Next, cryoEM was used to better understand the non-covalent interaction between UBA6 and BIRC6 in the absence of ubiquitin. During the initial optimisation of UbDha cross-linking a cryoEM dataset was collected on a sample with extremely low cross-linking efficiency, which was attributed to a bad batch of UbDha probe. While very little UBA6-UbDha-BIRC6 had been formed, coelution of BIRC6 with UBA6 was still observed, suggesting that the non-covalent complex would be present in the sample (**Fig. 29a**). Analysis of particles picked from this dataset (**Fig. 29b**) showed no sign of ubiquitin at either the adenylation or transthiolation sites. Instead, UBA6 was found in a range of different states, from no E2 bound ($UBA6^{APO}$, **Fig. 29c**) to two distinct UBA6-BIRC6 binding modes ($UBA6\text{-}BIRC6^{IN/OUT}$, **Fig. 29d, e**). Detailed descriptions of data processing and structure validation can be found in **Figures 30a-d, 31 a-c**.

$UBA6^{APO}$

Refinement of the $UBA6^{APO}$ particle stack produced a map at a nominal resolution of 3.2 Å. The corresponding atomic model was in good agreement with the previously reported UBA6 crystal structure (PDB: 7SOL[66]), however the UFD was slightly rotated inwards (**Fig. 32a**). While this represents a slight difference between the consensus UFD position from our data to the that seen in the crystal structure, local resolution of the UFD was poor, indicative of flexibility. As before, this was further using the 3D variability analysis tool in cryoSPARC, which is discussed in **Chapter 4.2.4**.

$UBA6\text{-}BIRC6^{IN}$

The $UBA6\text{-}BIRC6^{IN}$ map was refined to 3.4 Å, revealing an overall arrangement that is nearly identical to the UBA6-UbDha-BIRC6 complex. The only striking difference between the two models, besides the absence of ubiquitin, was the conformation of

the BIRC6 ‘L6’ (**Fig. 32b**). In contrast to the UbDha cross-linked structure, in which ‘L6’ opens to accommodate ubiquitin, ‘L6’ was closed in the UBA6-BIRC6^{IN} structure. The closed conformation matches that seen in a previously reported crystal structure of the BIRC6 UBC domain (PDB: 3CEG[109]). Overall, this structure demonstrates that, even in the absence of ubiquitin, BIRC6 can fully engage with UBA6 at both UFD and SCCH domains in the same manner as during ubiquitin transfer.

UBA6-BIRC6^{OUT}

The second BIRC6 conformation, refined to 3.6 Å, featured a novel E1-E2 configuration not observed in previous structures. Compared to the UBA6-BIRC6^{IN} state, BIRC6 was rotated 16° upwards, away from the UBA6 catalytic site (**Fig. 32c**). The UBA6 UFD was rotated out together with BIRC6, so that the interface with the BIRC6 ‘H1’ was generally maintained (**Fig. 32d**), however BIRC6 was placed at a slightly different angle, thereby introducing larger CA deviations towards the SCCH-facing side of BIRC6 (**Fig. 32d**). This coincided with lower local resolution throughout the BIRC6 density, which can be attributed to an increase in flexibility due to loss of stabilising contacts at the SCCH domain. Further 3D variability analysis of the BIRC6 movement is discussed in **Chapter 4.2.4**.

In contrast to the SCCH interface present in UBA6-BIRC6^{IN} and the UbDha cross-linked structures, the UBA6 Cys-cap loop was found sandwiched between the active sites of UBA6 and BIRC6 (**Fig. 32e**). This is the first example of the Cys-cap loop being observed in an E2-bound structure of an E1 enzyme, as in all previous structures the Cys-cap loop has been displaced from the active site[27,30,79,80,83,89].

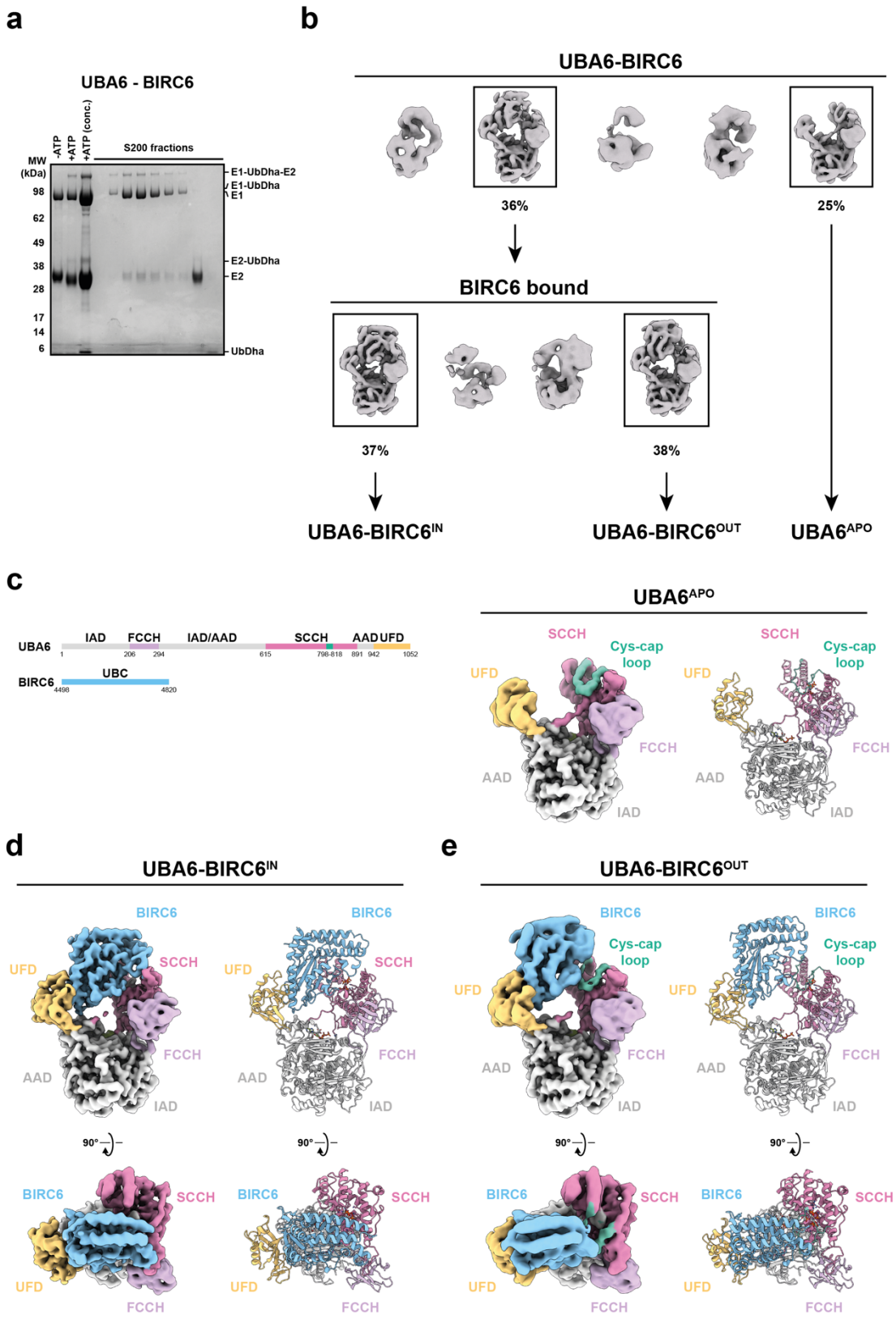
a
UBA6 - BIRC6
-ATP
+ATP
+ATP (conc.)
S200 fractions
MW (kDa)
98
62
49
38
28
17
14
6
E1-UbDha-E2
E1-UbDha
E1
E2-UbDha
E2
UbDha
b
UBA6-BIRC6
36%
25%
BIRC6 bound
37%
38%
UBA6-BIRC6IN
UBA6-BIRC6OUT
UBA6APO
c
UBA6
IAD
FCCH
IAD/AAD
SCCH
AAD
UFD
1
206
294
615
798-818
891
942
1052
BIRC6
UBC
4498
4820
UBA6APO
SCCH
Cys-cap loop
UFD
FCCH
AAD
IAD
d
UBA6-BIRC6IN
BIRC6
SCCH
UFD
FCCH
AAD
IAD
90°
e
UBA6-BIRC6OUT

Figure 29. CryoEM structures of non-covalent UBA6-BIRC6 interactions

a. SDS-PAGE of an early attempt at UBA6-UbDha-BIRC6 cross-linking with low cross-linking efficiency. The sample was still applied to SEC and fractions containing BIRC6 coeluting with UBA6 were applied to cryoEM grids.

b. Classed produced by 3D classification and heterogeneous refinement of the UBA6-BIRC6 dataset.

c. Domain schematic of UBA6 and BIRC6 constructs used (left). CryoEM density map and atomic model for $UBA6^{APO}$ (right).

d. CryoEM density map and atomic model for UBA6-$BIRC6^{IN}$.

e. CryoEM density map and atomic model for UBA6-$BIRC6^{OUT}$.

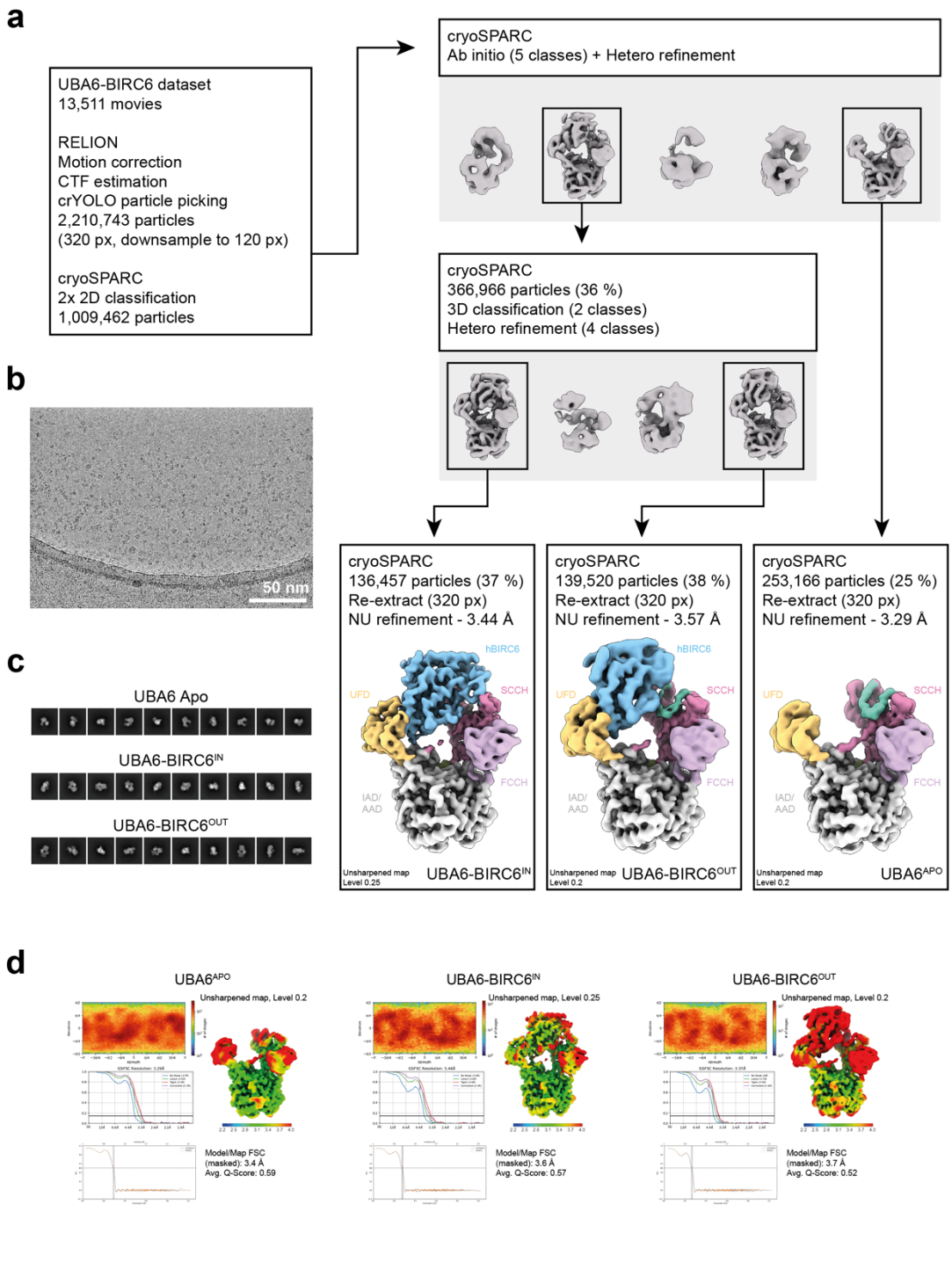
a
UBA6-BIRC6 dataset
13,511 movies
RELION
Motion correction
CTF estimation
crYOLO particle picking
2,210,743 particles
(320 px, downsample to 120 px)
cryoSPARC
2x 2D classification
1,009,462 particles
cryoSPARC
Ab initio (5 classes) + Hetero refinement
cryoSPARC
366,966 particles (36 %)
3D classification (2 classes)
Hetero refinement (4 classes)
b
50 nm
cryoSPARC
136,457 particles (37 %)
Re-extract (320 px)
NU refinement - 3.44 Å
cryoSPARC
139,520 particles (38 %)
Re-extract (320 px)
NU refinement - 3.57 Å
cryoSPARC
253,166 particles (25 %)
Re-extract (320 px)
NU refinement - 3.29 Å
c
UBA6 Apo
UBA6-BIRC6IN
UBA6-BIRC6OUT
hBIRC6
UFD
SCCH
FCCH
IAD/
AAD
Unsharpened map
Level 0.25
UBA6-BIRC6IN
Unsharpened map
Level 0.2
UBA6-BIRC6OUT
Unsharpened map
Level 0.2
UBA6APO
d
UBA6APO
Unsharpened map, Level 0.2
Model/Map FSC
(masked): 3.4 Å
Avg. Q-Score: 0.59
UBA6-BIRC6IN
Unsharpened map, Level 0.25
Model/Map FSC
(masked): 3.6 Å
Avg. Q-Score: 0.57
UBA6-BIRC6OUT
Unsharpened map, Level 0.2
Model/Map FSC
(masked): 3.7 Å
Avg. Q-Score: 0.52

Figure 30. CryoEM processing and validation for the UBA6-BIRC6 sample

a. Preprocessing, classification and refinement steps used to generate consensus maps for $UBA6^{APO}$, $UBA6\text{-}BIRC6^{IN}$ and $UBA6\text{-}BIRC6^{OUT}$.

b. A representative micrograph image.

c. Representative 2D classes for particles used in each class.

d. Particle orientation distribution diagram, local resolution map, GSFSC and model-map FSC curves for each consensus map.

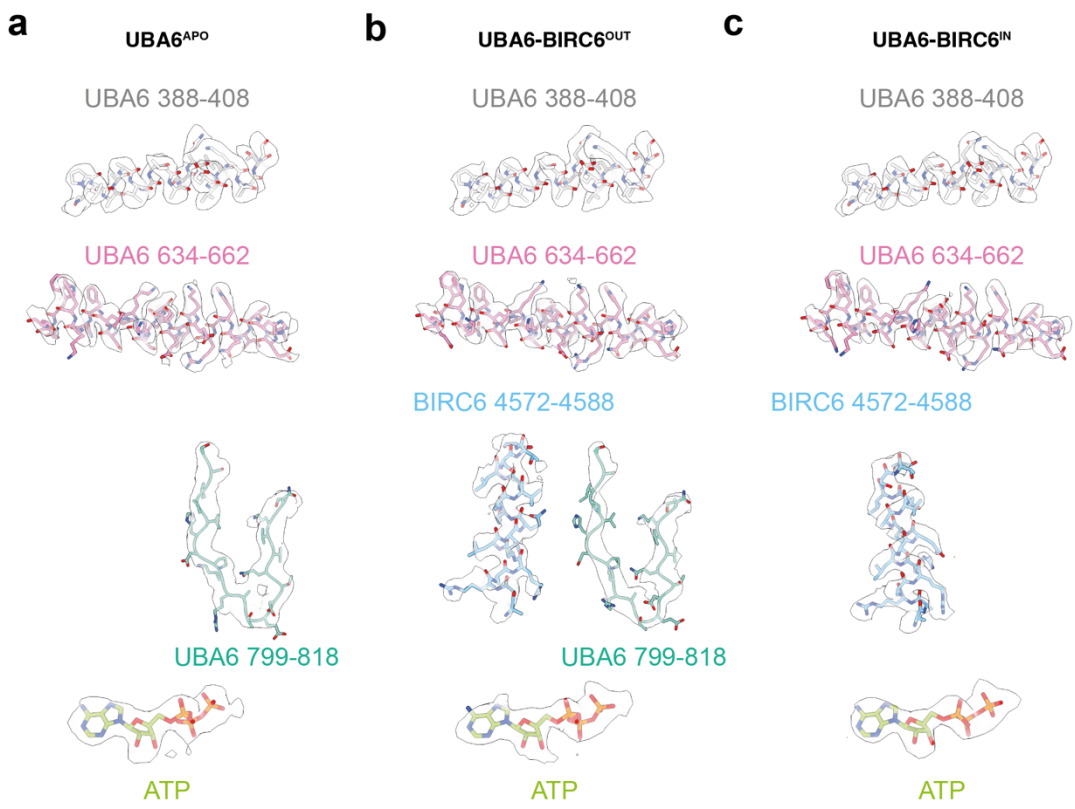

Figure 31. Representative densities for selected regions within UBA6-BIRC6 structures

Cryo-EM density and associated atomic model for selected regions in UBA6^{APO} (a), UBA6-BIRC6^{OUT} (b), and UBA6-BIRC6^{IN} structures: UBA6 core (residues 388-406), UBA6 SCCH domain (residues 634-662), BIRC6 helix 1 (residues 4572-4588), and ATP.

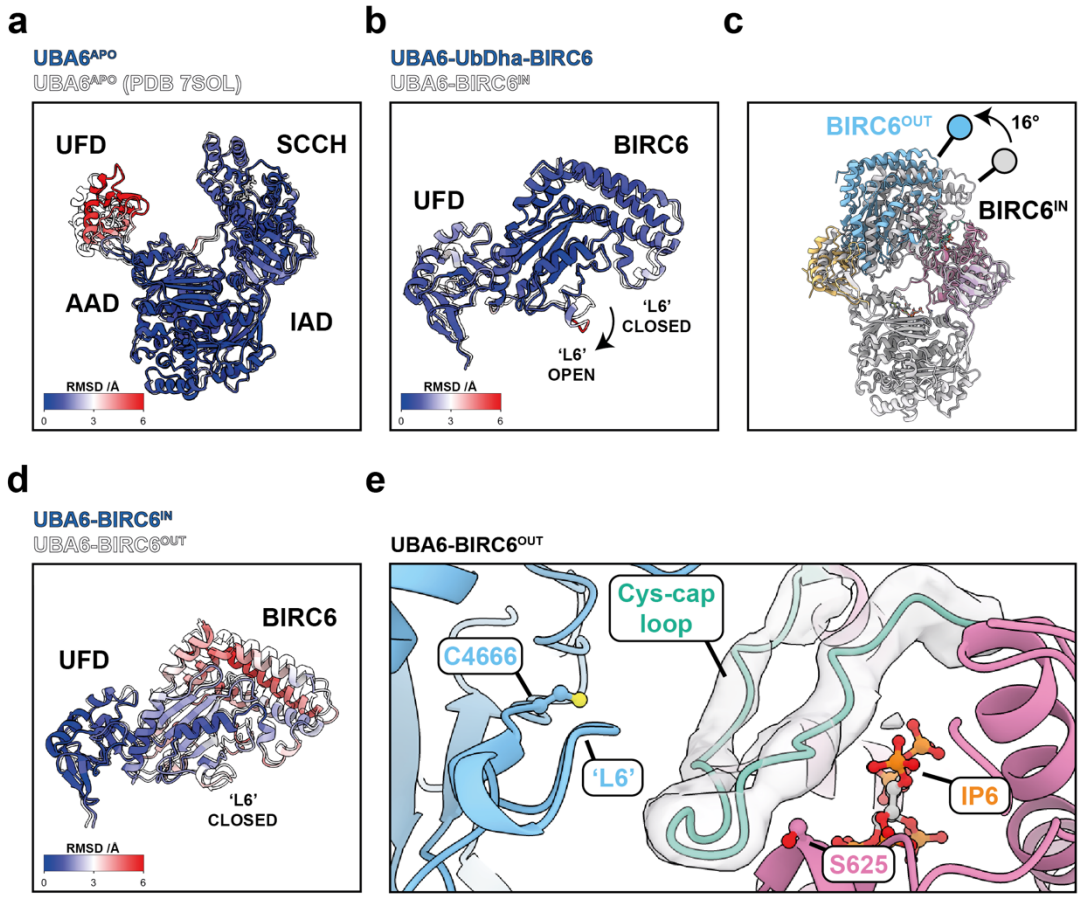
a
UBA6APO
UBA6APO (PDB 7SOL)
UFD
SCCH
AAD
IAD
RMSD /A
0
3
6
b
UBA6-UbDha-BIRC6
UBA6-BIRC6IN
BIRC6
UFD
'L6'
CLOSED
'L6'
OPEN
RMSD /A
0
3
6
c
BIRC6OUT
16°
BIRC6IN
d
UBA6-BIRC6IN
UBA6-BIRC6OUT
BIRC6
UFD
'L6'
CLOSED
RMSD /A
0
3
6
e
UBA6-BIRC6OUT
Cys-cap
loop
C4666
'L6'
IP6
S625

Figure 32. Comparing UBA6 and BIRC6 conformations from the non-covalent cryoEM dataset

a. Cα RMSD between the UBA6^{APO} model and a previously reported UBA6 crystal structure (PDB: 7SOL[66]).

b. Cα RMSD between the UBA6 UFD and BIRC6 in the UbDha cross-linked structure and the UBA6-BIRC6^{IN} state.

c. Alignment of the UBA6-BIRC6$^{IN/OUT}$ states. The angle between BIRC6 in each state is annotated.

d. Cα RMSD between the UBA6 UFD and BIRC6 in the UBA6-BIRC6$^{IN/OUT}$ states.

e. Close-up view of the UBA6 Cys-cap loop within the UBA6-BIRC6^{OUT} state.

4.2.4. 3D variability analysis of UBA6^{APO} and UBA6-BIRC6^{OUT}

3D variability analysis of UBA6^{APO} captured a claw-like motion of the UFD and SCCH domains, modulating the width of the E2-binding cavity of UBA6 (**Fig. 33a**). Concerted rotations of the UFD and SCCH domains by 14° and 6° narrow the cavity from a maximum diameter of ~41 Å to ~33 Å (**Fig. 33b**). Interestingly, the range of UFD motion for UBA6^{APO} correspond directly to the positions observed in the two UBA6-BIRC6$^{IN/OUT}$ states (**Fig. 33c**). Overall, the mobility of the UFD and SCCH domains observed across these datasets highlights the inherent structural plasticity of UBA6 and may additionally contribute towards its ability to accommodate E2s of different sizes.

In contrast to the rigidly bound UBA6-BIRC6^{IN} state, analysis of UBA6-BIRC6^{OUT} particles revealed a lateral rotation of the UBA6 UFD which was accompanied by the bound BIRC6 sliding across the E1 active site (**Fig. 33d**). While the furthest tip of BIRC6 travels 16 Å between either end of the 9° arc of UFD rotation (**Fig. 33e**), Cα RMSD comparisons show that the UFD interaction is maintained throughout (**Fig. 33f**).

Overall, the non-covalent UBA6-BIRC6 interaction appears much more dynamic than the transthiolation mimic state captured by the UbDha probe. It is unclear whether UBA6-BIRC6 can exchange between BIRC6$^{IN/OUT}$ states while remaining bound, however it may be the case that UBA6-BIRC6^{OUT} represents an initial recruitment stage of the interaction, and subsequent exclusion of the Cys-cap loop leads to formation of the BIRC6^{IN} conformation and ubiquitin transfer.

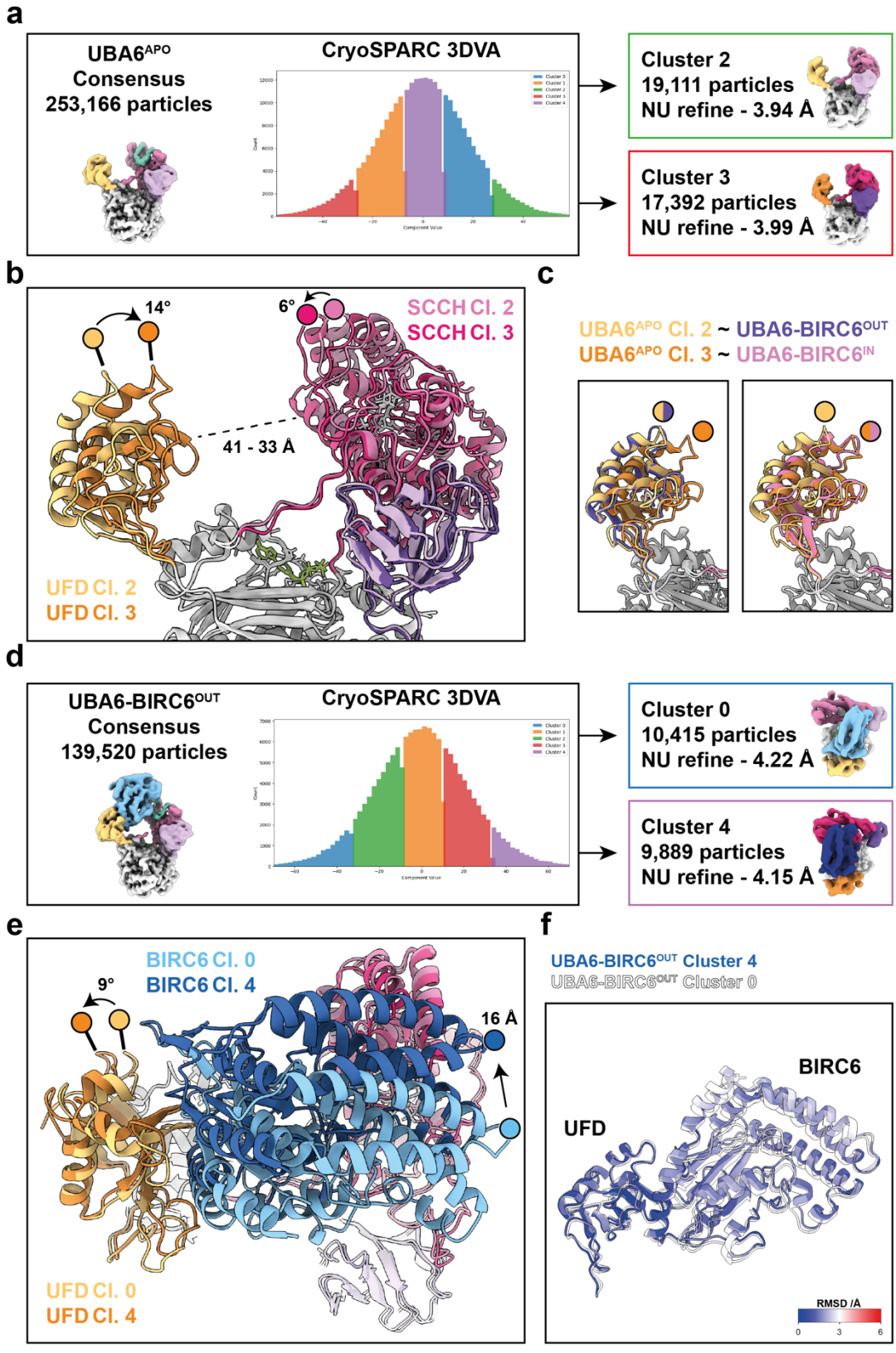
a
UBA6APO
Consensus
253,166 particles
CryoSPARC 3DVA
Cluster 2
19,111 particles
NU refine - 3.94 Å
Cluster 3
17,392 particles
NU refine - 3.99 Å
b
14°
6°
SCCH Cl. 2
SCCH Cl. 3
41 - 33 Å
UFD Cl. 2
UFD Cl. 3
c
UBA6APO Cl. 2 ~ UBA6-BIRC6OUT
UBA6APO Cl. 3 ~ UBA6-BIRC6IN
d
UBA6-BIRC6OUT
Consensus
139,520 particles
CryoSPARC 3DVA
Cluster 0
10,415 particles
NU refine - 4.22 Å
Cluster 4
9,889 particles
NU refine - 4.15 Å
e
BIRC6 Cl. 0
BIRC6 Cl. 4
9°
16 Å
UFD Cl. 0
UFD Cl. 4
f
UBA6-BIRC6OUT Cluster 4
UBA6-BIRC6OUT Cluster 0
BIRC6
UFD
RMSD /Å
0
3
6

Figure 33. Variability within the UBA6^{APO} and UBA6-BIRC6^{OUT} particle stacks

a. 3D variability analysis and clustering of particles from the UBA6^{APO} particle stack.

b. Comparison of atomic models fitted to UBA6^{APO} clusters 2 and 3. Angles of domain rotations and narrowing of the central cavity are annotated.

c. Comparison of UFD positioning between UBA6^{APO} clusters and UBA6-BIRC6$^{IN/OUT}$.

d. 3D variability analysis and clustering of particles from the UBA6-BIRC6^{OUT} particle stack.

e. Comparison of atomic models fitted to UBA6-BIRC6^{OUT} clusters 0 and 4. The angles of UFD rotation and distance between tips of BIRC6 positions are annotated.

f. Cα RMSD between UBA6-BIRC6^{OUT} clusters 0 and 4.

4.2.5. The UBA6 Cys-cap loop is required for efficient BIRC6 transthiolation

The placement of the Cys-cap loop between E1 and E2 catalytic sites in the UBA6-BIRC6^{OUT} structure highlights a potential role in regulating E1-E2 interactions. To test this, a UBA6 construct in which residues 797-817 were replaced by a shorter glycine-serine linker was generated (**Fig. 34a**). The UBA6 ΔCys-cap loop construct was then tested in time course multiple turnover transthiolation reactions with various E2s (**Fig. 34b-d**). While transthiolation to UBE2D2 and UBE2Z was not affected by removal of the Cys-cap loop, BIRC6~Ub formation was significantly reduced. Interestingly, the BIRC6 A4575D mutant (which shall be shown to interact less strongly with UBA6) did not show a further loss of activity with UBA6 ΔCys-cap loop. Overall, these results indicate that the UBA6 Cys-cap loop is specifically required for maximal E2 loading of high-affinity E2s, such as BIRC6.

Drosophila BIRC6 did not interact strongly with UBA6 in SEC (**Fig. 27g**). Consistent with this, drosophila BIRC6 does not show a reduction in transthiolation activity with the UBA6 ΔCys-cap loop construct (**Fig. 35a**, lanes 1, 2). Following from this, the panel of human/drosophila BIRC6 chimeras were tested to narrow down which regions of BIRC6 are required for the high-affinity UBA6 interaction, thus losing activity when the Cys-cap loop is deleted. BIRC6 constructs containing the human sequence between residues 4559 and 4590 showed reduced activity (**Fig. 35a**, lanes 1, 3, 6, 9, 11). These residues map on to the 'H1' region of BIRC6 and the immediately preceding loop (**Fig. 35b**), which directly contact UBA6 when BIRC6 is bound (**Fig. 35c**). As such, these results further validate the ‘H1’-UFD interface as the driver of the high-affinity UBA6-BIRC6 interaction.

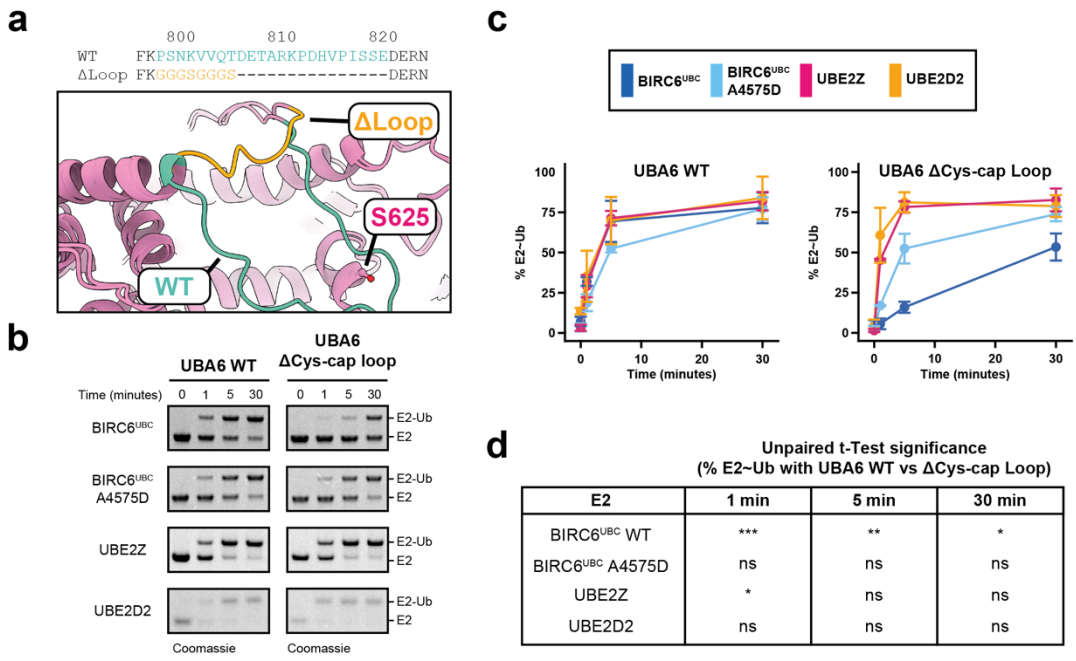

E2	1 min	5 min	30 min
BIRC6^{UBC} WT	***	**	*
BIRC6^{UBC} A4575D	ns	ns	ns
UBE2Z	*	ns	ns
UBE2D2	ns	ns	ns

Figure 34. Shortening the UBA6 Cys-cap loop specifically reduces turnover of BIRC6

a. Design of the UBA6 ΔCys-cap loop construct (top). Alignment of the UBA6APO structure to an AlphaFold3 model of UBA6 ΔCys-cap loop (bottom).

b-d. Time course transthiolation assays of E2s with WT and ΔCys-cap loop UBA6 constructs. Proportion of loaded E2 (E2~Ub) was measured by Coomassie stained SDS-PAGE analysis of transthiolation assays (b). Quantification was performed across three technical repeats, and the plot displays the mean ± standard deviation (c). Statistical analysis between reactions (d) was performed using an unpaired *t*-test, and significant differences are indicated with the following levels:

(*** $p < 0.001$, ** $p < 0.01$, * $p < 0.05$)

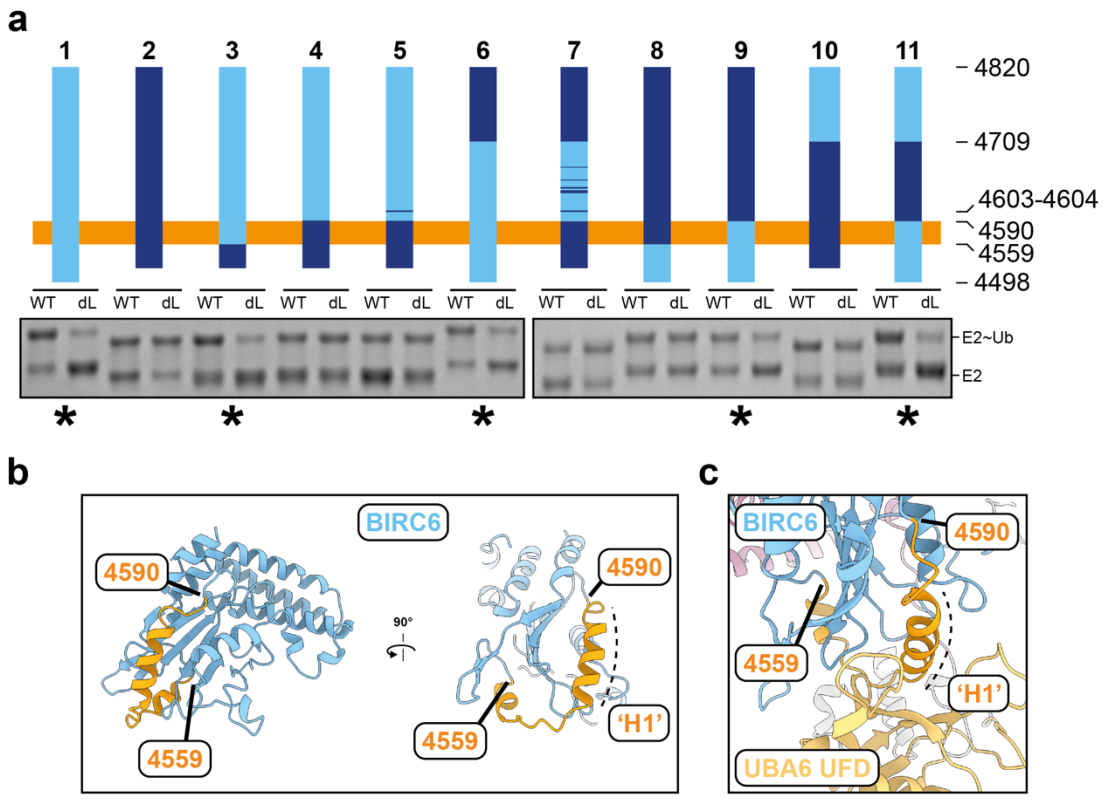

Figure 35. Only BIRC6 constructs containing the human 'H1' sequence show reduced transthiolation by UBA6 ΔCys-cap loop

a. Cartoon schematics of chimeric BIRC6 constructs (top). Image of Coomassie stained SDS-PAGE gel showing E2~Ub formation for each construct with either UBA6 WT (WT) or ΔCys-cap loop (dL). Constructs which have reduced activity with UBA6 ΔCys-cap loop are annotated with an asterisk.

b. Model of the human BIRC6 UBC domain with the residues 4559-4590 highlighted in orange.

c. View of the BIRC6-UBA6 interaction, emphasising the contact between BIRC6 residues 4559-4590 and the UBA6 UFD.

Domain boundaries of constructs used in (a):

1 hBIRC6 4590-4820

2 dBIRC6 4577-4646

3 dBIRC6 4577-4646, hBIRC6 4559-4820

4 dBIRC6 4577-4648, hBIRC6 4590-4820

5 dBIRC6 4577-4648, hBIRC6 4590-4820, E4603T, E4604D

6 hBIRC6 4498-4708, dBIRC6 4768-4879

7 dBIRC6 4577-4648, hBIRC6 4590-4708, dBIRC6 4768-4879: E4603T, E4604D, Y4631F, Q4634P, S4638N, S4639Q, G4650R, I4669V

8 hBIRC7 4498-4558, dBIRC6 4647-4879

9 hBIRC6 4498-4589, dBIRC6 4649-4879

10 dBIRC6 4577-4767, hBIRC6 4709-4820

11 hBIRC6 4498-4589, dBIRC6 4649-4767, hBIRC6 4709-4820

4.2.6. The UBA6 Cys-cap loop reduces E2 affinity

Either impaired recruitment or release of BIRC6 could explain the loss in BIRC6 activity with UBA6 ΔCys-cap loop. To clarify this, a fluorescence polarisation (FP) assay was used to measure the affinity of E1-E2 interactions. E2 proteins labelled with a sulfo-NHS Cy5 fluorophore were mixed with unlabelled UBA6, and the resulting Cy5 polarisation was measured at equilibrium (**Fig. 36a**). BIRC6 displayed robust binding to UBA6 with a Kd of 200 nM. As a control, the BIRC6 A4575D mutant, which had significantly reduced transthiolation activity (**Fig. 16a**) was included. This mutant showed weak binding to UBA6 in the FP assay, explaining the previous behaviour of this mutant in the priority and UBA6 ΔCys-cap loop transthiolation assays. However, while the A4575D mutation clearly makes recruitment to UBA6 less favourable, the sub-micromolar affinity of wild-type BIRC6 is not a requirement for E2s to be active with UBA6, since UBE2Z (for which only weak binding was detected) is still active with UBA6.

The binding assays were then repeated with the UBA6 ΔCys-cap loop construct. Surprisingly, increased binding for both BIRC6 variants and UBE2Z was observed (**Fig. 36b**). This was particularly striking for wild-type BIRC6, the affinity of which increased 20-fold to 10 nM. While all E2s tested (BIRC6 WT, BIRC6 A4575D, and UBE2Z) bind more strongly to the UBA6 ΔCys-cap loop construct, it appears that only the dramatic increase observed for BIRC6 WT reaches too high an affinity as to be detrimental to E2 turnover.

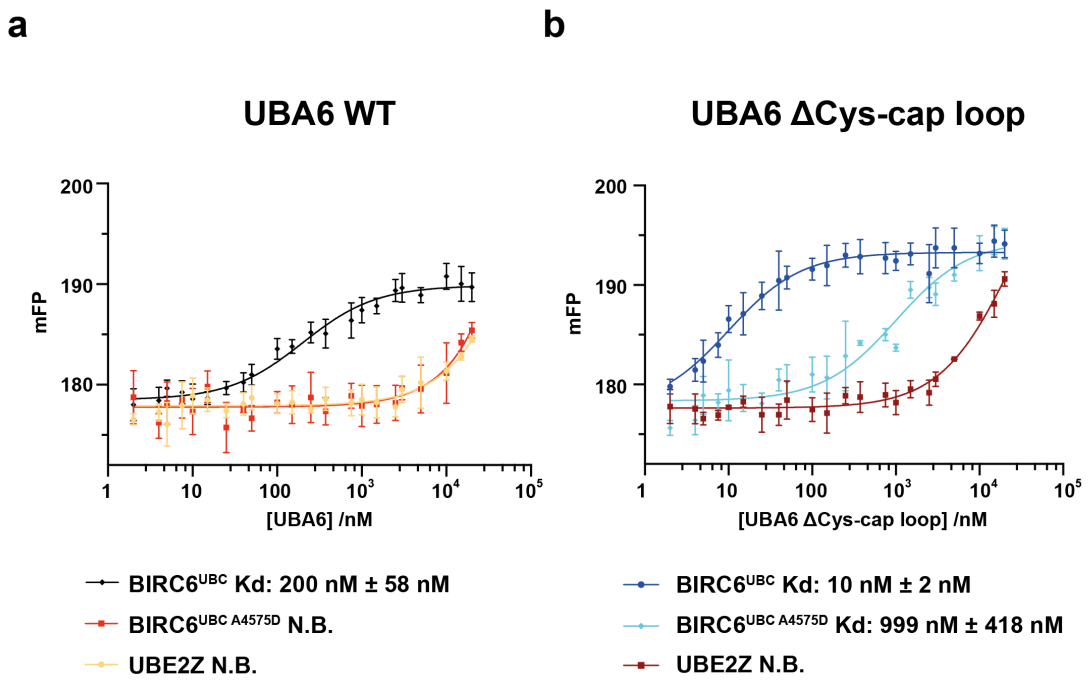

Figure 36. E2s bind to UBA6 ΔCys-cap loop more strongly than UBA6 WT

Fluorescence polarisation measurements for labelled E2s (BIRC6^{UBC}, BIRC6^{UBC} A4575D, and UBE2Z) binding to UBA6 WT (a) and UBA6 ΔCys-cap loop (b). An affinity to UBA6 WT was only fit for BIRC6^{UBC}, however weak interactions were detected for the remaining E2s. Stronger binding was detected for all E2s with UBA6 ΔCys-cap loop, which allowed models to be fit for BIRC6^{UBC} and BIRC6^{UBC} A4575D. Binding constants were fit in GraphPad Prism 9 using the equation for specific binding: $Y = B_{max} * X / (X + K_d)$.

4.2.7. The UBA6 Cys-cap loop reduces the effects of E2 competition

Next, the effect of Cys-cap loop removal on E2 competition for UBA6 was tested. Multiple turnover competition reactions were performed, in which UBE2D2 transthiolation was measured when paired with a concentration series of competitor E2s (**Fig. 37a-d**). When using WT UBA6, neither UBE2Z nor BIRC6 A4575D affected UBE2D2 loading. However, at concentrations equimolar and above, WT BIRC6 outcompeted UBE2D2 and suppressed its loading (**Fig. 37a**). Removal of the Cys-cap loop strengthened this effect (**Fig. 37b-d**), and even low concentrations of BIRC6 potently inhibited UBE2D2 loading. Furthermore, slight inhibition of UBE2D2 began to occur at the highest concentrations of BIRC6 A4575D used, consistent with the weak binding measured by FP. Together, these results show that the dampening of E2 binding by the Cys-cap loop allows UBA6 to function efficiently in reactions containing high-affinity E2s.

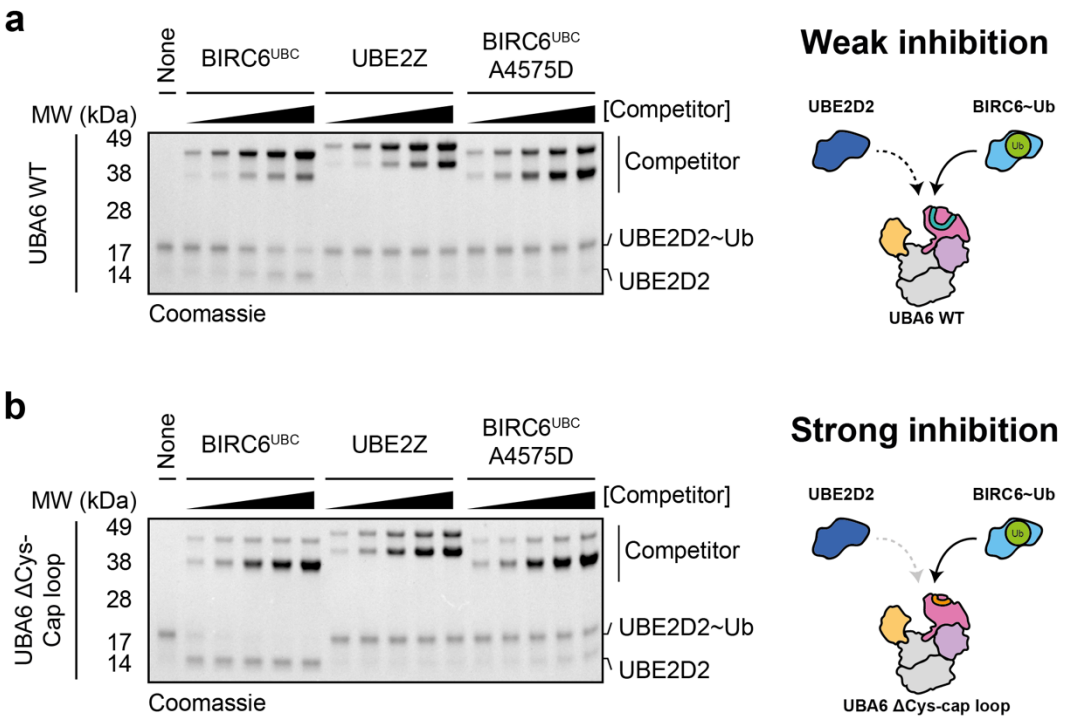

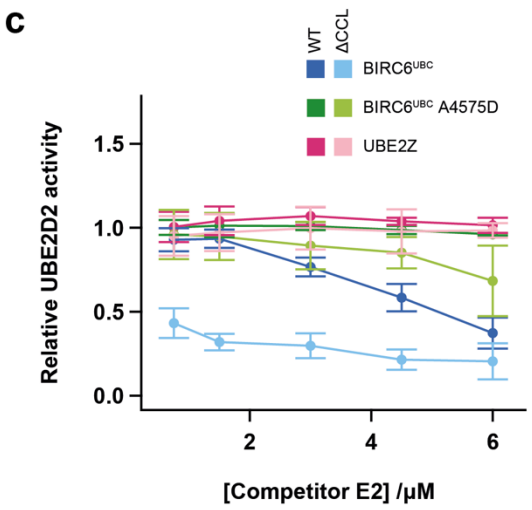

d

Unpaired t-Test significance
(% UBE2D2~Ub with competitor vs no competitor)
*** p < 0.05, ** p < 0.01, *** p < 0.001**

		[Competitor] /μM				
E1	**Competitor**	**0.75**	**1.5**	**3.0**	**4.5**	**6.0**
WT	BIRC6UBC	ns	ns	ns	*	**
WT	BIRC6UBC A4575D	ns	ns	ns	ns	ns
WT	UBE2Z	ns	ns	ns	ns	ns
ΔCCL	BIRC6UBC	*	*	*	**	*
ΔCCL	BIRC6UBC A4575D	ns	ns	ns	ns	ns
ΔCCL	UBE2Z	ns	ns	ns	ns	ns

Figure 37. The UBA6 Cys-cap loop is required for exclusion of BIRC6~Ub from UBA6, thereby allowing loading of other E2 enzymes

a-b. SDS-PAGE of end points taken from multiple-turnover E2 competition assays. Reactions contained UBE2D2 with active competitors combined with either wild-type (a) or ΔCys-cap loop (b) UBA6. Proportion of loaded E2 (E2~Ub) was measured by Coomassie stained SDS-PAGE analysis of 5-minute transthiolation assays. Summary cartoons describing the effect of BIRC6 competition of UBE2D2 loading are included to the right of each assay panel.

c. Quantification of UBE2D2 loading in each reaction relative to the no-competitor reaction. Quantification was performed across three technical repeats, and the plot displays the mean ± standard deviation.

d. Statistical significance when comparing UBE2D2 loading in each competitor reaction to the no-competitor reaction. Statistical analysis between reactions was performed using an unpaired *t*-test, and significant differences are indicated with the following levels:

(*** $p < 0.001$, ** $p < 0.01$, * $p < 0.05$)

4.2.8. The UBA6 thioester switch is ineffective after Cys-cap loop deletion

Presence of active UBE2Z did not disrupt UBE2D2 loading in competition assays, indicating that while UBA6 has the capacity to robustly load both competing E2s, something in the reactions containing the high-affinity E2 BIRC6 prevented efficient E2 turnover. This was particularly striking in the UBA6 ΔCys-cap loop reactions, where only a small proportion of BIRC6 appeared to receive ubiquitin before transthiolation was stalled. This apparent stalling invited further investigation into the release of loaded BIRC6.

As previously introduced, E2 release is facilitated by a thioester switch mechanism, specifically reducing the affinity of loaded E2s towards the E1 enzyme. To directly measure this effect for BIRC6, the UbDha cross-linking strategy was repurposed to generate a stable mimetic of ubiquitin-loaded BIRC6 for use in biophysical assays (**Fig. 38a**). Purified BIRC6-UbDha was then applied to the FP assay to measure binding to UBA6 variants (**Fig. 38b**). Loaded BIRC6-UbDha showed weaker binding to UBA6 WT, with the Kd reducing from 200 to 273 nM, consistent with a thioester switch mechanism.

Although the affinity for BIRC6-UbDha was still reduced when using UBA6 ΔCys-cap loop (from 10 to 22 nM), suggesting that a thioester switching mechanism was functioning, the affinity of BIRC6-UbDha was still significantly higher than that measured for unloaded BIRC6 and UBA6 WT. This would suggest that the UBA6 thioester switch cannot effectively release loaded BIRC6 from UBA6 ΔCys-cap loop, thereby explaining the stalling and inhibitory effects observed in the competition assays (**Fig. 37b**).

To demonstrate the necessity of the thioester switch for efficient E2 turnover by UBA6, the multiple turnover competition assays were repeated with catalytically inactive competitor E2s. As these competitor E2s are unable to receive ubiquitin, they would therefore not be subject to the affinity reduction caused by a thioester switch. Indeed, inhibitory effects were now observed at lower concentrations of BIRC6 C4666A when using UBA6 WT (**Fig. 39a, c-d**), and strong inhibition was observed with UBA6 ΔCys-cap loop (**Fig. 39b-d**). UBE2Z and BIRC6 A4575D still showed no inhibitory effect towards UBE2D2.

In summary, the FP binding assays show that a thioester switch lowers the affinity of loaded BIRC6 towards UBA6, however, deletion of the Cys-cap loop increases the affinity of BIRC6 to such a degree as to make the switch ineffective. This switch is required to prevent inhibition of UBA6. The inherently low affinity of UBE2Z to UBA6 prevents this behaviour, and weakening the BIRC6-UBA6 interaction with the A4575D mutation also abolishes the inhibitory effect (**Fig. 37, 39**).

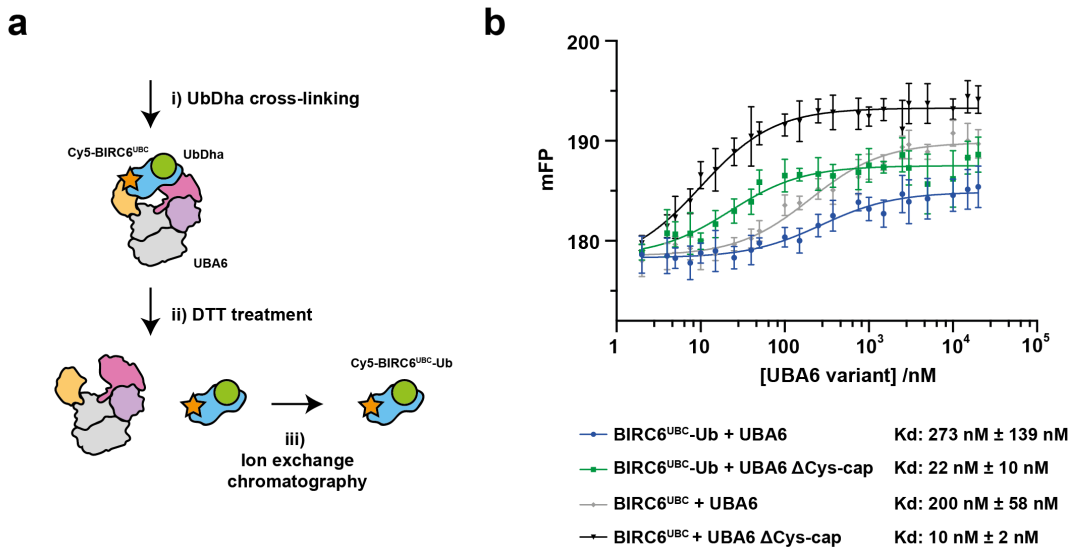

Figure 38. Measuring the effect of ubiquitin loading on UBA6-BIRC6 interactions

a. Schematic for the generation of a stable mimic of E2~Ub thioester. An E1-UbDha-E2 complex is prepared as previously described, then treated with 50 mM to reduce the E1-UbDha thioester bond. The E2-UbDha adduct is then isolated by ion exchange chromatography.

b. Fluorescence polarisation measurements for labelled BIRC6^{UBC} in loaded and unloaded states binding to UBA6 WT and UBA6 ΔCys-cap loop. Binding constants were fit in GraphPad Prism 9 using the equation for specific binding: $Y = B_{max} * X / (X + K_d)$.

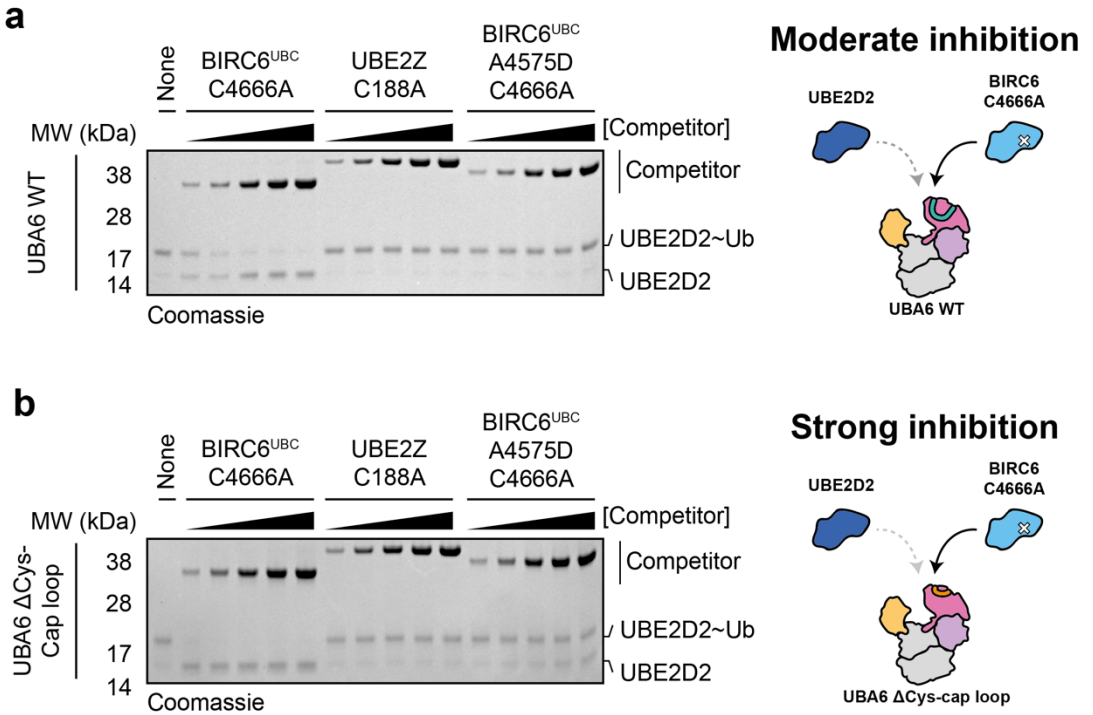

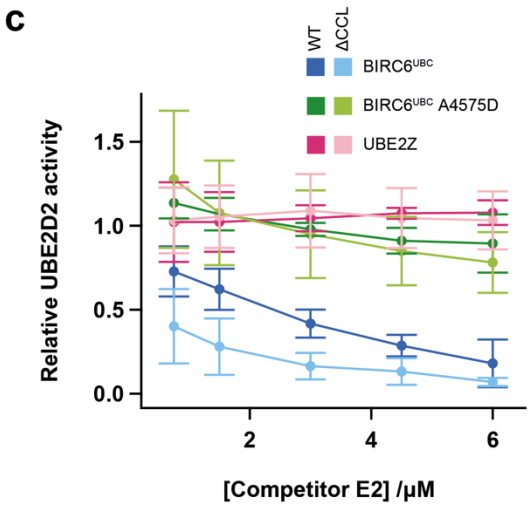

d

Unpaired t-Test significance
(% UBE2D2~Ub with competitor vs no competitor)
*** p < 0.05, ** p < 0.01, *** p < 0.001**

		[Competitor] /μM				
E1	**Competitor (C-A)**	**0.75**	**1.5**	**3.0**	**4.5**	**6.0**
WT	BIRC6UBC	ns	ns	*	*	**
WT	BIRC6UBC A4575D	ns	ns	ns	ns	ns
WT	UBE2Z	ns	ns	ns	ns	ns
ΔCCL	BIRC6UBC	*	*	*	*	**
ΔCCL	BIRC6UBC A4575D	ns	ns	ns	ns	ns
ΔCCL	UBE2Z	ns	ns	ns	ns	ns

Figure 39. Catalytically inactive BIRC6 evades the thioester switch to inhibit UBA6

a-b. SDS-PAGE of end points taken from multiple-turnover E2 competition assays. Reactions contained UBE2D2 with catalytically inactive competitors combined with either wild-type (a) or ΔCys-cap loop (b) UBA6. Proportion of loaded E2 (E2~Ub) was measured by Coomassie stained SDS-PAGE analysis of 5-minute transthiolation assays. Summary cartoons describing the effect of BIRC6 competition of UBE2D2 loading are included to the right of each assay panel.

c. Quantification of UBE2D2 loading in each reaction relative to the no-competitor reaction. Quantification was performed across three technical repeats, and the plot displays the mean ± standard deviation.

d. Statistical significance when comparing UBE2D2 loading in each competitor reaction to the no-competitor reaction. Statistical analysis between reactions was performed using an unpaired *t*-test, and significant differences are indicated with the following levels:

(*** $p < 0.001$, ** $p < 0.01$, * $p < 0.05$)

4.2.9. Microscopy of the non-covalent UBA6-BIRC6^{FL} complex

All the analysis of non-covalent interactions between UBA6 and BIRC6 presented in this thesis was performed using a truncated BIRC6 construct containing only the catalytic domain (residues 4498-4820). The catalytic domain of BIRC6 has the same E1 specificity as the full-length protein (**Fig. 9b**), however it remains to be shown if any other sections of BIRC6^{FL} contribute to interactions with UBA6. To investigate this, another cryoEM sample was prepared containing UBA6 and BIRC6^{FL}, this time without adding any UbDha probe.

1609 micrographs were collected from the UBA6-BIRC6^{FL} sample, in which UBA6 and BIRC6^{FL} particles could clearly be identified (**Fig. 40a**). UBA6 and BIRC6 particles were picked separately using existing 3D volumes as templates. After removal of junk and poorly aligned particles by 2D and heterogeneous refinement steps, UBA6 particles were sorted into two distinct classes based on presence of the BIRC6 UBC domain within the E1 central cavity (**Fig. 40b**). The UBA6-BIRC6^{OUT} atomic model fit well into the BIRC6-bound UBA6 volume (**Fig. 40c**). No density corresponding to other features from BIRC6 could be seen in the UBA6-BIRC6 class.

Although a higher resolution consensus volume for BIRC6^{FL} could be generated (**Fig. 40d, e**), additional focused 3D classification and 3D variability steps did not recover any density for the C-terminal UBC domain. A small unassigned density was present in the central cavity of BIRC6^{FL} (**Fig. 40e**, asterisk) however this is likely due to partial occupancy of BIRC6 substrates pulled out during purification, as has been previously reported[92].

A dissociation constant of ~200 nM was previously measured for the interaction between BIRC6^{UBC} and UBA6 by FP (**Fig. 36a**). Using this Kd value and the starting

concentrations used for the cryoEM sample (16 μM UBA6, 8 μM BIRC6^{FL}), ~7.8 μM UBA6-BIRC6 complex is expected to form at equilibrium. This would mean that UBA6-BIRC6 complexes should include 98% of BIRC6 particles and 49% of UBA6 particles. The proportion of bound UBA6 after 3D classification is not far off from this value (42%), and the slight decrease in binding may be explained by dissociation of complexes caused by processes during cryoEM grid preparation, such as interactions with the air-water interface.

Following from this, more than 90% of particles contributing to the consensus BIRC6^{FL} volume (**Fig. 40d, e**) should in fact be bound to UBA6. The lack of any signs of UBA6 density across the core and N-terminal domains of BIRC6^{FL}, despite such a high occupancy of UBA6, further points towards UBA6-BIRC6 interactions being solely mediated through the UBC domain.

The UBC domain is normally too small to provide sufficient signal for cryoEM analysis, however, once bound to UBA6, the BIRC6 UBC is visible (**Fig. 40b**). Therefore, UBA6-BIRC6 particles can be used to investigate positioning of the flexibly tethered BIRC6 UBC domain. To this end, distances between every UBA6 particle to the nearest BIRC6 particle were calculated for each micrograph in the UBA6-BIRC6^{FL} dataset (**Fig. 41a**). Histograms summarising distances for each class of UBA6 particles were then generated, and their distributions were compared to an equal number of randomly positioned BIRC6 and UBA6 particles (**Fig. 41b**).

UBA6-BIRC6 particles (UBA6^{BOUND}) showed a sharp peak in the distribution of distances to the nearest BIRC6, centred at 182 Å. Placement of cryoEM densities of BIRC6^{FL} and UBA6-BIRC6 particles 182 Å apart can produce a feasible interaction at certain angles (**Fig. 41c**). The distribution of distances extends beyond what could be reasonably expected for UBA6-BIRC6 interactions. This may be due to

misclassification of free UBA6 particles into the bound class, or failure to pick the true nearest BIRC6 particle. UBA6^{APO} particles showed a broader distribution and were more likely to be found further away from the nearest BIRC6 particle (237 Å). Distances for all UBA6 particles were on average much shorter than observed for fully random particle positions (516 Å). This may reflect physical constraints in the cryoEM micrographs, such as regions of carbon or thin ice in which particles are unlikely to be located.

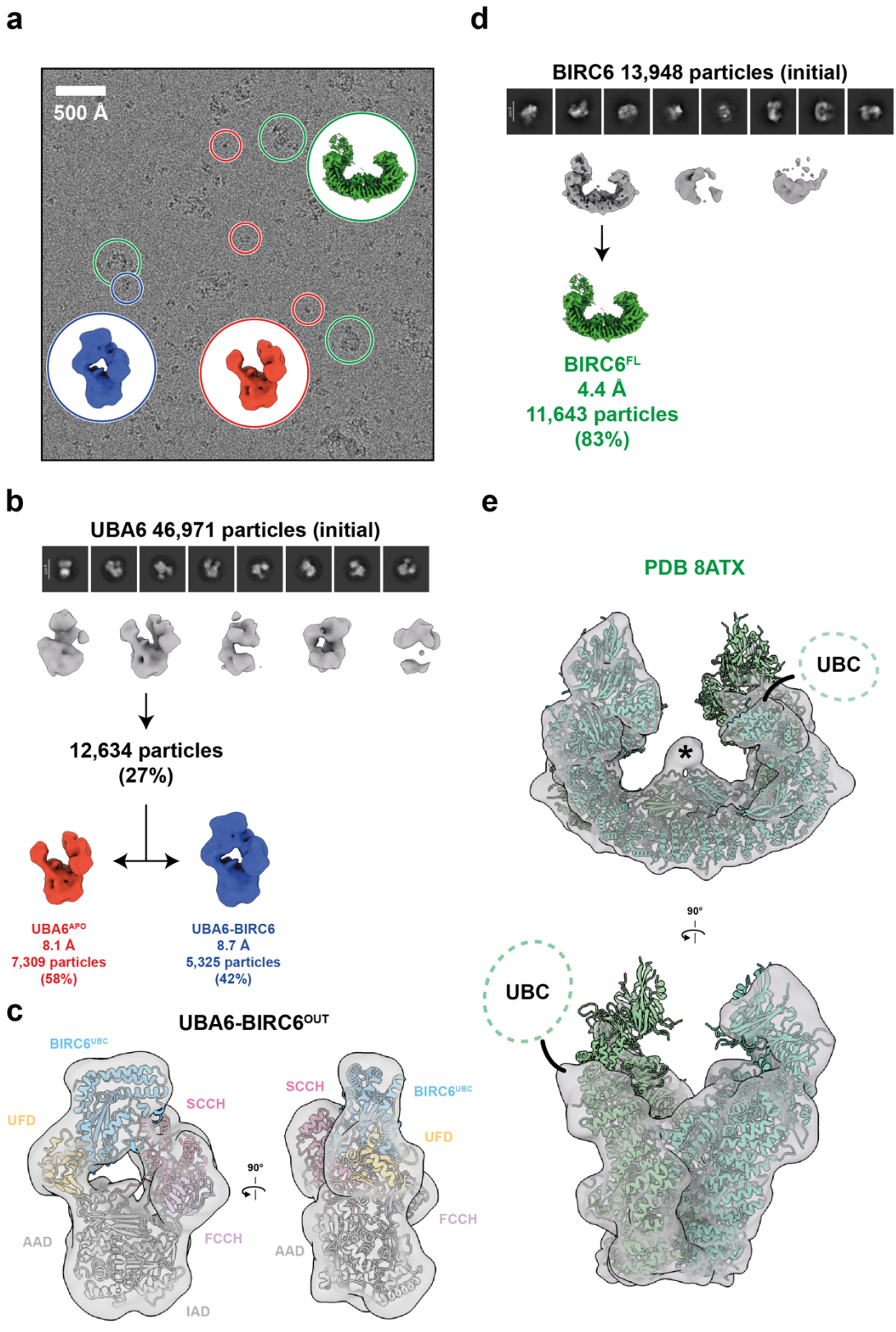
a
500 Å
d
BIRC6 13,948 particles (initial)
BIRC6FL
4.4 Å
11,643 particles
(83%)
b
UBA6 46,971 particles (initial)
12,634 particles
(27%)
UBA6APO
8.1 Å
7,309 particles
(58%)
UBA6-BIRC6
8.7 Å
5,325 particles
(42%)
e
PDB 8ATX
UBC
90°
UBC
c
UBA6-BIRC6OUT
BIRC6UBC
SCCH
UFD
AAD
FCCH
IAD
90°
SCCH
BIRC6UBC
UFD
FCCH
AAD

Figure 40. CryoEM volumes of UBA6 and BIRC6^{FL}

a. Manual annotation of BIRC6 and UBA6 particles on a representative micrograph.

b. 2D and 3D classification steps used to separate UBA6 particles into UBA6^{APO} and UBA6^{BOUND} classes.

c. Front and side views of the UBA6-BIRC6^{OUT} model (UBA6-BIRC6^{UBC} dataset) fit into the UBA6^{BOUND} volume (UAB6-BIRC6^{FL} dataset).

d. 2D and 3D classification steps used to generate the BIRC6^{FL} consensus volume. Further classification steps did not recover any density for the C-terminal UBC domain.

e. Front and side views of a BIRC6 model (PDB 8ATX) fit into the BIRC6^{FL} consensus volume (low-pass filtered). Expected location of the flexibly tethered C-terminal UBC domain is indicated with dashed lines. Unknown central density is annotated with an asterisk.

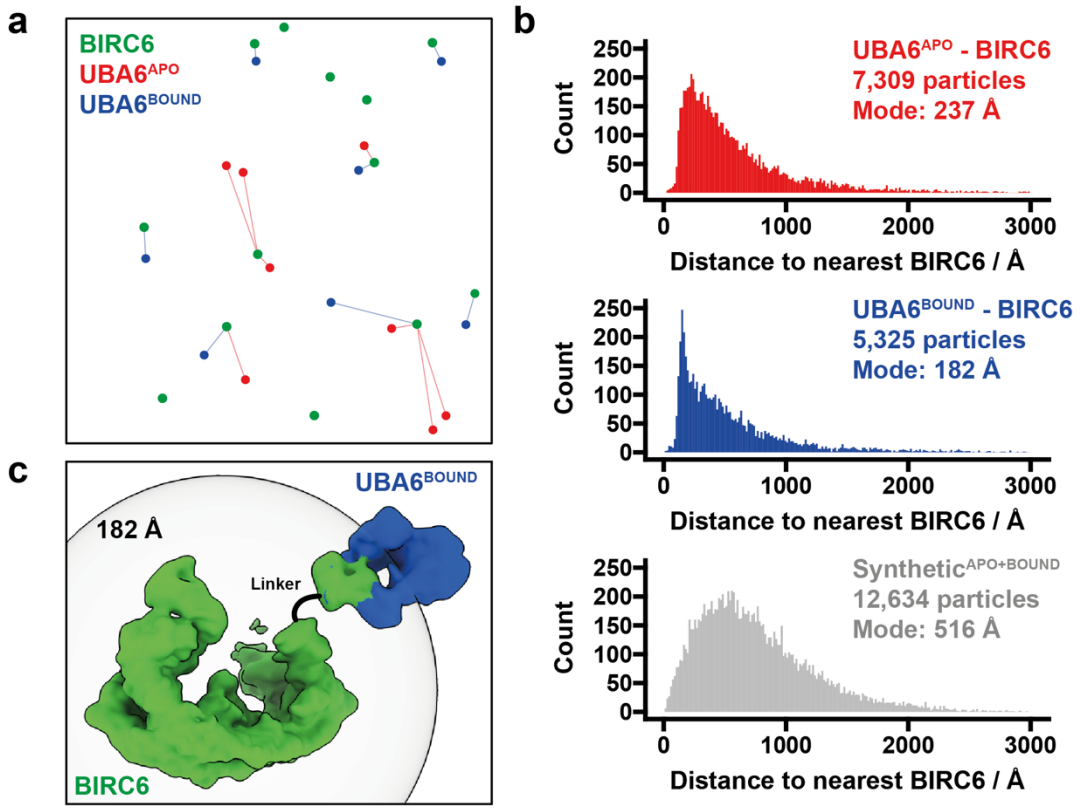

Figure 41. Analysis of distances between UBA6 and BIRC6^{FL} particles

a. Assignment of distances between UBA6$^{APO/BOUND}$ particles to the nearest BIRC6 particle on a representative micrograph.

b. Histograms of distances to the nearest BIRC6 particle for UBA6 particles from cryoEM data (UBA6^{APO} - top, UBA6^{BOUND} - middle) and randomly generated locations of an equal number of UBA6 particles (bottom).

c. Placement of BIRC6 (green) and UBA6^{BOUND} (UBA6 - blue, UBC domain - green) volumes at a distance of 182 Å (transparent sphere).

4.3. Discussion

4.3.1. Functional relevance of high-affinity E1-E2 interactions

BIRC6 appears to be an exception among ubiquitin E2 enzymes, binding to its unloaded E1 with low nanomolar affinity. Given the potency of BIRC6 in competition transthiolation assays, the higher relative affinity of BIRC6 for UBA6 appears to extend to the ubiquitin loaded state, despite the nanomolar Kds predicted for other E2s through kinetic assays[106].

Other examples of strong E1-E2 interactions have been found outside of the ubiquitin system: both human and yeast orthologues of UBE2I (the E2 for SUMO) form stable complexes with their cognate E1s[101,102] and similar results were found for UBE2M and NAE1-UBA3[24]. Despite these findings, the functional relevance of these stable E1-E2 interactions is not well understood.

In the case of UBE2M, it has been shown that combined binding of both the E2 'H1' and N-terminal extension is required for maximum activity, suggesting that the 'H1'-UFD interaction is not strong enough for optimal recruitment[17]. This is somewhat consistent with BIRC6, where we have seen that loss of the high affinity interaction through the A4575D mutation significantly reduces, but does not abolish, transthiolation activity. However, this trend is not conserved to other ubiquitin E2s which achieve high rates of transthiolation without high-affinity interactions.

Beyond simply enabling ubiquitin transthiolation to BIRC6, the high-affinity UBA6-BIRC6 interaction additionally bestows BIRC6 with priority for receiving ubiquitin over weaker binding E2s *in vitro*. Why might BIRC6 require such a priority mechanism? As previously discussed, BIRC6 regulates essential cellular functions through its ubiquitination activity[95,97,100]. However, compared to other UBA6-active E2s, BIRC6 is

expressed at a much lower level (**Table 7**) and is limited to only working with the less abundant E1, UBA6. As such, BIRC6 faces steep competition for access to UBA6 in cells, which the priority mechanism outlined here may allow BIRC6 to bypass.

The other UBA6-specific E2, UBE2Z, does not exhibit a similar high-affinity priority mechanism. This could be in part due to higher expression levels making it easier for the cell to maintain the required amount of ubiquitin-loaded UBE2Z, however the additional function of UBE2Z in FAT10 conjugation may also play a role. UBE2Z receives FAT10 significantly better than other UBA6-active E2s[78], which suggests that UBE2Z may utilise a UBL-driven mechanism to gain priority for UBA6 when UBE2Z-specific FAT10 conjugation pathways are required.

An additional consequence of the high-affinity E1-E2 interaction is the potential effect on localisation of proteins within the cell. Immunofluorescence imaging of high-affinity E2s BIRC6[97], UBE2M[110,111], and UBE2I[112,113] each show distinct localisation patterns related to their functions. Conversely, little is known about E1 localisation beyond broad distribution throughout both cytoplasm and nucleus[67,114]; however, it is possible that this could be altered on induction of the pathways influencing localisation of their downstream high-affinity E2s.

4.3.2. Role of the Cys-cap loop in E1-E2 binding

The high-affinity UBA6-BIRC6 interaction, while necessary for providing priority for BIRC6, poses a challenge for UBA6 to efficiently release ubiquitinated BIRC6. This results in impaired loading of other E2s when BIRC6 is present at high concentrations *in vitro*. UBA6 uses two methods to reduce this effect: Under normal conditions, the thioester switch reduces the affinity of loaded BIRC6 enough to dampen the inhibitory effect. Second, the UBA6 Cys-cap loop significantly lowers the affinity of the UBA6-

BIRC6 interactions such that the thioester switch can be effective. Removal of either mechanism, either by introducing catalytically inactive BIRC6 or deletion of the Cys-cap loop, causes inhibition of UBA6.

Interestingly, almost all canonical E1s feature a Cys-cap loop (**Fig. 42a**). Unlike regions critical for catalysis such as the ATP-binding site, the Cys-cap loop shows a high degree of variation across E1s (**Fig. 42b**). This points to a conserved function of the loop which does not necessarily depend on its exact sequence. Previous literature has suggested that this involves protection of the E1 catalytic cysteine from oxidation[115] and this has been followed up by a recent study showing that lengthening the UBA7 Cys-cap loop protects UBA7 from forming disulfide cross-links to UBE2L6 *in vitro*[105].

The data presented here suggests that the Cys-cap loop has a direct role in modulating E1-E2 interactions. Consistent with previous crystal structures of UBA6[18,66], the UBA6^{APO} structure places the Cys-cap loop directly over the catalytic site of the E1, thereby blocking recruitment of E2s to the SCCH interface. This is supported by FP data showing that E2s bind to UBA6 more strongly when the Cys-cap loop is removed, likely due to the additional binding interactions made at the SCCH interface.

Presence of the Cys-cap loop may contribute to the generally low affinity of E1-E2 interactions, revealing a potential mechanism by which general E2 recruitment may be regulated. Partial or full Cys-cap loop dissociation upon loading an E1 with ubiquitin would lower the barrier for E2 recruitment, selectively enhancing E2 recruitment when the E1 is primed for transfer (**Fig. 42c**). While this mechanism is speculative, a crystal structure of doubly loaded UBA1 (PDB: 4NNJ[19]) shows partial occupancy of the Cys-cap loop, and it is possible that in solution the loop would be even more disordered.

The data within this chapter describes how regulation of E2 binding by the Cys-cap loop, a mechanism which may be applicable to most E1-E2 pathways, has been coopted by UBA6-BIRC6 to facilitate a unique high-affinity interaction. As a result, BIRC6 enjoys priority access to UBA6 without disrupting other UBA6-dependent pathways.

a

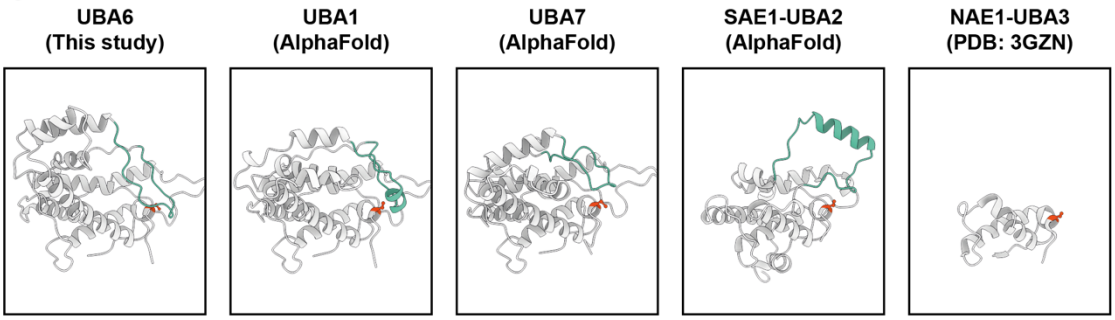

Cys-cap Loop
Catalytic Cys

b

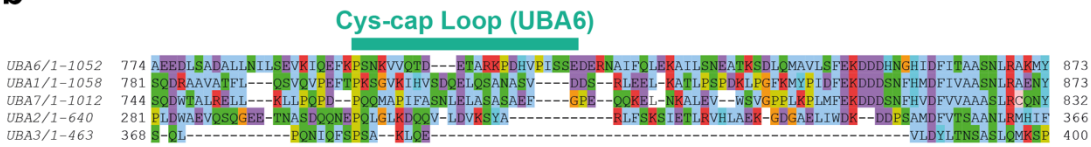

c

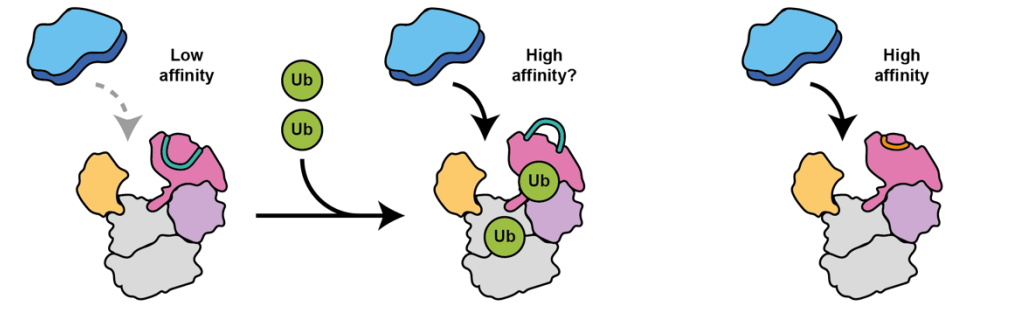

Figure 42. Role of the Cys-cap loop in regulating E1-E2 interactions

a. Experimental and predicted atomic models for canonical E1s, with the Cys-cap loop of each model coloured in teal. AlphaFold models were used in cases where the Cys-cap loop was not resolved in available experimental models.

b. Sequence alignment of SCCH-containing E1s covering the region corresponding to the UBA6 Cys-cap loop.

c. Cartoon summarising the proposed mechanism for regulation of E2 binding by the Cys-cap loop. The Cys-cap loop is ordered in an unloaded E1, discouraging E2 recruitment. Loading of ubiquitin to the E1 catalytic cysteine may displace the Cys-cap loop to promote E2 recruitment, as seen in the synthetic UBA6 ΔCys-cap loop construct.

5. Outlook

5.1. E1-E2 specificity

Because the ubiquitin system underpins so many essential processes, knockdown of either E1 has broad cellular consequences that can obscure the effects on individual E2 pathways. A key motivation for studying the determinants of E1-E2 recognition is to develop tools that allow selective investigation of E1-specific ubiquitination pathways. For example, it remains unclear whether dual reactivity with UBA1 and UBA6 is functionally important for non-specific ubiquitin E2s. Introducing specificity-altering mutations into E2s, guided by the principles of E1 recognition described in this thesis, would enable selective removal of UBA1 or UBA6 charging for a single E2 without disrupting other pathways.

Exploring E2-specific ubiquitination pathways may also clarify the molecular basis of VEXAS syndrome. It is unknown whether UBA6 can compensate for the loss of UBA1 to maintain ubiquitin loading of non-specific E2s in patients. If not, the cytotoxic effects observed in VEXAS could be attributed solely to the inactivation of UBA1-specific pathways. This question could be addressed by engineering E1 specificity into non-specific E2s and assessing whether the impact of UBA1 loss is exacerbated, or conversely, whether introducing UBA6 reactivity into UBA1-specific E2s can mitigate the phenotype.

The diversity of E1 recognition mechanisms among ubiquitin E2s also highlights opportunities for pathway-specific inhibition. Targeting E1-E2 interactions with small molecules has precedent; for instance, Auranofin, an FDA-approved treatment for rheumatoid arthritis, covalently binds the UBA1 UFD and enhances recruitment of a

broad range of E2s[116]. Structure-guided approaches could refine this strategy to design compounds that selectively modulate individual E1-E2 interactions. For example, the interaction of UBE2Z, but not BIRC6, with IP6 in the UBA6 SCCH domain suggests that small molecules targeting this pocket could modulate recruitment of specific E2s.

5.2. E2 priority

The novel observation that a high affinity E1-E2 interaction gives BIRC6 priority for receiving ubiquitin has wide implications for other E2s. It is thought that substrate ubiquitination by an E3 is the rate limiting step of the ubiquitin cascade; E2s are all expected to be loaded with ubiquitin under normal conditions[39,117]. However, under abnormal conditions, such as UBA1 depletion in VEXAS disease or situations where higher-than-normal rates of ubiquitin transfer are required, competition between E2s for receiving activated ubiquitin may become more relevant.

The low innate affinities of ubiquitin E2s to UBA1/UBA6 makes any predictions with regards to priority challenging. While no E2s tested in this thesis appear to have as strong an interaction as UBA6-BIRC6, it is possible that affinity differences between weaker binding E2s could also allow for priority mechanisms. A stable analogue for ubiquitin-loaded E1, or removal of the E1 Cys-cap loop, could be used to increase the strength of E1-E2 interactions, simplifying the measurement of affinities across the entire family and potentially revealing other priority E2s.

From an evolutionary perspective, the emergence of E1-E2 priority mechanisms may reflect a strategy to ensure robust ubiquitin transfer under fluctuating cellular demands. The exceptionally high affinity of UBA6-BIRC6 could represent an adaptation to safeguard critical ubiquitin-dependent processes when ubiquitin availability or UBA6

function is compromised. More broadly, subtle affinity differences across the E2 family may have been tuned to allow cells to prioritise specific E2s in times of stress while maintaining flexibility under normal conditions. Investigating the evolutionary conservation of these interactions across species could provide further insight into how E1-E2 hierarchies arose and how they contribute to the resilience of the ubiquitin system.

6. Bibliography

1. Zuin, A., Isasa, M. & Crosas, B. Ubiquitin signaling: extreme conservation as a source of diversity. *Cells* 3, 690–701 (2014).
2. Komander, D. & Rape, M. The ubiquitin code. *Annu Rev Biochem* 81, 203–29 (2012).
3. Dikic, I., Wakatsuki, S. & Walters, K. J. Ubiquitin-binding domains - from structures to functions. *Nat Rev Mol Cell Biol* 10, 659–71 (2009).
4. Komander, D., Clague, M. J. & Urbé, S. Breaking the chains: structure and function of the deubiquitinases. *Nat Rev Mol Cell Biol* 10, 550–563 (2009).
5. Ciechanover, A. & Schwartz, A. L. The ubiquitin-proteasome pathway: the complexity and myriad functions of proteins death. *Proc Natl Acad Sci U S A* 95, 2727–30 (1998).
6. Pines, J. Cubism and the cell cycle: the many faces of the APC/C. *Nat Rev Mol Cell Biol* 12, 427–38 (2011).
7. Hagting, A. *et al.* Human securin proteolysis is controlled by the spindle checkpoint and reveals when the APC/C switches from activation by Cdc20 to Cdh1. *J Cell Biol* 157, 1125–37 (2002).
8. Clute, P. & Pines, J. Temporal and spatial control of cyclin B1 destruction in metaphase. *Nat Cell Biol* 1, 82–7 (1999).
9. Chen, Z. J. Ubiquitination in signaling to and activation of IKK. *Immunol Rev* 246, 95–106 (2012).
10. Liu, T., Zhang, L., Joo, D. & Sun, S.-C. NF-κB signaling in inflammation. *Signal Transduct Target Ther* 2, 17023 (2017).
11. Harhaj, E. W. & Dixit, V. M. Regulation of NF-κB by deubiquitinases. *Immunol Rev* 246, 107–24 (2012).
12. Vijay-kumar, S., Bugg, C. E. & Cook, W. J. Structure of ubiquitin refined at 1.8 Å resolution. *J Mol Biol* 194, 531–544 (1987).
13. Schulman, B. A. & Harper, J. W. Ubiquitin-like protein activation by E1 enzymes: the apex for downstream signalling pathways. *Nat Rev Mol Cell Biol* 10, 319–31 (2009).
14. Haas, A. L. & Rose, I. A. The mechanism of ubiquitin activating enzyme. A kinetic and equilibrium analysis. *J Biol Chem* 257, 10329–37 (1982).
15. Haas, A. L., Warms, J. V, Hershko, A. & Rose, I. A. Ubiquitin-activating enzyme. Mechanism and role in protein-ubiquitin conjugation. *J Biol Chem* 257, 2543–8 (1982).
16. Lv, Z., Williams, K. M., Yuan, L., Atkison, J. H. & Olsen, S. K. Crystal structure of a human ubiquitin E1-ubiquitin complex reveals conserved functional elements essential for activity. *J Biol Chem* 293, 18337–18352 (2018).
17. Huang, D. T. *et al.* A unique E1-E2 interaction required for optimal conjugation of the ubiquitin-like protein NEDD8. *Nat Struct Mol Biol* 11, 927–35 (2004).
18. Truongvan, N., Li, S., Misra, M., Kuhn, M. & Schindelin, H. Structures of UBA6 explain its dual specificity for ubiquitin and FAT10. *Nat Commun* 13, 4789 (2022).
19. Schäfer, A., Kuhn, M. & Schindelin, H. Structure of the ubiquitin-activating enzyme loaded with two ubiquitin molecules. *Acta Crystallogr D Biol Crystallogr* 70, 1311–20 (2014).

20. Hann, Z. S. *et al.* Structural basis for adenylation and thioester bond formation in the ubiquitin E1. *Proc Natl Acad Sci U S A* 116, 15475–15484 (2019).
21. van Wijk, S. J. L. & Timmers, H. T. M. The family of ubiquitin-conjugating enzymes (E2s): deciding between life and death of proteins. *FASEB J* 24, 981–93 (2010).
22. Stewart, M. D., Ritterhoff, T., Klevit, R. E. & Brzovic, P. S. E2 enzymes: more than just middle men. *Cell Res* 26, 423–440 (2016).
23. Walden, H. *et al.* The structure of the APPBP1-UBA3-NEDD8-ATP complex reveals the basis for selective ubiquitin-like protein activation by an E1. *Mol Cell* 12, 1427–37 (2003).
24. Walden, H., Podgorski, M. S. & Schulman, B. A. Insights into the ubiquitin transfer cascade from the structure of the activating enzyme for NEDD8. *Nature* 422, 330–4 (2003).
25. Huang, D. T. *et al.* Basis for a ubiquitin-like protein thioester switch toggling E1-E2 affinity. *Nature* 445, 394–8 (2007).
26. Huang, D. T. *et al.* Structural basis for recruitment of Ubc12 by an E2 binding domain in NEDD8's E1. *Mol Cell* 17, 341–50 (2005).
27. Yuan, L., Lv, Z., Adams, M. J. & Olsen, S. K. Crystal structures of an E1-E2-ubiquitin thioester mimetic reveal molecular mechanisms of transthioesterification. *Nat Commun* 12, 2370 (2021).
28. Tokgöz, Z., Bohnsack, R. N. & Haas, A. L. Pleiotropic effects of ATP.Mg2+ binding in the catalytic cycle of ubiquitin-activating enzyme. *J Biol Chem* 281, 14729–37 (2006).
29. Pickart, C. M., Kasperek, E. M., Beal, R. & Kim, A. Substrate properties of site-specific mutant ubiquitin protein (G76A) reveal unexpected mechanistic features of ubiquitin-activating enzyme (E1). *J Biol Chem* 269, 7115–23 (1994).
30. Kochańczyk, T. *et al.* Structural basis for transthiolation intermediates in the ubiquitin pathway. *Nature* 633, 216–223 (2024).
31. Spratt, D. E. & Shaw, G. S. Association of the disordered C-terminus of CDC34 with a catalytically bound ubiquitin. *J Mol Biol* 407, 425–38 (2011).
32. Kolman, C. J., Toth, J. & Gonda, D. K. Identification of a portable determinant of cell cycle function within the carboxyl-terminal domain of the yeast CDC34 (UBC3) ubiquitin conjugating (E2) enzyme. *EMBO J* 11, 3081–90 (1992).
33. Schumacher, F.-R., Wilson, G. & Day, C. L. The N-terminal extension of UBE2E ubiquitin-conjugating enzymes limits chain assembly. *J Mol Biol* 425, 4099–111 (2013).
34. Summers, M. K., Pan, B., Mukhyala, K. & Jackson, P. K. The unique N terminus of the UbcH10 E2 enzyme controls the threshold for APC activation and enhances checkpoint regulation of the APC. *Mol Cell* 31, 544–556 (2008).
35. Brown, N. G. *et al.* Mechanism of polyubiquitination by human anaphase-promoting complex: RING repurposing for ubiquitin chain assembly. *Mol Cell* 56, 246–260 (2014).
36. Bartke, T., Pohl, C., Pyrowolakis, G. & Jentsch, S. Dual role of BRUCE as an antiapoptotic IAP and a chimeric E2/E3 ubiquitin ligase. *Mol Cell* 14, 801–11 (2004).
37. Yanagitani, K., Juszkiewicz, S. & Hegde, R. S. UBE2O is a quality control factor for orphans of multiprotein complexes. *Science* 357, 472–475 (2017).

38. Pruneda, J. N., Stoll, K. E., Bolton, L. J., Brzovic, P. S. & Klevit, R. E. Ubiquitin in motion: structural studies of the ubiquitin-conjugating enzyme~ubiquitin conjugate. *Biochemistry* 50, 1624–33 (2011).
39. Wenzel, D. M., Stoll, K. E. & Klevit, R. E. E2s: structurally economical and functionally replete. *Biochemical Journal* 433, 31–42 (2011).
40. Metzger, M. B., Pruneda, J. N., Klevit, R. E. & Weissman, A. M. RING-type E3 ligases: Master manipulators of E2 ubiquitin-conjugating enzymes and ubiquitination. *Biochimica et Biophysica Acta (BBA) - Molecular Cell Research* 1843, 47–60 (2014).
41. Ye, Y. & Rape, M. Building ubiquitin chains: E2 enzymes at work. *Nat Rev Mol Cell Biol* 10, 755–764 (2009).
42. Harper, J. W. & Schulman, B. A. Cullin-RING Ubiquitin Ligase Regulatory Circuits: A Quarter Century Beyond the F-Box Hypothesis. *Annu Rev Biochem* 90, 403–429 (2021).
43. Wang, Y., Argiles-Castillo, D., Kane, E. I., Zhou, A. & Spratt, D. E. HECT E3 ubiquitin ligases - emerging insights into their biological roles and disease relevance. *J Cell Sci* 133, (2020).
44. Wang, X. S. *et al.* The unifying catalytic mechanism of the RING-between-RING E3 ubiquitin ligase family. *Nat Commun* 14, 168 (2023).
45. Bedford, L., Lowe, J., Dick, L. R., Mayer, R. J. & Brownell, J. E. Ubiquitin-like protein conjugation and the ubiquitin-proteasome system as drug targets. *Nat Rev Drug Discov* 10, 29–46 (2011).
46. Cappadocia, L. & Lima, C. D. Ubiquitin-like Protein Conjugation: Structures, Chemistry, and Mechanism. *Chem Rev* 118, 889–918 (2018).
47. Pickart, C. M. & Raasi, S. Controlled synthesis of polyubiquitin chains. *Methods Enzymol* 399, 21–36 (2005).
48. Caesar, J. *et al.* SIMPLE 3.0. Stream single-particle cryo-EM analysis in real time. *J Struct Biol X* 4, 100040 (2020).
49. Punjani, A., Rubinstein, J. L., Fleet, D. J. & Brubaker, M. A. cryoSPARC: algorithms for rapid unsupervised cryo-EM structure determination. *Nat Methods* 14, 290–296 (2017).
50. Zivanov, J., Nakane, T. & Scheres, S. H. W. A Bayesian approach to beam-induced motion correction in cryo-EM single-particle analysis. *IUCrJ* 6, 5–17 (2019).
51. Scheres, S. H. W. RELION: implementation of a Bayesian approach to cryo-EM structure determination. *J Struct Biol* 180, 519–30 (2012).
52. Zheng, S. Q. *et al.* MotionCor2: anisotropic correction of beam-induced motion for improved cryo-electron microscopy. *Nat Methods* 14, 331–332 (2017).
53. Rohou, A. & Grigorieff, N. CTFFIND4: Fast and accurate defocus estimation from electron micrographs. *J Struct Biol* 192, 216–21 (2015).
54. Wagner, T. *et al.* SPHIRE-crYOLO is a fast and accurate fully automated particle picker for cryo-EM. *Commun Biol* 2, 218 (2019).
55. Horstmann, A. *et al.* A service-based approach to cryoEM facility processing pipelines at eBIC. *Acta Crystallogr D Struct Biol* 80, 174–180 (2024).
56. Jumper, J. *et al.* Highly accurate protein structure prediction with AlphaFold. *Nature* 596, 583–589 (2021).

57. Croll, T. I. ISOLDE: a physically realistic environment for model building into low-resolution electron-density maps. *Acta Crystallogr D Struct Biol* 74, 519–530 (2018).
58. Liebschner, D. *et al.* Macromolecular structure determination using X-rays, neutrons and electrons: recent developments in Phenix. *Acta Crystallogr D Struct Biol* 75, 861–877 (2019).
59. Emsley, P. & Cowtan, K. Coot: model-building tools for molecular graphics. *Acta Crystallogr D Biol Crystallogr* 60, 2126–2132 (2004).
60. Punjani, A. & Fleet, D. J. 3D variability analysis: Resolving continuous flexibility and discrete heterogeneity from single particle cryo-EM. *J Struct Biol* 213, 107702 (2021).
61. Pelzer, C. *et al.* UBE1L2, a novel E1 enzyme specific for ubiquitin. *J Biol Chem* 282, 23010–4 (2007).
62. Chiu, Y.-H., Sun, Q. & Chen, Z. J. E1-L2 activates both ubiquitin and FAT10. *Mol Cell* 27, 1014–23 (2007).
63. Jin, J., Li, X., Gygi, S. P. & Harper, J. W. Dual E1 activation systems for ubiquitin differentially regulate E2 enzyme charging. *Nature* 447, 1135–8 (2007).
64. Ciechanover, A., Finley, D. & Varshavsky, A. Mammalian cell cycle mutant defective in intracellular protein degradation and ubiquitin-protein conjugation. *Prog Clin Biol Res* 180, 17–31 (1985).
65. Finley, D., Ciechanover, A. & Varshavsky, A. Thermolability of ubiquitin-activating enzyme from the mammalian cell cycle mutant ts85. *Cell* 37, 43–55 (1984).
66. Yuan, L. *et al.* Crystal structures reveal catalytic and regulatory mechanisms of the dual-specificity ubiquitin/FAT10 E1 enzyme Uba6. *Nat Commun* 13, 4880 (2022).
67. Itzhak, D. N., Tyanova, S., Cox, J. & Borner, G. H. Global, quantitative and dynamic mapping of protein subcellular localization. *Elife* 5, (2016).
68. Liu, X. *et al.* Orthogonal ubiquitin transfer identifies ubiquitination substrates under differential control by the two ubiquitin activating enzymes. *Nat Commun* 8, 14286 (2017).
69. Schlabach, M. R. *et al.* Cancer proliferation gene discovery through functional genomics. *Science* 319, 620–4 (2008).
70. Beck, D. B. *et al.* Somatic Mutations in UBA1 and Severe Adult-Onset Autoinflammatory Disease. *N Engl J Med* 383, 2628–2638 (2020).
71. Collins, J. C. *et al.* Shared and distinct mechanisms of UBA1 inactivation across different diseases. *EMBO J* 43, 1919–1946 (2024).
72. Lee, P. C. W., Sowa, M. E., Gygi, S. P. & Harper, J. W. Alternative ubiquitin activation/conjugation cascades interact with N-end rule ubiquitin ligases to control degradation of RGS proteins. *Mol Cell* 43, 392–405 (2011).
73. Lee, P. C. W. *et al.* Altered social behavior and neuronal development in mice lacking the Uba6-Use1 ubiquitin transfer system. *Mol Cell* 50, 172–84 (2013).
74. Canaan, A. *et al.* Extended lifespan and reduced adiposity in mice lacking the FAT10 gene. *Proc Natl Acad Sci U S A* 111, 5313–8 (2014).
75. Canaan, A. *et al.* FAT10/diubiquitin-like protein-deficient mice exhibit minimal phenotypic differences. *Mol Cell Biol* 26, 5180–9 (2006).

76. Hunkeler, M., Jin, C. Y. & Fischer, E. S. Structures of BIRC6-client complexes provide a mechanism of SMAC-mediated release of caspases. *Science* 379, 1105–1111 (2023).
77. Ehrmann, J. F. *et al.* Structural basis for regulation of apoptosis and autophagy by the BIRC6/SMAC complex. *Science* 379, 1117–1123 (2023).
78. Dietz, L. *et al.* Structural basis for SMAC-mediated antagonism of caspase inhibition by the giant ubiquitin ligase BIRC6. *Science* 379, 1112–1117 (2023).
79. Wallace, I. *et al.* Insights into the ISG15 transfer cascade by the UBE1L activating enzyme. *Nat Commun* 14, 7970 (2023).
80. Afsar, M. *et al.* Cryo-EM structures of Uba7 reveal the molecular basis for ISG15 activation and E1-E2 thioester transfer. *Nat Commun* 14, 4786 (2023).
81. Huang, D. T., Zhuang, M., Ayrault, O. & Schulman, B. A. Identification of conjugation specificity determinants unmasks vestigial preference for ubiquitin within the NEDD8 E2. *Nat Struct Mol Biol* 15, 280–7 (2008).
82. Williams, K. M. *et al.* Structural insights into E1 recognition and the ubiquitin-conjugating activity of the E2 enzyme Cdc34. *Nat Commun* 10, 3296 (2019).
83. Olsen, S. K. & Lima, C. D. Structure of a ubiquitin E1-E2 complex: insights to E1-E2 thioester transfer. *Mol Cell* 49, 884–96 (2013).
84. Mulder, M. P. C. *et al.* A cascading activity-based probe sequentially targets E1-E2-E3 ubiquitin enzymes. *Nat Chem Biol* 12, 523–30 (2016).
85. Domingues, C. & Ryoo, H. D. Drosophila BRUCE inhibits apoptosis through non-lysine ubiquitination of the IAP-antagonist REAPER. *Cell Death Differ* 19, 470–7 (2012).
86. Vernooy, S. Y. *et al.* Drosophila Bruce can potently suppress Rpr- and Grim-dependent but not Hid-dependent cell death. *Curr Biol* 12, 1164–8 (2002).
87. Tokgöz, Z. *et al.* E1-E2 interactions in ubiquitin and Nedd8 ligation pathways. *J Biol Chem* 287, 311–321 (2012).
88. Huang, D. T. *et al.* Structural basis for recruitment of Ubc12 by an E2 binding domain in NEDD8's E1. *Mol Cell* 17, 341–50 (2005).
89. Lv, Z. *et al.* S. pombe Uba1-Ubc15 Structure Reveals a Novel Regulatory Mechanism of Ubiquitin E2 Activity. *Mol Cell* 65, 699-714.e6 (2017).
90. Cervia, L. D. *et al.* A Ubiquitination Cascade Regulating the Integrated Stress Response and Survival in Carcinomas. *Cancer Discov* 13, 766–795 (2023).
91. Tsherniak, A. *et al.* Defining a Cancer Dependency Map. *Cell* 170, 564-576.e16 (2017).
92. Liu, S.-S. *et al.* Molecular mechanisms underlying the BIRC6-mediated regulation of apoptosis and autophagy. *Nat Commun* 15, 891 (2024).
93. Huang, Y. *et al.* Structural basis of caspase inhibition by XIAP: differential roles of the linker versus the BIR domain. *Cell* 104, 781–90 (2001).
94. Riedl, S. J. *et al.* Structural basis for the inhibition of caspase-3 by XIAP. *Cell* 104, 791–800 (2001).
95. Hao, Y. *et al.* Apollon ubiquitinates SMAC and caspase-9, and has an essential cytoprotection function. *Nat Cell Biol* 6, 849–60 (2004).
96. Suzuki, Y., Nakabayashi, Y. & Takahashi, R. Ubiquitin-protein ligase activity of X-linked inhibitor of apoptosis protein promotes proteasomal degradation of caspase-3 and enhances its anti-apoptotic effect in Fas-induced cell death. *Proc Natl Acad Sci U S A* 98, 8662–7 (2001).

97. Jia, R. & Bonifacino, J. S. Negative regulation of autophagy by UBA6-BIRC6-mediated ubiquitination of LC3. *Elife* 8, (2019).
98. Kabeya, Y. *et al.* LC3, GABARAP and GATE16 localize to autophagosomal membrane depending on form-II formation. *J Cell Sci* 117, 2805–12 (2004).
99. Birgisdottir, Å. B., Lamark, T. & Johansen, T. The LIR motif - crucial for selective autophagy. *J Cell Sci* 126, 3237–47 (2013).
100. Ren, J. *et al.* The Birc6 (Bruce) gene regulates p53 and the mitochondrial pathway of apoptosis and is essential for mouse embryonic development. *Proc Natl Acad Sci U S A* 102, 565–70 (2005).
101. Lois, L. M. & Lima, C. D. Structures of the SUMO E1 provide mechanistic insights into SUMO activation and E2 recruitment to E1. *EMBO J* 24, 439–51 (2005).
102. Bencsath, K. P., Podgorski, M. S., Pagala, V. R., Slaughter, C. A. & Schulman, B. A. Identification of a multifunctional binding site on Ubc9p required for Smt3p conjugation. *J Biol Chem* 277, 47938–45 (2002).
103. Pickart, C. M. & Rose, I. A. Functional heterogeneity of ubiquitin carrier proteins. *J Biol Chem* 260, 1573–81 (1985).
104. Hershko, A., Heller, H., Elias, S. & Ciechanover, A. Components of ubiquitin-protein ligase system. Resolution, affinity purification, and role in protein breakdown. *J Biol Chem* 258, 8206–14 (1983).
105. Chen, P.-T., Yeh, J.-Y., Weng, J.-H. & Wu, K.-P. Elucidating the Mechanism Underlying UBA7•UBE2L6 Disulfide Complex Formation. Preprint at https://doi.org/10.7554/eLife.105638.1 (2025).
106. Haas, A. L., Bright, P. M. & Jackson, V. E. Functional diversity among putative E2 isozymes in the mechanism of ubiquitin-histone ligation. *J Biol Chem* 263, 13268–75 (1988).
107. Scott, D. C. *et al.* Structure of a RING E3 trapped in action reveals ligation mechanism for the ubiquitin-like protein NEDD8. *Cell* 157, 1671–84 (2014).
108. Lee, I. & Schindelin, H. Structural insights into E1-catalyzed ubiquitin activation and transfer to conjugating enzymes. *Cell* 134, 268–78 (2008).
109. Sheng, Y. *et al.* A human ubiquitin conjugating enzyme (E2)-HECT E3 ligase structure-function screen. *Mol Cell Proteomics* 11, 329–41 (2012).
110. Brown, J. S. *et al.* Neddylation promotes ubiquitylation and release of Ku from DNA-damage sites. *Cell Rep* 11, 704–14 (2015).
111. Ma, T. *et al.* RNF111-dependent neddylation activates DNA damage-induced ubiquitination. *Mol Cell* 49, 897–907 (2013).
112. Sahin, U. *et al.* Oxidative stress-induced assembly of PML nuclear bodies controls sumoylation of partner proteins. *J Cell Biol* 204, 931–45 (2014).
113. Ihara, M., Stein, P. & Schultz, R. M. UBE2I (UBC9), a SUMO-conjugating enzyme, localizes to nuclear speckles and stimulates transcription in mouse oocytes. *Biol Reprod* 79, 906–13 (2008).
114. Thul, P. J. *et al.* A subcellular map of the human proteome. *Science* 356, (2017).
115. Olsen, S. K., Capili, A. D., Lu, X., Tan, D. S. & Lima, C. D. Active site remodelling accompanies thioester bond formation in the SUMO E1. *Nature* 463, 906–12 (2010).
116. Yan, W. *et al.* Auranofin targets UBA1 and enhances UBA1 activity by facilitating ubiquitin trans-thioesterification to E2 ubiquitin-conjugating enzymes. *Nat Commun* 14, 4798 (2023).

117. Siepmann, T. J., Bohnsack, R. N., Tokgöz, Z., Baboshina, O. V & Haas, A. L. Protein interactions within the N-end rule ubiquitin ligation pathway. *J Biol Chem* 278, 9448–57 (2003).

7. Supplementary tables

Table 1. Human E2 enzymes and related constructs used in the E2 panel

Human gene	Other names	UBL(s)	Included in panel?	Residues (full-length)	N-terminal UBC extension	C-terminal UBC extension	Residue boundaries used
UBE2A	Ubc2a, Rad6A	Ubiquitin	+	1-152	3	3	1-152
UBE2B	Ubc2b, Rad6B	Ubiquitin	+	1-152	3	3	1-152
UBE2C	UbcH10	Ubiquitin	+	1-179	29	4	1-179
UBE2D1	Ubc4/5, UbcH5A	Ubiquitin	+	1-147	0	0	1-147
UBE2D2	Ubc4/5, UbcH5B	Ubiquitin	+	1-147	0	0	1-147
UBE2D3	Ubc4/5, UbcH5C	Ubiquitin	+	1-147	0	0	1-147
UBE2D4	Ubc4/5, UbcH5D	Ubiquitin	+	1-147	0	0	1-147
UBE2E1	UbcH6	Ubiquitin	+	1-193	46	0	1-193
UBE2E2	UbcH8	Ubiquitin	+	1-201	54	0	1-201
UBE2E3	UbcH9, UbcM2	Ubiquitin	+	1-207	60	0	1-207
UBE2F		NEDD8	-	1-185			
UBE2G1	Ubc7	Ubiquitin	+	1-170	4	5	1-170
UBE2G2	Ubc7	Ubiquitin	+	1-165	3	2	1-165
UBE2H	Ubc8, UbcH2, E2-20K	Ubiquitin	+	1-183	5	32	1-183
UBE2I	Ubc9	SUMO	-	1-158			
UBE2J1	Ubc6	Ubiquitin	+	1-285	9	173	1-285
UBE2J2	Ubc6	Ubiquitin	+	1-230	11	112	1-230
UBE2K	Ubc1, E2-25K	Ubiquitin	+	1-200	2	46	1-200
UBE2L3	UbcH7, UbcM4	Ubiquitin	+	1-154	1	5	1-154
UBE2L6	UbcH8	ISG15	-	1-153			
UBE2M	Ubc12	NEDD8	-	1-183			
UBE2N	Ubc13	Ubiquitin	+	1-152	1	3	1-152
UBE2NL		N/A	-	1-153			
UBE2O	E2-230K	Ubiquitin	+	1-1292	952	180	1-1292
UBE2Q1		Ubiquitin	+	1-422	250	N/A	1-422
UBE2Q2		Ubiquitin	+	1-375	203	N/A	1-375
UBE2QL		Ubiquitin	-	1-161			

UBE2R1	Cdc34, UbcH3	Ubiquitin	+	1-236	7	63	1-236
UBE2R2	Cdc34b, Ubc3B	Ubiquitin	+	1-238	7	65	1-238
UBE2S		Ubiquitin	+	1-222	10	65	1-222
UBE2T		Ubiquitin	+	1-197	1	45	1-197
UBE2U		Ubiquitin	+	1-321	3	172	1-150
UBE2V1	Uev1	N/A	-	1-147			
UBE2V2	Uev2, Mms2	N/A	-	1-145			
UBE2W	Ubc16	Ubiquitin	+	1-151	2	N/A	1-151
UBE2Z		Ubiquitin, FAT10	+	1-354	98	101	1-354
BIRC6	Bruce, Apollon	Ubiquitin	+	1-4857	4572	117	1-4857, 4498-4820
ATG3		ATG12	-	1-314			
ATG10		ATG8	-	1-220			

Table 2. Details of recombinant protein expression and purification

Protein	Construct length	Vector	Affinity tag	Expression system	Ion exchange column	Size exclusion chromatography column
Ubiquitin	1-76	Mod. pOPINB	None	*E. coli*	SP	Superdex 75
MC-Ubiquitin	1-78	Mod. pOPINB	None	*E. coli*	SP	Superdex 75
Ubiquitin G76C	1-76	Mod. pOPINB	None	*E. coli*	SP	Superdex 75
UBA1	1-1058	pACEBAC	Twin-Strep-3C	*Sf9*	Resource Q	Superdex 200
UBA1-6UFD	1-1053	pACEBAC	Twin-Strep-3C	*Sf9*	Resource Q	Superdex 200
UBA1-6SCCH	1-1065	pACEBAC	Twin-Strep-3C	*Sf9*	Resource Q	Superdex 200
UBA6	1-1052	pACEBAC	Twin-Strep-3C	*Sf9*	Resource Q	Superdex 200
UBA6-1UFD	1-1057	pACEBAC	Twin-Strep-3C	*Sf9*	Resource Q	Superdex 200
UBA6-1SCCH	1-1045	pACEBAC	Twin-Strep-3C	*Sf9*	Resource Q	Superdex 200
UBA6 ΔCys-Cap loop	1-1037	pACEBAC	Twin-Strep-3C	*Sf9*	Resource Q	Superdex 200
UBA6 C625S	1-1052	pACEBAC	Twin-Strep-3C	*Sf9*	Resource Q	Superdex 200
UBA6-UFD	940-1052	pOPINS	His_6-SUMO	*E. coli*	Resource S	Superdex 75
dUBA1	184-1191	pACEBAC	Twin-Strep-3C	*Sf9*	Resource Q	Superdex 200
UBE2A	1-152	pOPINB	His_6-3C	*E. coli*	Resource Q	Superdex 75
UBE2B	1-152	pOPINB	His_6-3C	*E. coli*	Resource Q	Superdex 75
UBE2C	1-179	pOPINB	His_6-3C	*E. coli*	N/A	Superdex 75
UBE2D1	1-147	pOPINB	His_6-3C	*E. coli*	N/A	Superdex 75
UBE2D2	1-147	pOPINB	His_6-3C	*E. coli*	N/A	Superdex 75
UBE2D3	1-147	pOPINB	His_6-3C	*E. coli*	N/A	Superdex 75
UBE2D4	1-147	pOPINB	His_6-3C	*E. coli*	N/A	Superdex 75
UBE2E1	1-193	pOPINB	His_6-3C	*E. coli*	Resource S	Superdex 75
UBE2E2	1-201	pOPINB	His_6-3C	*E. coli*	N/A	Superdex 75
UBE2E3	1-207	pOPINB	His_6-3C	*E. coli*	N/A	Superdex 75
UBE2G1	1-170	pOPINB	His_6-3C	*E. coli*	Resource Q	Superdex 75
UBE2G2	1-165	pOPINB	His_6-3C	*E. coli*	Resource Q	Superdex 75
UBE2H	1-183	pOPINB	His_6-3C	*E. coli*	Resource Q	Superdex 75
UBE2J1	1-285	pOPINB	His_6-3C	*E. coli*	N/A	Superdex 75
UBE2J2	1-230	pOPINB	His_6-3C	*E. coli*	N/A	Superdex 75
UBE2K	1-200	pOPINB	His_6-3C	*E. coli*	Resource Q	Superdex 75
UBE2L3	1-154	pOPINK	His_6-GST-3C	*E. coli*	Resource S	Superdex 75

UBE2N	1-152	pGEX6P1	GST-3C	*E. coli*	Resource Q	Superdex 75
UBE2O	1-1292	pGB	C-terminal His_6	*Sf9*	Resource Q	Superdex 200
UBE2Q1	1-422	pOPINB	His_6-3C	*E. coli*	Resource Q	Superdex 75
UBE2Q1 ΔN	246-422	pOPINB	His_6-3C	*E. coli*	N/A	Superdex 75
UBE2Q1 ΔC	1-399	pOPINB	His_6-3C	*E. coli*	Resource Q	Superdex 75
UBE2Q1 ΔNC	246-399	pOPINB	His_6-3C	*E. coli*	N/A	Superdex 75
UBE2Q2	1-375	pOPINB	His_6-3C	*E. coli*	Resource Q	Superdex 75
UBE2Q2 ΔN	197-375	pOPINB	His_6-3C	*E. coli*	Resource Q	Superdex 75
UBE2Q2 ΔC	1-352	pOPINB	His_6-3C	*E. coli*	Resource Q	Superdex 75
UBE2Q2 ΔNC	197-352	pOPINB	His_6-3C	*E. coli*	Resource Q	Superdex 75
UBE2R1	1-236	pOPINB	His_6-3C	*E. coli*	Resource Q	Superdex 75
UBE2R2	1-238	pOPINB	His_6-3C	*E. coli*	Resource Q	Superdex 75
UBE2S	1-222	pOPINB	His_6-3C	*E. coli*	Resource S	Superdex 75
UBE2T	1-197	pOPINB	His_6-3C	*E. coli*	N/A	Superdex 75
UBE2U	1-150	pOPINB	His_6-3C	*E. coli*	Resource Q	Superdex 75
UBE2W	1-151	pOPINB	His_6-3C	*E. coli*	N/A	Superdex 75
UBE2Z	1-354	pOPINB	His_6-3C	*E. coli*	Resource Q	Superdex 75
$BIRC6^{UBC}$	4498-4820	pOPINS	His_6-SUMO	*E. coli*	Resource Q	Superdex 75
BIRC6	1-4857	pACEBAC	Twin-Strep-3C	*Sf9*	MonoQ	Superose 6
dBIRC6	4577-4879	pOPINB	His_6-3C	*E. coli*	N/A	Superdex 75
h/dBIRC6 chimeras	various	pOPINS	His_6-SUMO	*E. coli*	N/A	Superdex 75

Table 3. Buffers used for protein purifications

Buffer name	Buffer contents
Sf9 Lysis buffer	20 mM Tris (pH 8.5)
	200 mM NaCl
	4 mM Dithiothreitol
	10% (v/v) glycerol
Nickel A buffer	20 mM Tris (pH 8.5)
	300 mM NaCl
	20 mM Imidazole
	2 mM β-mercaptoethanol
Nickel B buffer	20 mM Tris (pH 8.5)
	300 mM NaCl
	500 mM Imidazole
	2 mM β-mercaptoethanol
Anion exchange buffer A	20 mM Tris (pH 8.5)
	4 mM Dithiothreitol
Anion exchange buffer B	20 mM Tris (pH 8.5)
	1 M NaCl
	4 mM Dithiothreitol
Cation exchange buffer A	20 mM MES (pH 6.5)
	4 mM Dithiothreitol
Cation exchange buffer B	20 mM MES (pH 6.5)
	1 M NaCl
	4 mM Dithiothreitol
SP buffer A	20 mM Na Acetate (pH 4.5)
SP buffer B	20 mM Na Acetate (pH 4.5)
	1 M NaCl
SEC buffer	20 mM HEPES (pH 7.5)
	200 mM NaCl
	4 mM Dithiothreitol

Table 4. Details of structure determination of Dha-linked E1-E2 structures

	UBA6-UbDha-BIRC6^{UBC} (Doubly loaded) Consensus	**UBA6-UbDha-BIRC6^{UBC} (Doubly loaded) Cluster 0**	**UBA6-UbDha-BIRC6^{UBC} (Doubly loaded) Cluster 2**	**UBA6-UbDha-BIRC6^{UBC} (Singly loaded)**	**UBA6-UbDha-UBE2Z (Singly loaded)**	**dUBA1-UbDha-dBIRC6^{UBC} (Doubly loaded) Consensus**	**dUBA1-UbDha-dBIRC6^{UBC} (Doubly loaded) Cluster 2**	**dUBA1-UbDha-dBIRC6^{UBC} (Doubly loaded) Cluster 4**
EMDB ID	**EMD-53155**	**EMD-53170**	**EMD-53183**	**EMD-53149**	**-**	**EMD-53130**	**EMD-53131**	**EMD-53147**
PDB ID	**9QH5**	**9QHI**	**9QIA**	**9QGW**	**-**	**9QGG**	**9QGI**	**9QGR**
Data collection								
Microscope	Krios (COSMIC)	Krios (COSMIC)	Krios (COSMIC)	Krios (COSMIC)	Krios (COSMIC)	Krios (COSMIC)	Krios (COSMIC)	Krios (COSMIC)
Voltage (kV)	300	300	300	300	300	300	300	300
Detector	K3 BioQuantum	K3 BioQuantum	K3 BioQuantum	K3 BioQuantum	K3 BioQuantum	K3 BioQuantum	K3 BioQuantum	K3 BioQuantum
Slit width (eV)	20	20	20	20	20	20	20	20
Total Dose (e^{-} Å^{-2})	37.84	37.84	37.84	37.84	40.10	36.1	36.1	36.1
Defocus range (μm)	-0.5, -2.5	-0.5, -2.5	-0.5, -2.5	-0.5, -2.5	-0.5, -2.5	-0.5, -2.1	-0.5, -2.1	-0.5, -2.1
Pixel size (Åpx^{-1})	0.85*	0.85*	0.85*	0.85*	0.85*	0.83*	0.83*	0.83*
Micrographs	13,888	13,888	13,888	13,888	6,392	15,362	15,362	15,362
Processing								
Picking software	SIMPLE	SIMPLE	SIMPLE	SIMPLE	SIMPLE	SIMPLE	SIMPLE	SIMPLE
Particles (initial)	4,653,678	4,653,678	4,653,678	4,653,678	4,791,444	7,193,985	7,193,985	7,193,985
Particles (final)	188,172	9,014	6,504	170,986	206,197	333,479	23,467	20,475
Symmetry imposed	C1	C1	C1	C1	C1	C1	C1	C1
Map resolution	3.09	4.27	4.38	3.62	2.93	2.58	3.16	3.10
FSC cut-off	0.143	0.143	0.143	0.143	0.143	0.143	0.143	0.143
Map resolution range 25th, 75th percentile (Å)	3.22, 6.73	6.06, 10.04	7.05, 11.04	3.67, 7.59	3.04, 6.55	2.62, 5.79	3.57, 8.26	3.47, 8.28
Map-sharpening B-factor (Å^2)	124.9	86.6	79.8	151.1	102.4	100.5	76.8	73.8
Refinement								
Model-map Resolution (Å^2)	3.4	4.8	7.1	3.7	3.0	2.8	3.3	3.3
Model-map FSC cut-off	0.5	0.5	0.5	0.5	0.5	0.5	0.5	0.5
CC Mask	0.85	0.84	0.79	0.90	0.90	0.91	0.89	0.87
CC Volume	0.85	0.83	0.77	0.89	0.90	0.91	0.88	0.87
Average protein B-factor (Å^2)	189.08	247.73	249.07	166.92	137.19	119.51	125.99	146.47
Bonds (RMSD)								
Lengths (Å)	0.005	0.004	0.004	0.004	0.004	0.006	0.005	0.006
Angles (°)	0.943	0.946	0.962	0.490	0.547	0.993	0.964	1.033
Validation								
MolProbity score	1.02	1.87	1.56	1.09	0.97	1.04	1.20	1.24
Clashscore	2.36	11.53	9.03	3.04	2.00	2.57	4.21	4.70
Poor rotamers (%)	1.00	2.45	0.71	0.80	0.60	0.85	0.80	0.64
Ramachandran plot								
Disallowed (%)	0.00	0.00	0.00	0.00	0.00	0.00	0.00	0.00
Allowed (%)	1.78	1.97	2.39	1.88	1.68	1.05	1.63	1.42
Favoured (%)	98.22	98.03	97.61	98.12	98.32	98.95	98.37	98.58

Table 5. Details of structure determination of non-covalent E1-E2 structures

	UBA6^{APO} Consensus	UBA6^{APO} Cluster 2	UBA6^{APO} Cluster 3	UBA6-BIRC6^{UBC-IN}	UBA6-BIRC6$^{UBC-OUT}$ Consensus	UBA6-BIRC6$^{UBC-OUT}$ Cluster 0	UBA6-BIRC6$^{UBC-OUT}$ Cluster 4
EMDB ID	**EMD-53184**	**EMD-53187**	**EMD-53188**	**EMD-53195**	**EMD-53190**	**EMD-53192**	**EMD-53193**
PDB ID	**9QIC**	**9QIG**	**9QII**	**9QIV**	**9QIM**	**9QIO**	**9QIP**
Data collection							
Microscope	Krios (eBIC)	Krios (eBIC)	Krios (eBIC)	Krios (eBIC)	Krios (eBIC)	Krios (eBIC)	Krios (eBIC)
Voltage (kV)	300	300	300	300	300	300	300
Detector	K3 BioQuantum	K3 BioQuantum	K3 BioQuantum	K3 BioQuantum	K3 BioQuantum	K3 BioQuantum	K3 BioQuantum
Slit width (eV)	20	20	20	20	20	20	20
Total Dose (e^{-}Å^{-2})	37.45	37.45	37.45	37.45	37.45	37.45	37.45
Defocus range (μm)	-0.5, -2.5	-0.5, -2.5	-0.5, -2.5	-0.5, -2.5	-0.5, -2.5	-0.5, -2.5	-0.5, -2.5
Pixel size (Åpx^{-1})	0.825	0.825	0.825	0.825	0.825	0.825	0.825
Micrographs	13,511	13,511	13,511	13,511	13,511	13,511	13,511
Processing							
Picking software	crYOLO	crYOLO	crYOLO	crYOLO	crYOLO	crYOLO	crYOLO
Particles (initial)	2,210,743	2,210,743	2,210,743	2,210,743	2,210,743	2,210,743	2,210,743
Particles (final)	253,166	19,111	17,392	136,457	139,520	10,415	9,889
Symmetry imposed	C1	C1	C1	C1	C1	C1	C1
Map resolution	3.29	3.94	3.99	3.44	3.57	4.22	4.15
FSC cut-off	0.143	0.143	0.143	0.143	0.143	0.143	0.143
Map resolution range 25^{th}, 75^{th} percentile (Å)	3.32, 6.91	5.19, 8.12	5.33, 8.13	3.42, 7.42	3.91, 7.66	5.94, 9.40	5.66, 9.28
Map-sharpening B-factor (Å^2)	165.5	125.3	122.9	147.6	155.3	122.7	119.9
Refinement							
Model-map Resolution (Å^2)	3.4	4.1	4.2	3.6	3.7	4.6	4.5
Model-map FSC cut-off	0.5	0.5	0.5	0.5	0.5	0.5	0.5
CC Mask	0.90	0.87	0.87	0.90	0.87	0.86	0.86
CC Volume	0.89	0.85	0.86	0.89	0.87	0.84	0.85
Average protein B-factor (Å^2)	168.79	223.60	208.95	141.14	191.60	265.36	261.75
Bonds (RMSD)							
Lengths (Å)	0.003	0.004	0.005	0.002	0.002	0.002	0.002
Angles (°)	0.455	0.685	0.702	0.443	0.438	0.586	0.595
Validation							
MolProbity score	1.14	1.62	1.82	1.25	1.15	1.36	1.36
Clashscore	3.54	9.31	13.79	4.85	3.56	6.55	6.46
Poor rotamers (%)	0.45	0.45	0.78	0.79	0.26	0.00	0.00
Ramachandran plot							
Disallowed (%)	0.00	0.00	0.00	0.00	0.00	0.00	0.00
Allowed (%)	1.39	2.68	2.97	1.49	1.00	1.84	1.38
Favoured (%)	98.61	97.32	97.03	98.51	99.00	98.16	98.62

Table 6. Details of cryoEM analysis of the UBA6-BIRC6^{FL} sample

	UBA6^{APO}	**UBA6-BIRC6^{FL}**	**BIRC6^{FL}**
EMDB ID	**-**	**-**	**-**
PDB ID	**-**	**-**	**-**
Data collection			
Microscope	Arctica (COSMIC)	Arctica (COSMIC)	Arctica (COSMIC)
Voltage (kV)	200	200	200
Detector	Falcon 4	Falcon 4	Falcon 4
Slit width (eV)	-	-	-
Total Dose (e^{-}Å^{-2})	44.10	44.10	44.10
Defocus range (μm)	-1.0, -2.6	-1.0, -2.6	-1.0, -2.6
Pixel size (Åpx^{-1})	0.95	0.95	0.95
Micrographs	2,153	2,153	2,153
Processing			
Picking software	cryoSPARC template picker	cryoSPARC template picker	cryoSPARC template picker
Particles (initial)	46,971	46,971	13,948
Particles (final)	7,309	5,325	11,643
Symmetry imposed	C1	C1	C1
Map resolution	8.13	8.72	4.40
FSC cut-off	0.143	0.143	0.143
Map resolution range 25th, 75th percentile (Å)	9.81-11.94	11.22-13.01	7.05-11.79
Map-sharpening B-factor (Å^2)	706.9	821.6	39.4

Table 7. Estimated protein levels for selected proteins within the ubiquitin cascade

Estimation of protein abundance within a HeLa cell for selected E1 and E2 enzymes, data adapted from Itzhak *et al.*[67]. Values rounded to two significant figures.

Protein	E1 specificity	Copies per cell	Concentration /nM
UBA1	N/A	3,000,000	1,900
UBA6	N/A	440,000	270
UBE2A	Non-specific	100,000	62
UBE2D1	Non-specific	73,000	45
UBE2D3	Non-specific	1,700,000	1,000
UBE2G2	Non-specific	480,000	300
UBE2J2	Non-specific	16,000	9.7
UBE2L3	Non-specific	2,400,000	1,500
UBE2N	Non-specific	7,400,000	4,600
UBE2O	Non-specific	220,000	140
UBE2S	Non-specific	240,000	150
UBE2T	Non-specific	700,000	430
UBE2Z	UBA6-specific	500,000	310
BIRC6	UBA6-specific	58,000	36

8. Appendix

8.1. Appendix Figures

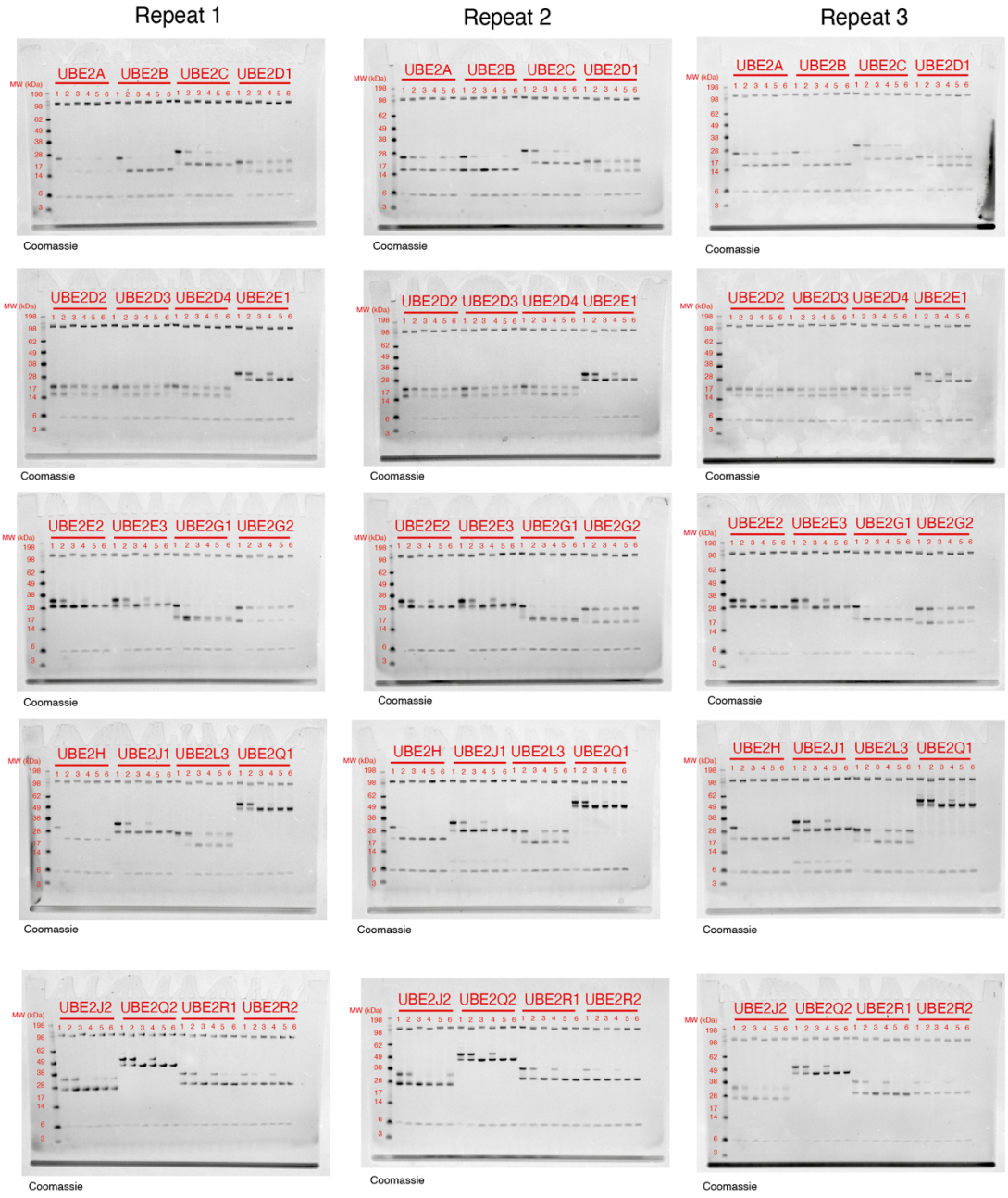

1. UBA1
2. UBA1-UBA6^{SCCH}
3. UBA1-UBA6^{UFD}
4. UBA6-UBA1^{UFD}
5. UBA6-UBA1^{SCCH}
6. UBA6

Appendix Figure 1. Unprocessed gel images for Figures 8b, 9b

Unprocessed images showing all three repeats for the E1-E2 specificity panel transthiolation assay in **Figures 8b, 9b**. Reactions were analysed by SDS-PAGE and Coomassie stained for quantification.

Repeat 1 | Repeat 2 | Repeat 3

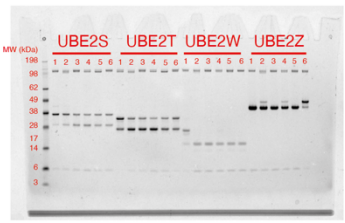

Coomassie

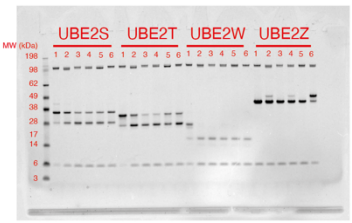

Coomassie

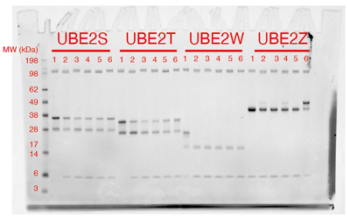

Coomassie

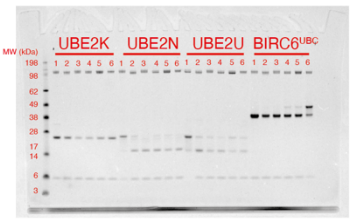

Coomassie

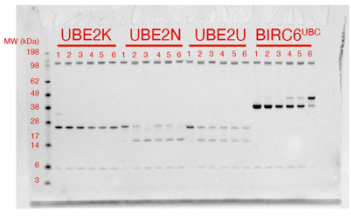

Coomassie

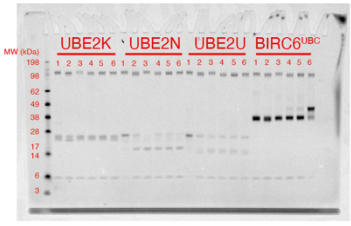

Coomassie

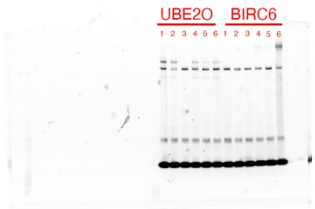

Fluorescence 488 nm

Fluorescence 488 nm

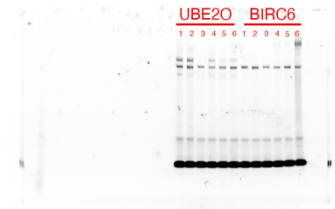

Fluorescence 488 nm

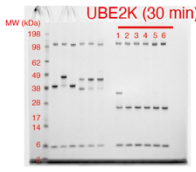

Coomassie

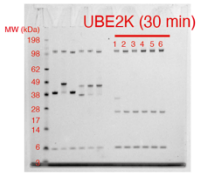

Coomassie

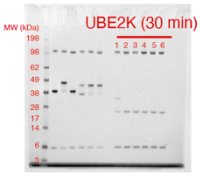

Coomassie

Coomassie

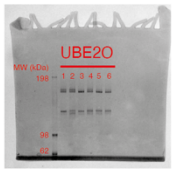

Coomassie

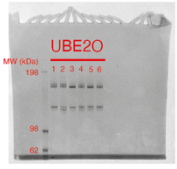

Coomassie

1. UBA1
2. UBA1-UBA6^{SCCH}
3. UBA1-UBA6^{UFD}
4. UBA6-UBA1^{UFD}
5. UBA6-UBA1^{SCCH}
6. UBA6

Appendix Figure 2. Unprocessed gel images for Figures 8b, 9b (continued)

Unprocessed images showing all three repeats for the E1-E2 specificity panel transthiolation assay in **Figures 8b, 9b**. Reactions were analysed by SDS-PAGE and Coomassie stained for quantification. A reaction with fluorescently labelled ubiquitin was used for full-length BIRC6, which is too large to observe a mobility shift upon ubiquitin loading.

a

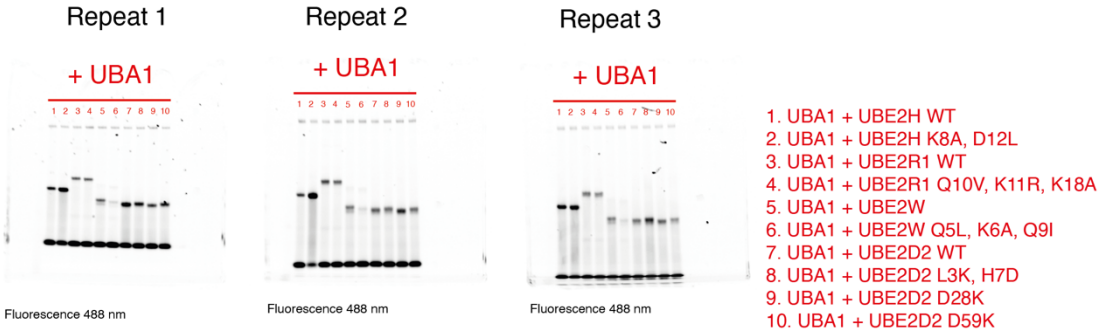

1. UBA1 + UBE2H WT
2. UBA1 + UBE2H K8A, D12L
3. UBA1 + UBE2R1 WT
4. UBA1 + UBE2R1 Q10V, K11R, K18A
5. UBA1 + UBE2W
6. UBA1 + UBE2W Q5L, K6A, Q9I
7. UBA1 + UBE2D2 WT
8. UBA1 + UBE2D2 L3K, H7D
9. UBA1 + UBE2D2 D28K
10. UBA1 + UBE2D2 D59K

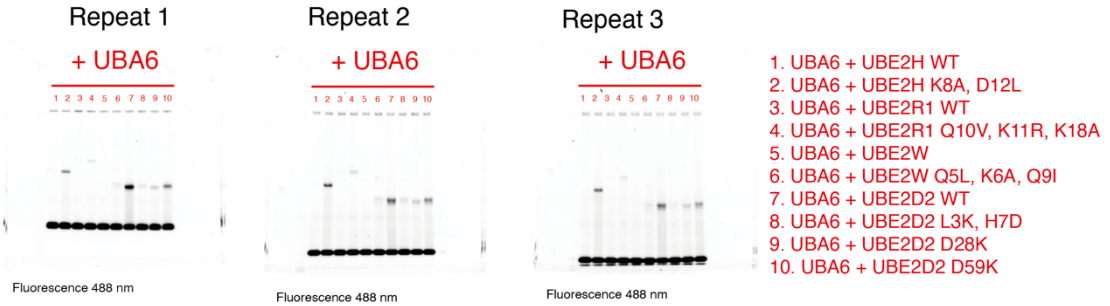

1. UBA6 + UBE2H WT
2. UBA6 + UBE2H K8A, D12L
3. UBA6 + UBE2R1 WT
4. UBA6 + UBE2R1 Q10V, K11R, K18A
5. UBA6 + UBE2W
6. UBA6 + UBE2W Q5L, K6A, Q9I
7. UBA6 + UBE2D2 WT
8. UBA6 + UBE2D2 L3K, H7D
9. UBA6 + UBE2D2 D28K
10. UBA6 + UBE2D2 D59K

b

Dashed green box - region used for quantification.

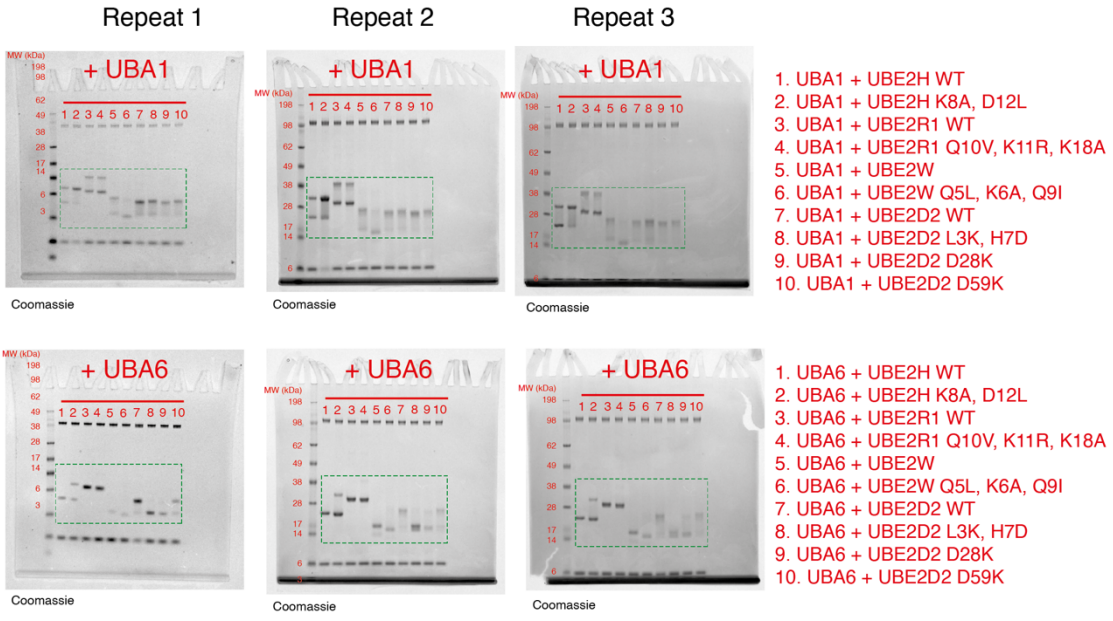

1. UBA1 + UBE2H WT
2. UBA1 + UBE2H K8A, D12L
3. UBA1 + UBE2R1 WT
4. UBA1 + UBE2R1 Q10V, K11R, K18A
5. UBA1 + UBE2W
6. UBA1 + UBE2W Q5L, K6A, Q9I
7. UBA1 + UBE2D2 WT
8. UBA1 + UBE2D2 L3K, H7D
9. UBA1 + UBE2D2 D28K
10. UBA1 + UBE2D2 D59K

1. UBA6 + UBE2H WT
2. UBA6 + UBE2H K8A, D12L
3. UBA6 + UBE2R1 WT
4. UBA6 + UBE2R1 Q10V, K11R, K18A
5. UBA6 + UBE2W
6. UBA6 + UBE2W Q5L, K6A, Q9I
7. UBA6 + UBE2D2 WT
8. UBA6 + UBE2D2 L3K, H7D
9. UBA6 + UBE2D2 D28K
10. UBA6 + UBE2D2 D59K

Appendix Figure 3. Unprocessed gel images for Figure 22.

a-b. Unprocessed images showing all three repeats for the transthiolation assay in **Fig. 22**. Reactions were analysed by SDS-PAGE and imaged first for fluorescence (a), then Coomassie stained for quantification (b).